Studies on Catalytic Conversion of Biomass-derived C6-Furanics for Polymer Applications

(高分子材料への応用を志向した

バイオマス由来 C6 フラン化合物の触媒変換に関する研究)

Nirupama Sheet

Hokkaido University

北海道大学

2024

Table of Contents

Chapter 1: General Introduction

1.1 Background

In recent decades, the continuous depletion of fossil fuels leads to the finding of an alternative renewable carbon source for energy and chemicals.[1–3] The conversion of renewable and non-edible biomass resources into useful commodity chemicals is of great importance to building up a sustainable society alleviating our dependency on fossil fuels.[1–6] Biomass, a biological material derived from living or recently living organisms, often refers to plant-derived materials (**Figure 1.1A**). The energy stored in biomass, in the chemical form is released when the chemical bonds in their component (such as C-H, C-O, and C-C, etc.) are broken via combustion, digestion or other chemical reactions, which can be utilized in several fields, such as to produce liquid and gaseous fuels, electricity, and a variety of chemicals contributing about 10–14% of the world's energy supply (**Figure 1.1B**).[7–8] In brief, biomass refinery is one of the promising methods for the sustainable development of human society and economy.[1–8]

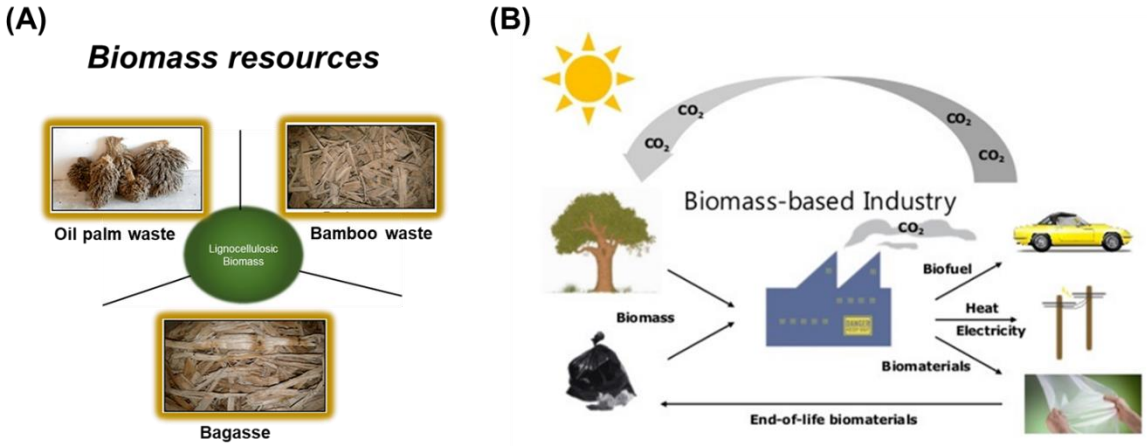

Figure 1.1. (A) Biomass resources and (B) Applications of biomass in real field (Slideshare.net.).

Recently, lignocellulosic biomass is one of the promising biomass feedstocks that has gained tremendous attention for valorization to useful chemicals owing to the advantages of low-cost, non-edible, fast growth, carbon-rich and high abundance in nature.[9–13] It is

comprised of three main parts: i) cellulose (long linear chain of glucopyranose unit), ii) hemicellulose (polysaccharide like xylose), and iii) lignin (highly branched and substituted aromatic polymer) (**Figure 1.2**).[9–10] The difference in their inherent structure makes the separation of different fractions less critical. Nevertheless, after the separation of each fraction, cannot be used directly due to their high oxygen content and low energy density. Instead, they can be converted into a variety of platform molecules (such as furfural, 5-hydroxymethylfurfural (HMF), levulinic acid, phenol, vanillin and so on) via several cascade reactions (such as hydrolysis, dehydration, aldol condensation, dealkylation, etc.), which further can be upgraded to the fuel-derivatives and other valuable chemicals (**Figure 1.2**).[9–13]

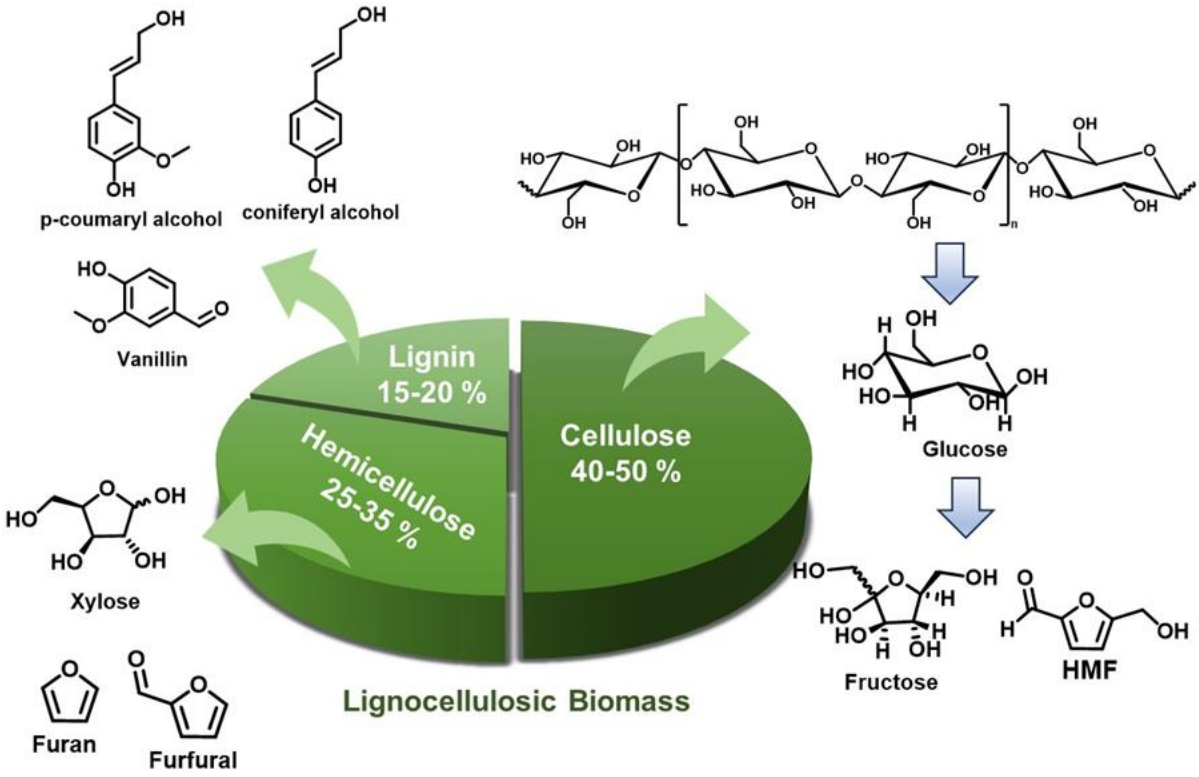

Figure 1.2. Valorization of lignocellulosic biomass.

1.2 Significance of biomass-derived C6-furanics

Nowadays, the conversion of biomass-derived carbohydrates (such as glucose, fructose and xylose) into furanic aldehydes (such as furfural, HMF, 5-choloromethylfurfural (CMF) and 5-bromoromethylfurfural (BMF)) have been recognized as a promising strategy for the synthesis of a broad range of commodity chemicals.[13] For example, furfural is the dehydration product of xylose and can be converted to a range of valuable chemicals such as furfuryl alcohol, 2-methylfuran (MF), 2-methyltetrahydrofuran (MTHF), linear alkanes, phenol-formaldehyde resin, furoic acid, maleic acid and so on.[13] HMF is obtained by acid-catalyzed dehydration of glucose and is identified as one of the versatile platform molecules.[12] A variety of building blocks used potentially to produce essential polymers can be obtained from HMF originating from its unique structure through selective tailoring of its functional groups by hydrogenation, hydrodeoxygenation, oxidation, reductive amination, and so on (**Scheme 1.1**).[3–6] For example, aerobic oxidation of HMF produces 2,5-furandicarboxylic acid (FDCA).[14–16] FDCA and its ester derivatives can be used as a substitute for petroleum-based terephthalic acid for polymer application, because polymerization of FDCA with biobased ethylene glycol makes a 100% biomass-derived polyester, poly(ethylene furanoate) (PEF), which can be potentially replaced with petroleum-derived poly(ethylene terephthalate) (PET, global annual production >50 MT) (**Scheme 1.2**). PEF has superior gas barrier and glass transition properties than PET.[6] Hydrogenation of HMF produces aromatic (2,5-bis(hydroxymethyl)furan, BHMF)[17–18] and aliphatic diols (2,5-bis(hydroxymethyl)tetrahydrofuran (BHMTHF) and 1,6-hexanediol (1,6-HDO)[19–22] that can be utilized as building blocks for polyesters and polyurethanes. Hydrodeoxygenation of HMF affords 2,5-dimethylfuran (DMF) which has a high-octane number, an ideal for transportation fuels.[23] In addition, 2,5-bis(aminomethyl)furan (BAMF), a value-added primary amine, can be synthesized directly via reductive amination of HMF and 2,5-diformylfuran (DFF).[24–25] Most recently, CMF and BMF were used to produce valuable fuels and chemicals such as DMF, 5-ethoxymethylfurfural (EMF) or LA.[13] However, the low yield and high production cost limit their potential application in chemical industries.

Several catalytic reaction systems for the conversion of HMF and HMF-derivatives to monomers of biobased polymers are summarized below.

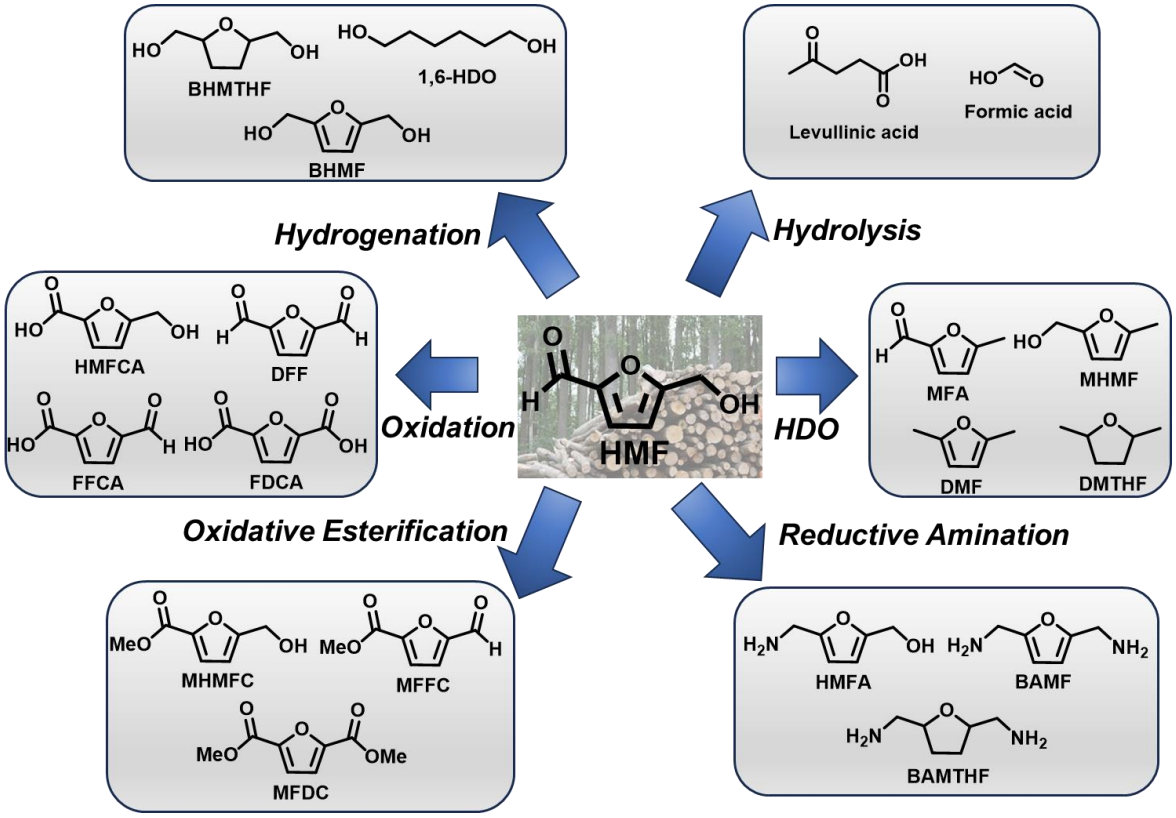

Scheme 1.1. Conversion of lignocellulosic biomass derived 5-HMF into valuable platform molecules.

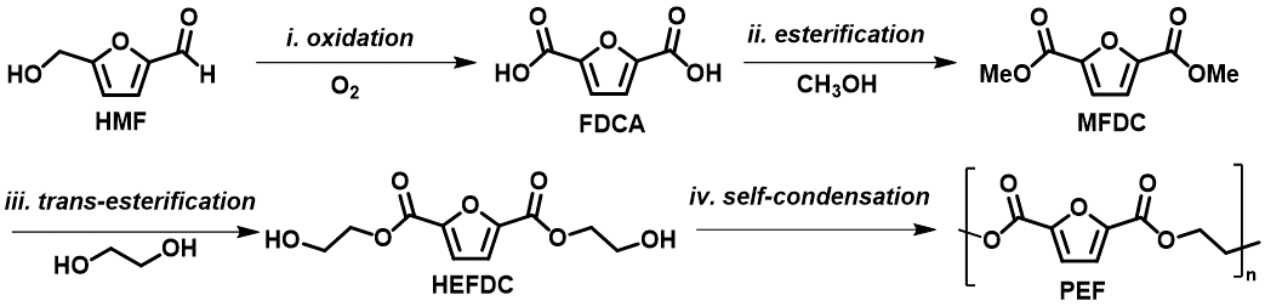

Scheme 1.2. Schematic illustration to synthesize PEF form HMF. HEFDC refers to the bis(2-hydroxyethyl)furan-2,5-dicaroxylate.

1.3 Aerobic Oxidation and Oxidative esterification of HMF

Traditionally, the oxidation of HMF to FDCA involved use of oxidizing agents such as nitric acid, potassium permanganate and so on.[26–28] However, low efficiency and severe hazards limits the industrialization of this process.[26–28] Several homogeneous catalytic systems were developed to make the efficient process, but still, reactor corrosion and catalyst recovery remain serious challenges.[26-28] To date, several supported noble metal (e.g., Au, Pd, Pt, Ru and their alloys) and non-noble metal nanoparticles (e.g., Co, Mn, Cu) have been extensively investigated for the catalytic oxidation of HMF to FDCA and its dimethyl ester (Dimethyl furan-2,5-dicarboxylate, MFDC) (**Table 1.1**).[26–49] For example, Casanova et al. studied the oxidation of HMF using a wide range of supported (such as C, CeO_2, Fe_2O_3 and TiO_2) Au catalysts.[14] Among them, Au/CeO_2 showed the best catalytic activity to produce FDCA in >99% yields at 60 °C for 8 h under 10 bar air, while Au-Cu supported on TiO_2 produced FDCA in 99% yield at 110 °C for 4 h under 20 bar O_2.[28] The addition of homogeneous bases such as NaOH or Na_2CO_3 is essential for the oxidation of HMF into FDCA due to the neutralization.[14] Later, Lilga et al.[29] and Gupta et al.[27] reported that Pt/ZrO_2 and Au/HT catalysts can form FDCA in water with 98% and 99% yields, respectively, under moderate reaction conditions without any base. Conventional purification methods such as vacuum distillation and recrystallization are not applicable on FDCA production.[26] To overcome these issues, direct conversion from HMF to MFDC is an alternative approach, which can be easily purified and transformed to FDCA via hydrolysis.[26] Moreover, MFDC is used directly to synthesize polyesters (such as poly(ethylene furanoate), PEF) via trans-esterification reactions with ethylene glycol. The conversion of HMF to MFDC can proceed following one of the two reaction pathways; i) oxidative esterification of the formyl (-CHO) group of HMF to 5-hydroxymethyl-2-methyl-furoate (MHMFC) followed by oxidation of hydroxymethyl functionality (-CH_2OH) to 5-formyl-2-methyl-furoate (MFFC), and subsequent oxidative esterification to convert formyl (-CHO) group of MFFC to MFDC, ii) the oxidation of -CH_2OH group of HMF to 2,5-diformylfuran (DFF), and then subsequent oxidative esterification of the -CHO groups to MFFC followed by MFDC (**Scheme 1.3**).[28] The reaction pathways depend on the catalytic nature and reaction conditions.[26–49]

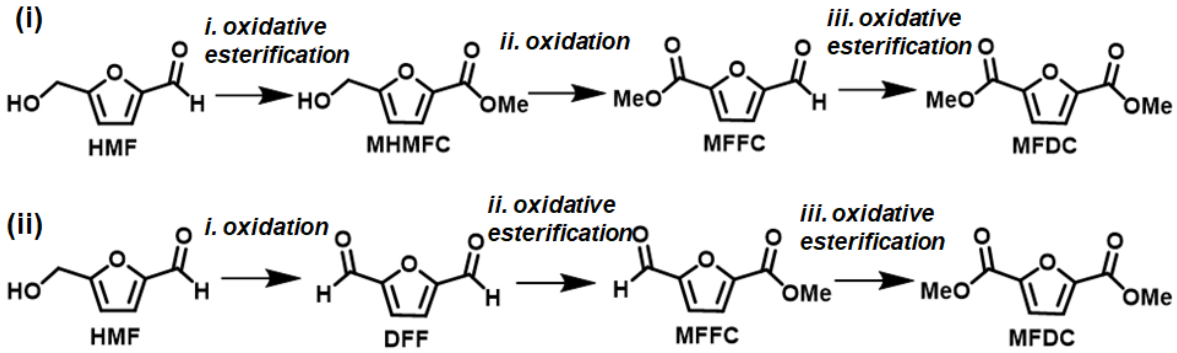

Scheme 1.3. Reaction Pathways for the conversion of HMF to MFDC via oxidative esterification.

Table 1.1. Literature survey for oxidative esterification of HMF to MFDC.

#	Catalyst	Conc. (wt%)	Additives	T/P(O_2)/t (° C/bar/h)	MFDC Yield (%)	Ref.
1	Au/TiO_2	5.0	MeONa	130/4/3	98	[34]
2	$Au\text{-}Pd/Fe_3O_4$	1.6	K_2CO_3	rt./1/24	92	[35]
3	PdCoBi/C	4.0	K_2CO_3	60/1/14	96	[36]
4	Au/CeO_2	1.2	-	130/10/5	>99	[33]
5	Au/ZrO_2	0.2	-	130/3/5	30	[38]
6	$Au\text{-}Cu/\gamma\text{-}Al_2O_3$	0.8	-	105/10/5	98	[37]
7	CoxOy-N@C	2.0	K-OMS-2, K_2CO_3	100/10/6	96	[26]
8	Co@NC	1.6	Na_2CO_3	100/20/12	95	[48]
9	Co SAC-N@C	1.3	-	65/1/9	83	[46]

In 2008, Chtistensen group first reported Au/TiO_2 catalyzed the oxidative esterification of HMF to MFDC with 98% yield at 130 °C for 3 h under 4 bar of O_2 using sodium methoxide (MeONa) as a base.[34] The reaction did not proceed without MeONa even prolonging the reaction time. It is reported that the activation of C-H and O-H bonds of -CH_2OH with Brønsted base (hydroxyl ion) is the key in the oxidation of HMF.[31] Kim et al.

developed AuPd-Fe_3O_4 nanoparticles catalyst for MFDC synthesis in the presence of K_2CO_3 under mild reaction conditions (rt., 24 h, 1 bar of O_2).[35] In addition, PdCoBi/C afforded a 96% MFDC yield under optimum reaction conditions (60 °C, 1 atm O_2, 14 h, 20% K_2CO_3).[36] In contrast, the Au/CeO_2 catalyst showed high MFDC productivity in the absence of base and its activity is superior to other Au catalysts with different supports.[33] The characterization of the catalyst revealed the formation of superoxide molecules on nanocrystalline CeO_2 due to the electronic defects caused by the presence of an unsaturated Ce atom (Ce^{3+}), which induces providing a sufficient oxygen source for the reaction.[33] More interestingly, the similar atomic radii of Au and Cu enhanced the miscibility, which favor the formation of homogeneous Au-Cu hybrids.[37] To date, Au-Cu/Al_2O_3 showed the highest MFDC productivity in the oxidative esterification of HMF at 105 °C in 5 h under 10 bar of O_2.[37]

Recently, the use of supported non-noble metal catalysts has gained significant attention for the oxidative esterification processes.[42–49] Cobalt and cobalt oxides are earth-abundant, and their catalytic activity can be enhanced by immobilization of their nanoparticles on nitrogen-doped carbon support.[42–48] Several nitrogen-doped carbon-supported Co catalysts has been studied in the catalytic oxidation and oxidative esterification reactions of HMF. For example, Fu et al. developed CoxOy-N@C catalyst via an incipient wetness impregnation method and obtained MFDC in 96% yield under optimum conditions (100 °C, 1 MPa O_2, 6 h, K-OMS-2, 0.2 eq. K_2CO_3).[26] An alternative method to synthesize Co@NC is the carbonization of zeolite imidazole ester frameworks (ZIFs), wherein high calcination temperatures are applied to ensuring uniform formation of Co@NC. The imidazole ligands in ZIF transformed into nitrogen-doped carbon by calcination in an inert gas atmosphere, while the hollow structure of ZIF provides a large specific surface area in the resulting material. Lin et al. reported ZIF-67 derived Co@NC to produce MFDC in a 95% yield under mild reaction conditions using Na_2CO_3 as the base additive.[48] Liu et al. synthesized single atom catalysts (SACs) (Fe, Co, Ni, Cu) supported on nitrogen-doped carbon materials, where the natural phenolic structure of lignin was utilized to confine metal ions via metal-lignin complex formation.[46] The Co SACs-N@C afforded MFDC in a 86% yield (65 °C, 1 MPa O_2, 9 h) without any base-additive.[46] Although the uses of inexpensive

and reusable transition metal nanoparticles are attractive alternatives, the relatively poor stability and activity limit their practical applications.

1.4 Reductive amination of biomass-derived C6-furanics

Primary diamines are the most versatile nitrogen-containing compound having wide applications in polymer industry to produce polyamides and polyurea.[50–55] For example, 1,6-hexanediamine (HAD) is a monomer of PA-6,6, a commercial polyamide, which had an annual production of 1400 thousand tons in 2022. In addition, nitrogen-containing compounds are key components in diverse bioactive molecules including peptides, alkaloids, nucleic acids and other natural products.[58] Moreover, they have extensive applications in the synthesis of pharmaceuticals, food additives, detergents, and agrochemicals.[55] Traditionally, the synthesis of primary amines mainly relies on fossil resources, harsh reaction conditions, and toxic intermediates rendering sustainable production.[55–58] Therefore, the applications of biomass-derived substrates to synthesize primary diamines will be one of the promising methods to meet the global demand. There are several strategies for the sustainable production of nitrogen-containing compounds from biomass-derived substrates such as catalytic fast pyrolysis of carbohydrates in ammonia, conversion of nitrogen-containing carbohydrates, and reductive amination of biomass-derived aldehydes.[55] Catalytic reductive amination of biomass-derived furanics is promising for synthesizing corresponding primary amines.[55] Several reductants, including gaseous hydrogen (H_2), formic acid, sodium borohydride and hydrosilane, have been used, but H_2 is more viable compared to others due to no byproduct formation.[55–57] Reductive amination with NH_3 starts from the formation of a primary imine, followed by hydrogenation with a catalyst and a reductant molecule to obtain the target nitrogen-containing compound. Recent progress for the catalytic reductive amination of several biomass-derived furanics has been summarized in **Table 1.2**.[55–63] The reductive amination of HMF with NH_3 and H_2 delivers two aminated products, 5-hydroxymethyl-2-furfuryl amine (HMFA) and 2,5-Bis(aminomethyl)furan (BAMF).[25,67–69] HMFA is a useful intermediate in the synthesis of several bioactive molecules and a monomer of biopolymers such as 6-amino-1-hexanol.[67–

[69] BAMF, a primary diamine, is widespread for the synthesis of polyamides, polyurethanes and polyurea due to their superior gas barrier performance, miscibility, processibility and biocompatibility.[55–56] Methyl-5-formyl-2-furancarboxylate (MFFC) produced via selective aerobic oxidative esterification of HMF can be utilized to synthesize another valuable bio-based primary amine, Methyl-5-(aminomethyl)-2-furancarboxylate (MAMFC). MAMFC further can be used to synthesize an attractive polyamide, poly(iminomethylene(cis-tetrahydro-2,5-furandiyl)carbonyl) (PITC) via the formation of 8-oxa-3-azabicyclo[3.2.1]octan-2-one and several precursors of anticancer drugs such as G-quadruplex[75–78].

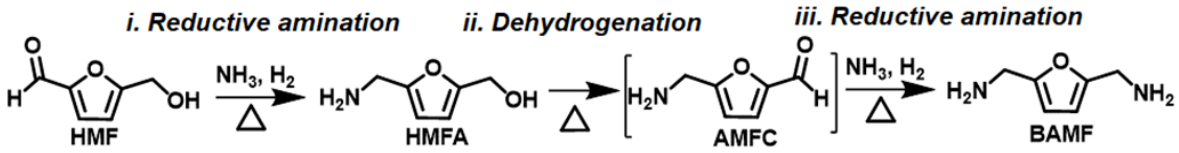

Scheme 1.4. Reaction pathways for subsequent reductive amination of HMF to HMFA, followed by BAMF.

BAMF formation from HMF is a stepwise conversion process that converts formyl group (-CHO) and hydroxymethyl group (-CH_2OH) to -CH_2NH_2 (**Scheme 1.4**). The conversion of -CH_2OH consists of three consecutive steps: 1) dehydrogenation of -CH_2OH to formyl group, 2) imination of the resulting formyl group with NH_3 to a primary imine, and 3) hydrogenation of the imine to -CH_2NH_2.[25, 67–69] The dehydrogenation of -CH_2OH is the rate-determining step in the overall process,[25,67–69] which is thermodynamically unfavorable.[67–69] Yuan et al. reported Ni_6AlO_x catalyst with optimum Ni/Al ratio, produces HMFA in a quantitative yield (99%) in the reductive amination of HMF in the presence of aq. NH_3 and H_2.[67] Gokhale et al. developed the montmorillonite clay (MMT)-impregnated Ni nanoparticles (12.5 wt% Ni/MMT) to aminate HMF in an aq. NH_3 solution, giving HMFA in a 79% yield at 94% HMF conversion.[69] Ru/MMT catalyst synthesized by the similar procedures produced HMFA in a 86% yield at 98% conversion.[69] Several multi-step methods were developed to obtain BAMF from HMF. Komonoya et al. developed a two-step process, wherein HMF was first converted to HMFA over Ru/Nb_2O_5 catalyst and then

transformed into BAMF over a homogeneous [Ru(CO)ClH(PPh_3)$_3$]/Xantphos catalyst.[68] Similar results were reported by Wei et al., where BAMF can be obtained in a 88.3% yield at full conversion over Raney Ni catalyst in THF under optimized reaction conditions (0.35 MPa NH_3, 1 MPa H_2, 160 °C, 6 h).[25] Recently, hydrotalcite-like Ni_2Al-600 catalyst gave a moderate BAMF yield of 70.5% in the reductive amination of HMFA with 0.4 MPa NH_3 at 160 °C in 18 h.[70] In addition, various strategies to selectively obtain BAMF from HMF derivatives have also been demonstrated.[71] For instance, BAMF can be produced directly via the reductive amination of DFF (**Scheme 1.1**). The reductive amination of DFF to BAMF involves the imination of -CHO groups with a nitrogen (N) source to generate a di-imine intermediate which on hydrogenation in the presence of a suitable catalyst gave BAMF (**Scheme 1.5**).[24]

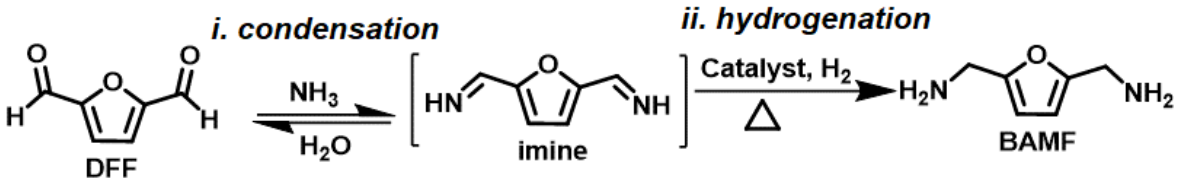

Scheme 1.5. Reaction pathways for reductive amination of DFF to BAMF.

However, an efficient process towards direct synthesis of BAMF from DFF has been not yet established due to the imination of amine group in HMFA and BAMF with formyl group in DFF and HMFA forming secondary and tertiary imines, which is then hydrogenated to polymeric amine species. Kim et al. obtained only a 42.6% yield of BAMF in the reductive amination of DFF over acid-treated RANEY-Ni catalysts.[24] To overcome such challenges, a few multi-step processes have been developed currently. Xu and co-workers demonstrated that the oximation of DFF, followed by hydrogenation of 2,5-diformylfuran dioxime gave a high yield of BAMF (94.5%).[71] Zhang et al. introduced *n*-butylamine as a protecting agent of dialdehydes.[74] *n*-Butylamine first reacts with DFF to form primary di-imine, which undergoes *trans*-imination reaction with NH_3. Then, the hydrogenation with Co/ZrO_2 catalysts (P_{H2} = 2 MPa) affords BAMF in a high yield of 95% (**Scheme 1.6**).[74] Increasing the substrate concentration to 10 wt% significantly drops the BAMF yield from 95% to 71%,

which makes this process less promising.[74] Therefore, it is still in demand to develop an efficient heterogeneous catalytic process for the synthesis of BAMF from biomass-derived substrates.

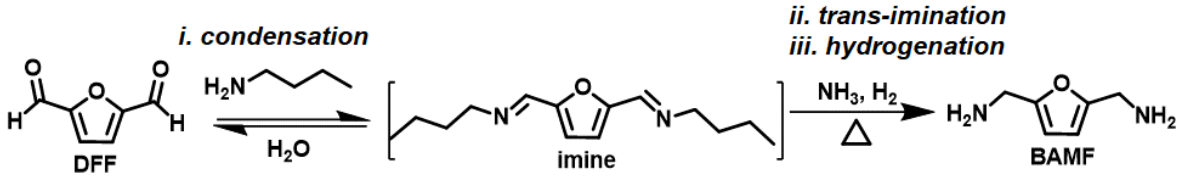

Scheme 1.6. Strategy of *trans*-imination for the synthesis of BAMF from DFF.[83]

Recently, metal phosphide nanoparticles emerged as an efficient catalyst in several organic transformations such as hydrogenation, reductive amination, cyclization and so on.[79–91] The incorporation of phosphorus atoms into metal alloys significantly upgrades their catalytic efficiency and stability. The P-alloying i) modulates the electronic state of metals, ii) stabilizes the zero-valent metal species and iii) creates well-defined active sites preciously.[91–97] Mitsudome *et al.* reported single-crystal cobalt phosphide nanorods (Co_2P NRs) for the reductive amination of several biomass-derived compounds (such as furfural and HMF) with aqueous NH_3 and obtained corresponding primary amine-derivatives in high yields.[85] The higher hydrogenation efficiency of Co_2P NRs is associated with its unique rod-shaped morphology, which generates a large content of surface unsaturated Co-Co active sites.[85] The coordination number (CN) ratio, $CN_{Co\text{-}Co}/CN_{Co\text{-}P}$ calculated from the crystal structure of orthorhombic Co_2P, reveals that NRs (1.6) is smaller than bulk Co_2P (2.0) indicating a high number of coordinatively unsaturated Co-Co sites present on the nanorod surface.[85]

Table 1.2. Representative report on reductive amination of biomass-derived C6-furanics to subsequent primary amines.

#	Catalyst	Reactant	Conc. (wt%)	Additives	T/P_{H2}/t (° C/MPa/h)	Product	Yield (%)	Ref.
1	Ni_6AlO_x	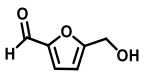 HMF	4.2	NH_3, H_2O	100/0.1/6	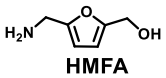 HMFA	99	[64]
2	Ni/MMT		1.6	NH_3, H_2O	130/1.5/7		79	[69]
3	Ru/MMT		1.6	NH_3, H_2O	90/1.0/3		86	[69]
4	Co_2P NRs		1.8	NH_3, H_2O	100/0.5/10		87	[85]
5	Ru/Nb_2O_5 & Ru complex[a] /Xantphos		1.2	NH_3, CH_3OH, t-amyl alcohol	90/4/4 140/-/14		93	[68]
6	$Cu_4Ni_1Al_4O_x$	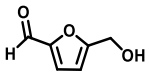 HMF	19.4	NH_3, Na_2CO_3, 1,4-dioxane	90/4.5/6 210/4.5/18	 BAMF	86	[61]
7	Ni/Al_2O_3		3.7	NH_3, THF	160/1/36		86	[25]
8	NiMn(4:1) $/Al_2O_3$				160/1/24		82	[25]
9	Raney Ni		1.1	NH_3, THF-H_2O	120/1/6		43	[24]
10	Co/ZrO_2	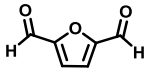 DFF	1.3	NH_3, CH_3OH, butylamine	100/2/10	 BAMF	95	[74]
11			10		100/4/10		71	[74]

[a] $[Ru(Co)ClH(PPh_3)_3]$

1.5 Dehydrogenation of 5-Hydroxymethylfurfural (HMF)

HMF can be oxidatively converted to a variety of valuable compounds as shown in **scheme 1.1**.[26–49] DFF is an attractive platform molecule, which can be not only used as a precursor for adhesives, binders, heterocyclic ligands, and furan–urea resins, but also further upgraded to FDCA, MFDC, BAMF, BHMF, and so on.[92] However, the oxidation of HMF in water proceeds via 5-(hydroxymethyl)furan-2-carboxylic acid (HMFCA) and 5-

formylfuran-2-carboxylic acid (FFCA) as intermediates (**Scheme 1.8**),[93] and another route via DFF is a minor path. Formyl group in DFF is present in the geminal diol form with water, which leads to the formation of carboxylic group through oxidative dehydrogenation (**Scheme 1.9**).[93] Selective oxidation of HMF to DFF has been developed using anhydrous and non-protic solvents (such as *N,N*-dimethylformamide (DMF), toluene, and so on) with several supported noble metal (Ru, Pd, Au) and metal oxide catalysts containing Mn, V, Cu, Co and Fe. Takagaki et al. reported a 92% yield of DFF via aerobic oxidation of HMF in DMF over a Ru/hydrotalcite catalyst.[94] Nie et al. obtained a 96% selectivity of DFF in toluene using Ru/C under an oxygen pressure of 2 MPa.[95]

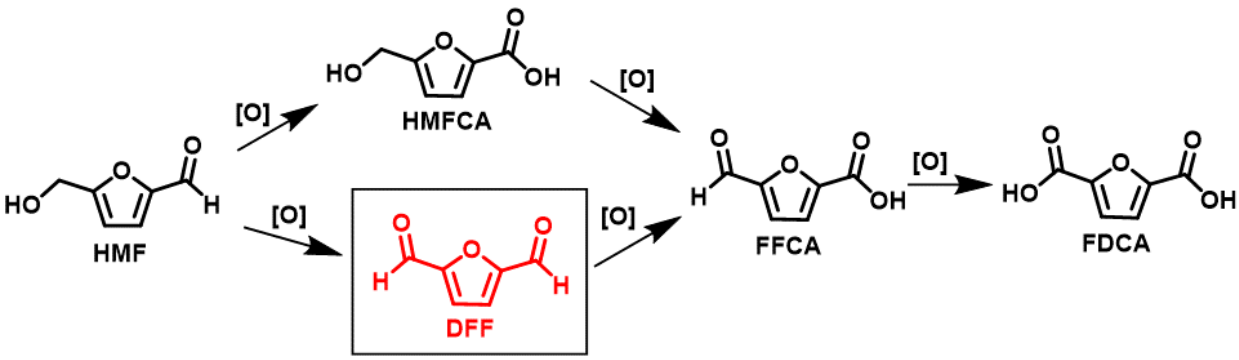

Scheme 1.8. Reaction pathways for oxidative transformation of HMF to FDCA.

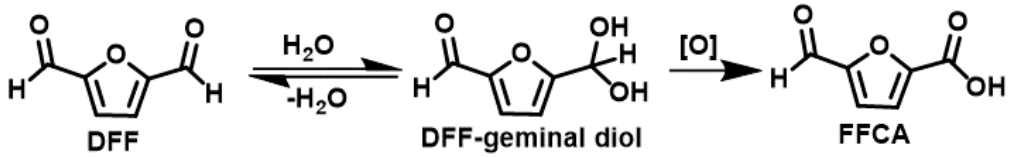

Scheme 1.9. Reaction mechanism for the conversion of DFF to FFCA.

The dehydrogenation of HMF (an oxidant free methodology) could be an alternative approach to produce DFF,[96–100] but efficient synthetic procedures have not yet been developed. Chatterjee et al. reported the dehydrogenation of HMF to DFF over activated carbon-supported rhodium catalyst (Rh/C) using compressed carbon dioxide media ($scCO_2$).[96] In the absence of CO_2, the conversion of HMF was very poor resulting in unknown byproducts. While $scCO_2$ facilitates the reaction due to the shift of the equilibrium

to the product,[96] a high CO_2 (8 MPa) pressure was required for efficient DFF formation, which significantly reduced the sustainability of the process.

1.6 Protection strategies for the selective conversion of biomass-derived C6-furanics to desirable building blocks.

The intrinsic reactive nature of furanics requires milder operation conditions in the chemocatalytic valorization processes to avoid undesirable byproducts formation such as humins. Significant efforts have been made to develop catalytic systems and optimize process conditions to minimize such byproducts, but still practical implementation of furanics as a feedstock on an industrial scale remains restricted.[101] All previous processes focused on the use of dilute substrate solutions to mitigate humin formation and obtained excellent product yields (90-95%) with extremely low space-time productivity. However, the use of large amount of solvents and a huge-sized reactor remains serious challenges for their large-scale production (**Table 1.1 and Table 1.2**).[1–100]

Protection/deprotection strategies are an efficient way to passivate the reactive groups in biomass-derived furanic aldehydes and realize sustainable production of desired chemicals with minimizing side-reactions.[101–106] Such chemical modification approaches are well known in multistep organic synthesis for the manufacture of pharmaceuticals.[101] However, there are very few applications in the valorization of biomass-derived furanics.[101] The major disadvantage of protection strategies is that it decreases the atom efficiency of the process, which affects the process costs and elevates the environmental burden.[101] Process transformation could overcome such challenges via rendering the modified approach beneficial over the conventional method. [101] For example, the use of concentrated solutions in all reaction steps, together with low catalyst loading can make this approach economically feasible. [101] The applicable strategy relies mainly on the type of functionality in the furanic compounds, which are mostly carbonyl, hydroxyl and carboxyl moiety.[101] Acetal protection strategies are frequently applied to protect the carbonyl functionality, while both hydroxyl group and carboxyl group are mainly esterified. [101] Acetalization is based on the conversion of reactive carbonyl group to acetal or ketal by the reaction with alcohol. [101] Reaction

efficiency and stability of the resulting acetal can be tuned by the choice of alcohol. Conventional mono-ols (e.g., methanol) yield acyclic acetals, while di-ols (e.g., ethylene glycol and propane-di-ol) afford cyclic acetals. [101] In general, acyclic acetals are less stable compared to cyclic acetals due to the entropically favored hydrolysis of acyclic acetals.[101] Our group applied a protection strategy based on acetalization of -CHO in HMF with 1,3-propanediol (PD) to the efficient production of FDCA and MFDC using Au/CeO_2 catalyst as shown in **Figure 1.3**.[102–104] FDCA and MFDC could be obtained in high yields (> 90%) using concentrated solutions (10–20 wt%) of HMF-acetal (PD-HMF) under optimized reaction conditions. The six-membered cyclic acetal ring in PD-HMF suppresses by-product formation in concentrated solutions, while the non-protected HMF under the same reaction conditions produced mostly humin-type byproducts. In the oxidative esterification of PD-HMF to MFDC, a catalytic amount of water added to the reaction mixture acts as a key role in efficiently converting the six-membered ring acetal to methyl carboxylate, which is the rate determining step.[103] DFT calculations revealed that corresponding hemiacetal formed with Lewis acid site of CeO_2 support is oxidatively dehydrogenated with molecular oxygen on Au nanoparticle, and the resulting alkyl carboxylate with protecting 1,3-propanediol undergoes *trans*-esterification with the solvent (methanol) to afford MFDC.[103] The addition of small amount of water accelerates the formation of hemiacetal species. Our group also found that the presence of cyclic acetal increases the oxidation rate of -CH_2OH bonded to the same furan ring, presumably due to the electron-donating effect of the acetal group on the furan ring.[102-104] Such an acetal protection strategy is also highly beneficial in the hydrogenation reactions of HMF.[106] The selective hydrogenation of HMF affords two valuable monomers of polyesters, such as bis(hydroxymethyl)furan (BHMF) and bis(hydroxymethyl)tetrahydrofuran (BHMTHF). The protecting groups are highly stable under reducing atmosphere.[101,106] Thus, careful control of the deprotection rate in concentrated solutions was proved to be vital in obtaining BHMF in high yields.[101,106] A too fast deprotection rate resulted in the increase in HMF concentration leading to humin formation, while a slow rate causes the formation of ring hydrogenated product (BHMTHF).[101,106] BHMF was obtained in high yield under optimal the protection-

deprotection rate, which can be realized by tuning the pH of the reaction mixture carefully.[101,106] The acetalization agent was recovered in high yield (> 90%) in all studies, making these reactions attractive for large-scale applications. Such protection strategies can be explored for the selective conversion of other biomass-derived furanics to produce several valuable chemicals.[102–106]

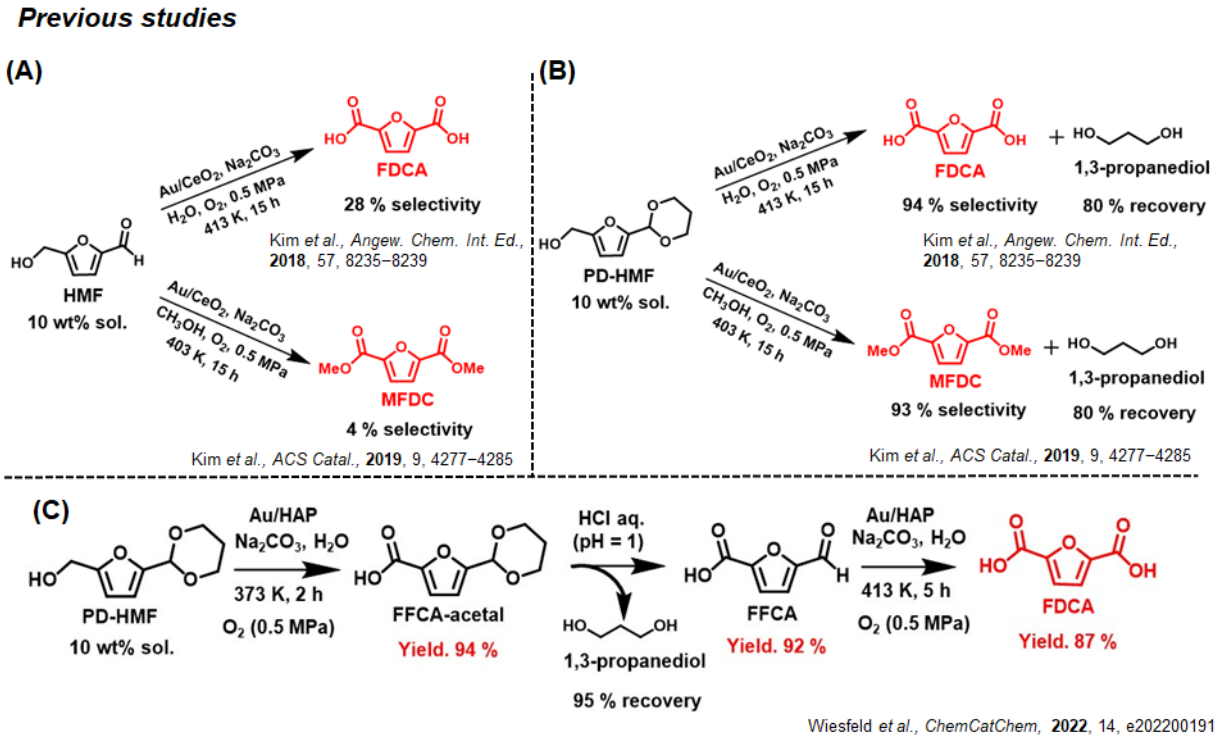

Figure 1.3. Reaction pathways for direct oxidation and oxidative esterification of (A) HMF and (B) PD-HMF to FDCA and MFDC respectively; stepwise approach for (C) oxidation of PD-HMF to FDCA.

1.7 Scope of the thesis

This thesis deals with the transformation of biomass-derived C6-furanics using concentrated solutions (10–20 wt%) to produce possible building blocks of bio-based polymers aiming at developing a sustainable society. The highly reactive formyl groups in biomass-derived furanics cause severe and complex side reactions, which are predominant in concentrated solutions.[102–106] Our group has already demonstrated that protection of the

reactive formyl group of HMF as its acetal with 1,3-propanediol (PD) enabled the use of concentrated solutions (10–20 wt%) in various redox reactions and ensured high productivity of the intended products (**Figure 1.3**).[101–106] Therefore, my aim is to further develop the current reaction systems along with the acetal protection strategy for the synthesis of valuable chemicals to mitigate our dependency on limited fossil-based feedstocks.

In Chapter 2, I reported an efficient process for the stepwise synthesis of MFDC from a concentrated HMF-acetal solution with ceria-supported Au catalyst (Au/CeO_2). Earlier reported processes were limited to the use of dilute HMF solution to produce MFDC, which significantly lowered the productivity.[26–46] I utilized dimethylacetal form of HMF as a substrate in the oxidative esterification with Au/CeO_2 catalyst and designed a new stepwise reaction system using concentrated solutions (10-20 wt%) with largely reducing Na_2CO_3 loading.

In Chapter 3, an acetal protection strategy was explored for the synthesis of 2,5-bis(aminomethyl)furan (BAMF) by reductive amination of biomass-derived acetal-protected 2,5-diformylfuran (DFF) using Co_2P nanorods (NRs) catalyst. A six-membered ring acetal of mono-acetalized DFF retained intact during the reaction, while a bare formyl group was converted to a primary amine group in the presence of NH_3 and Co_2P NRs, affording an acetal form of 5-aminomethyl-2-formylfuran (AMF-acetal). *In-situ* deprotection and subsequent reductive amination of AMF-acetal with NH_3 and Co_2P NRs produced BAMF.

In Chapter 4, I reported the reductive amination of MFFC to synthesize methyl 5-aminomethylfuran-2-carboxylate (MAMFC) with Co_2P NRs. MFFC is a versatile platform molecule and can be obtained in both high yield and purity by oxidative esterification of HMF-dimethylacetal and subsequent deprotection as reported in Chapter 2. Herein, I extended the application of Co_2P NRs to synthesize MAMFC via reductive amination of MFFC and its activity was comprehensively compared with those of other representative catalysts. Finally, I summarized my works and discussed the future scope in Chapter 5.

1.8 References

[1] M. A. Hillmyer, *Science* **2017**, 358, 868−870.

[2] Y. Zhu, C. Romain, C. K. Williams, *Nature* **2016**, 540, 354364.

[3] M. Jin, L. Yu, H. Chen, X. Ma, K. Cui, Z. Wen, Z. Ma, Y. Sang, M. Chen, Y. Li, Catal. Today **2021**, *367*, 2–8.

[4] A. F. Sousa, C. Vilela, A. C. Fonseca, M. Matos, C. S. R. Freire, G.-J. M. Gruter, J. F. J. Coelho, A. J. D. Silvestre, *Polym. Chem.* **2015**, 6, 5961−5983.

[5] A. J. J. E. Eerhart, A. P. C. Faaij, M. K. Patel, *Energy Environ. Sci.* **2012**, *5*, 6407.

[6] S. K. Burgess, J. E. Leisen, B. E. Kraftschik, C. R. Mubarak, R. M. Kriegel, W. J. Koros, *Macromolecules* **2014**, *47*, 1383–1391.

[7] Z. Guo, Y. Chen, N. L. Lu, *Multifunctional Nanocomposites for Energy and Environmental Applications*, Wiley, **2018**.

[8] C. Zhao, J. He, A. A. Lemonidou, X. Li, J. A. Lercher, *J. Catal.* **2011**, *280*, 8–16.

[9] X. Li, P. Jia, T. Wang, *ACS Catal.* **2016**, *6*, 7621–7640.

[10] R.-J. Van Putten, J. C. Van Der Waal, E. De Jong, C. B. Rasrendra, H. J. Heeres, J. G. De Vries, *Chem. Rev.* **2013**, *113*, 1499–1597.

[11] A. Herbst, C. Janiak, *CrystEngComm* **2017**, *19*, 4092–4117.

[12] D. Esposito, M. Antonietti, *Chem. Soc. Rev.* **2015**, *44*, 5821–5835.

[13] L. Hu, G. Zhao, W. Hao, X. Tang, Y. Sun, L. Lin, S. Liu, *RSC Adv.* **2012**, *2*, 11184.

[14] O. Casanova, S. Iborra, A. Corma, *ChemSusChem* **2009**, *2*, 1138–1144.

[15] S. Xu, P. Zhou, Z. Zhang, C. Yang, B. Zhang, K. Deng, S. Bottle, H. Zhu, *J. Am. Chem. Soc.* **2017**, *139*, 14775–14782.

[16] Z. Zhang, K. Deng, *ACS Catal.* **2015**, *5*, 6529–6544.

[17] Y. Takeda, M. Tamura, Y. Nakagawa, K. Okumura, K. Tomishige, *Catal. Sci. Technol.* **2016**, *6*, 5668–5683.

[18] M. Tamura, K. Tokonami, Y. Nakagawa, K. Tomishige, *Chem. Commun.* **2013**, *49*, 7034.

[19] T. Buntara, S. Noel, P. H. Phua, I. Melián-Cabrera, J. G. de Vries, H. J. Heeres, *Angew. Chem. Int. Ed.* **2011**, *50*, 7083–7087.

[20] X. Kong, R. Zheng, Y. Zhu, G. Ding, Y. Zhu, Y.-W. Li, *Green Chem.* **2015**, *17*, 2504–2514.

[21] S. Yao, X. Wang, Y. Jiang, F. Wu, X. Chen, X. Mu, *ACS Sustain. Chem. Eng.* **2014**, *2*, 173–180.

[22] T. Buntara, I. Melián-Cabrera, Q. Tan, J. L. G. Fierro, M. Neurock, J. G. De Vries, H. J. Heeres, *Catal. Today* **2013**, *210*, 106–116.

[23] A. T. Hoang, S. Nižetić, A. I. Ölçer, *Fuel* **2021**, *285*, 119140.

[24] N.-T. Le, A. Byun, Y. Han, K.-I. Lee, H. Kim, *Green Sustain. Chem.* **2015**, *05*, 115–127.

[25] Z. Wei, Y. Cheng, H. Huang, Z. Ma, K. Zhou, Y. Liu, *ChemSusChem* **2022**, *15*, e202200233.

[26] J. Deng, H.-J. Song, M.-S. Cui, Y.-P. Du, Y. Fu, *ChemSusChem* **2014**, *7*, 3334–3340.

[27] N. K. Gupta, S. Nishimura, A. Takagaki, K. Ebitani, *Green Chem.* **2011**, *13*, 824.

[28] Y. Sun, H. Ma, X. Jia, J. Ma, Y. Luo, J. Gao, J. Xu, *ChemCatChem* **2016**, *8*, 2907–2911.

[29] T. Pasini, M. Piccinini, M. Blosi, R. Bonelli, S. Albonetti, N. Dimitratos, J. A. Lopez-Sanchez, M. Sankar, Q. He, C. J. Kiely, G. J. Hutchings, F. Cavani, *Green Chem.* **2011**, *13*, 2091.

[30] M. A. Lilga, R. T. Hallen, M. Gray, *Top. Catal.* **2010**, *53*, 1264–1269.

[31] D. Zhao, T. Su, C. Len, R. Luque, Z. Yang, Green Chem. **2022**, *24*, 6782–6789.

[32] A. Abad, P. Concepción, A. Corma, H. García, Angew. Chem. Int. Ed. **2005**, *44*, 4066–4069.

[33] O. Casanova, S. Iborra, A. Corma, J. Catal. **2009**, *265*, 109–116.

[34] E. Taarning, I. S. Nielsen, K. Egeblad, R. Madsen, C. H. Christensen, ChemSusChem **2008**, *1*, 75–78.

[35] A. Cho, S. Byun, J. H. Cho, B. M. Kim, *ChemSusChem* **2019**, *12*, 2310–2317.

[36] F. Li, X.-L. Li, C. Li, J. Shi, Y. Fu, Green Chem. **2018**, *20*, 3050–3058.

[37] J. Du, H. Fang, H. Qu, J. Zhang, X. Duan, Y. Yuan, Appl. Catal. Gen. **2018**, *567*, 80–89.

[38] F. Menegazzo, M. Signoretto, D. Marchese, F. Pinna, M. Manzoli, J. Catal. **2015**, *326*, 1–8.

[39] A. Salazar, P. Hünemörder, J. Rabeah, A. Quade, R. V. Jagadeesh, E. Mejia, ACS Sustain. Chem. Eng. **2019**, acssuschemeng.9b00914.

[40] M. Jin, L. Yu, H. Chen, X. Ma, K. Cui, Z. Wen, Z. Ma, Y. Sang, M. Chen, Y. Li, Catal. Today **2021**, *367*, 2–8.

[41] H. Liu, W. Jia, X. Yu, X. Tang, X. Zeng, Y. Sun, T. Lei, H. Fang, T. Li, L. Lin, *ACS Catal.* **2021**, *11*, 7828–7844.

[42] H. Su, K.-X. Zhang, B. Zhang, H.-H. Wang, Q.-Y. Yu, X.-H. Li, M. Antonietti, J.-S. Chen, *J. Am. Chem. Soc.* **2017**, *139*, 811–818.

[43] S. Xu, P. Zhou, Z. Zhang, C. Yang, B. Zhang, K. Deng, S. Bottle, H. Zhu, *J. Am. Chem. Soc.* **2017**, *139*, 14775–14782.

[44] Q. Zhu, F. Wang, F. Zhang, Z. Dong, *Nanoscale* **2019**, *11*, 17736–17745.

[45] W. Zhong, H. Liu, C. Bai, S. Liao, Y. Li, *ACS Catal.* **2015**, *5*, 1850–1856.

[46] Y. Lu, Z. Zhang, H. Wang, Y. Wang, *Appl. Catal. B Environ.* **2021**, *292*, 120162.

[47] Y. Sun, H. Ma, X. Jia, J. Ma, Y. Luo, J. Gao, J. Xu, *ChemCatChem* **2016**, *8*, 2907–2911.

[48] Y. Feng, W. Jia, G. Yan, X. Zeng, J. Sperry, B. Xu, Y. Sun, X. Tang, T. Lei, L. Lin, *J. Catal.* **2020**, *381*, 570–578.

[49] A. E. Demet, O. Gimello, R. Arletti, N. Tanchoux, M. T. Sougrati, L. Stievano, F. Quignard, G. Centi, S. Perathoner, F. Di Renzo, *Catalysts* **2022**, *12*, 814.

[50] J. M. García, F. C. García, F. Serna, J. L. De La Peña, *Prog. Polym. Sci.* **2010**, *35*, 623–686.

[51] J. Reglero Ruiz, M. Trigo-López, F. García, J. García, *Polymers* **2017**, *9*, 414.

[52] H. Zeng, Z. Guan, *J. Am. Chem. Soc.* **2011**, *133*, 1159–1161.

[53] A. Kumar, D. Armstrong, G. Peters, M. Nagala, S. Shirran, *Chem. Commun.* **2021**, *57*, 6153–6156.

[54] D. Pingen, J. B. Schwaderer, J. Walter, J. Wen, G. Murray, D. Vogt, S. Mecking, *ChemCatChem* **2018**, *10*, 3027–3033.

[55] J. He, L. Chen, S. Liu, K. Song, S. Yang, A. Riisager, *Green Chem.* **2020**, *22*, 6714–6747.

[56] L. Bini, C. Müller, J. Wilting, L. Von Chrzanowski, A. L. Spek, D. Vogt, *J. Am. Chem. Soc.* **2007**, *129*, 12622–12623.

[57] M. Niwa, *J. Catal.* **1981**, *70*, 1–13.

[58] I. Delidovich, P. J. C. Hausoul, L. Deng, R. Pfützenreuter, M. Rose, R. Palkovits, *Chem. Rev.* **2016**, *116*, 1540–1599.

[59] K. Zhou, R. Xie, M. Xiao, D. Guo, Z. Cai, S. Kang, Y. Xu, J. Wei, *ChemCatChem* **2021**, *13*, 2074–2085.

[60] Y. Kita, M. Kuwabara, S. Yamadera, K. Kamata, M. Hara, *Chem. Sci.* **2020**, *11*, 9884–9890.

[61] H. Yuan, B. T. Kusema, Z. Yan, S. Streiff, F. Shi, *RSC Adv.* **2019**, *9*, 38877–38881.

[62] Yogita, K. T. V. Rao, P. M. Kumar, N. Lingaiah, *Sustain. Energy Fuels* **2022**, *6*, 4692–4705.

[63] M. Chatterjee, T. Ishizaka, H. Kawanami, *Green Chem.* **2016**, *18*, 487–496.

[64] H. Yuan, J.-P. Li, F. Su, Z. Yan, B. T. Kusema, S. Streiff, Y. Huang, M. Pera-Titus, F. Shi, *ACS Omega* **2019**, *4*, 2510–2516.

[65] G. Hahn, P. Kunnas, N. De Jonge, R. Kempe, *Nat. Catal.* **2018**, *2*, 71–77.

[66] Y. Zhang, H. Yang, Q. Chi, Z. Zhang, *ChemSusChem* **2019**, *12*, 1246–1255.

[67] C. C. Truong, D. K. Mishra, Y. Suh, *ChemSusChem* **2023**, *16*, e202201846.

[68] T. Komanoya, T. Kinemura, Y. Kita, K. Kamata, M. Hara, *J. Am. Chem. Soc.* **2017**, *139*, 11493–11499.

[69] T. A. Gokhale, A. B. Raut, B. M. Bhanage, *Mol. Catal.* **2021**, *510*, 111667.

[70] K. Zhou, R. Xie, M. Xiao, D. Guo, Z. Cai, S. Kang, Y. Xu, J. Wei, *ChemCatChem* **2021**, *13*, 2074–2085.

[71] Y. Xu, X. Jia, J. Ma, J. Gao, F. Xia, X. Li, J. Xu, *Green Chem.* **2018**, *20*, 2697–2701.

[72] Z.-Z. Yang, J. Deng, T. Pan, Q.-X. Guo, Y. Fu, *Green Chem.* **2012**, *14*, 2986.

[73] R. Fang, R. Luque, Y. Li, *Green Chem.* **2017**, *19*, 647–655.

[74] H. Qi, F. Liu, L. Zhang, L. Li, Y. Su, J. Yang, R. Hao, A. Wang, T. Zhang, *Green Chem.* **2020**, *22*, 6897–6901.

[75] C. P. Woroch, A. W. Lankenau, M. W. Kanan, *Macromolecules* **2021**, *54*, 9978–9983.

[76] A. W. Lankenau, M. W. Kanan, *Chem. Sci.* **2020**, *11*, 248–252.

[77] H. Singh, K. Arora, S. Tapadar, T. K. Chakraborty, *J. Theor. Comput. Chem.* **2004**, *03*, 555–566.

[78] T. K. Chakraborty, A. Arora, S. Roy, N. Kumar, S. Maiti, *J. Med. Chem.* **2007**, *50*, 5539–5542.

[79] S. Carenco, D. Portehault, C. Boissière, N. Mézailles, C. Sanchez, *Chem. Rev.* **2013**, *113*, 7981–8065.

[80] Y. Shi, B. Zhang, *Chem. Soc. Rev.* **2016**, *45*, 1529–1541.

[81] Y. Wang, B. Kong, D. Zhao, H. Wang, C. Selomulya, *Nano Today* **2017**, *15*, 26–55.

[82] T. Liu, D. Liu, F. Qu, D. Wang, L. Zhang, R. Ge, S. Hao, Y. Ma, G. Du, A. M. Asiri, L. Chen, X. Sun, *Adv. Energy Mater.* **2017**, *7*, 1700020.

[83] A. Sumboja, T. An, H. Y. Goh, M. Lübke, D. P. Howard, Y. Xu, A. D. Handoko, Y. Zong, Z. Liu, *ACS Appl. Mater. Interfaces* **2018**, *10*, 15673–15680.

[84] H. Zhang, D.-H. Ha, R. Hovden, L. F. Kourkoutis, R. D. Robinson, *Nano Lett.* **2011**, *11*, 188–197.

[85] M. Sheng, S. Fujita, S. Yamaguchi, J. Yamasaki, K. Nakajima, S. Yamazoe, T. Mizugaki, T. Mitsudome, *JACS Au* **2021**, *1*, 501–507.

[86] H. Ishikawa, M. Sheng, A. Nakata, K. Nakajima, S. Yamazoe, J. Yamasaki, S. Yamaguchi, T. Mizugaki, T. Mitsudome, *ACS Catal.* **2021**, *11*, 750–757

[87] M. Sheng, S. Yamaguchi, A. Nakata, S. Yamazoe, K. Nakajima, J. Yamasaki, T. Mizugaki, T. Mitsudome, *ACS Sustain. Chem. Eng.* **2021**, *9*, 11238–11246.

[88] P. Liu, J. A. Rodriguez, *J. Am. Chem. Soc.* **2005**, *127*, 14871–14878.

[89] R. Gao, L. Pan, H. Wang, X. Zhang, L. Wang, J.-J. Zou, *ACS Catal.* **2018**, *8*, 8420–8429.

[90] S. Yamaguchi, S. Fujita, K. Nakajima, S. Yamazoe, J. Yamasaki, T. Mizugaki, T. Mitsudome, *ACS Sustain. Chem. Eng.* **2021**, *9*, 6347–6354.

[91] S. Yamaguchi, S. Fujita, K. Nakajima, S. Yamazoe, J. Yamasaki, T. Mizugaki, T. Mitsudome, *Green Chem.* **2021**, *23*, 2010–2016.

[92] C. P. Woroch, A. W. Lankenau, M. W. Kanan, *Macromolecules* **2021**, *54*, 9978–9983.

[93] W. Liang, R. Zhu, X. Li, J. Deng, Y. Fu, *Green Chem.* **2021**, *23*, 6604–6613.

[94] A. Takagaki, M. Takahashi, S. Nishimura, K. Ebitani, *ACS Catal.* **2011**, *1*, 1562–1565.

[95] J. Nie, J. Xie, H. Liu, *J. Catal.* **2013**, *301*, 83–91.

[96] M. Chatterjee, T. Ishizaka, A. Chatterjee, H. Kawanami, *Green Chem.* **2017**, *19*, 1315–1326.

[97] T. Mitsudome, Y. Mikami, H. Funai, T. Mizugaki, K. Jitsukawa, K. Kaneda, *Angew. Chem. Int. Ed.* **2008**, *47*, 138–141.

[98] T. Mitsudome, Y. Mikami, K. Ebata, T. Mizugaki, K. Jitsukawa, K. Kaneda, *Chem. Commun.* **2008**, 4804.

[99] D. Huang, H. Wang, Y. Wu, *Molecules* **2022**, *27*, 8537.

[100] J. Dai, *Green Energy Environ.* **2021**, *6*, 22–32.

[101] F. J. A. G. Coumans, Z. Overchenko, J. J. Wiesfeld, N. Kosinov, K. Nakajima, E. J. M. Hensen, *ACS Sustain. Chem. Eng.* **2022**, *10*, 3116–3130.

[102] M. Kim, Y. Su, A. Fukuoka, E. J. M. Hensen, K. Nakajima, *Angew. Chem. Int. Ed.* **2018**, *57*, 8235–8239.

[103] M. Kim, Y. Su, T. Aoshima, A. Fukuoka, E. J. M. Hensen, K. Nakajima, *ACS Catal.* **2019**, *9*, 4277–4285.

[104] J. J. Wiesfeld, M. Asakawa, T. Aoshima, A. Fukuoka, E. J. M. Hensen, K. Nakajima, *ChemCatChem* **2022**, *14*, e202200191.

[105] T. Boonyakarn, J. J. Wiesfeld, M. Asakawa, L. Chen, A. Fukuoka, E. J. M. Hensen, K. Nakajima, *ChemSusChem* **2022**, *15*, e202200059.

[106] J. J. Wiesfeld, M. Kim, K. Nakajima, E. J. M. Hensen, *Green Chem.* **2020**, *22*, 1229–1238.

Chapter 2

A Protection Strategy for High-yield Synthesis of Dimethyl Furan-2,5-dicarboxylate from 5-Hydroxymethylfurfural Using Methanol as an Acetalizing Agent

Abstract

Developing efficient catalytic processes for obtaining biobased monomers for plastics can significantly contribute to a more sustainable economy. The biomass-derived and chemical platform 5-hydroxymethylfurfural (HMF) can be converted to various key intermediates, which is often hampered by side reactions due to the reactive nature of the formyl group in HMF. Here, a stepwise approach is demonstrated involving a protecting agent to obtain dimethyl furan-2,5-dicarboxylate (MFDC), which is a monomer for polyalkylene furanoates, a new class of biobased polyesters. Methanol is used as a solvent, reactant, and protecting agent for HMF's formyl group. In the first step, the oxidative esterification of the hydroxymethyl group to methyl carboxylate in HMF-dimethylacetal catalyzed by Au/CeO_2 affords methyl 5-formylfuran-2-carboxylate dimethylacetal (MFFC-acetal) in high yields (> 90%) from concentrated methanolic solutions (~ 20 wt%). Without protecting agent, a mixture of methyl-5-hydroxymethylfuran-2-carboxylate (MHMFC), MFDC, and humin by-product was obtained. The deprotection of MFFC-acetal in the second step proceeded efficiently in acetone with Amberlyst-15, affording MFFC in a >90% yield. In the final step, oxidative esterification of MFFC in methanol (10 wt%) afforded MFDC in a 93% yield using Au/CeO_2. The acetal protection strategy with methanol offers an efficient route toward MFDC in two oxidative esterification steps.

2.1 Introduction

In the last decades, the energy crisis and environmental pollution, which has been linked to large-scale rapid consumption of fossil fuel resources, have become a substantial concern. The substitution of petroleum-based commodities with biomass-derived alternatives is essential in the transition to a more sustainable future.[1,2] Manufacturing commodity chemicals from renewable and preferably non-edible biomass can contribute substantially to lowering the pressure on the environment. 5-Hydroxymethylfurfural (HMF) is a biobased platform molecule, which can be obtained from biomass resources via the hydrolysis of cellulose, followed by glucose dehydration. HMF can be converted into many valuable compounds, such as building blocks for biobased polymers like 2,5-bis(hydroxymethyl)furan, 2,5-furandicarboxylic acid (FDCA), dimethyl furan-2,5-dicarboxylate (MFDC) and 2,5-bis(aminomethyl)furan.[3–5] FDCA, which can be made by aerobic oxidation of HMF, has received most attention. The co-polymerization of FDCA with ethylene glycol yields the biobased poly(ethylene furanoate) polyester (PEF) (**Scheme 1.3**). Its superiority in terms of gas permeability and tensile strength makes PEF a suitable replacement for petroleum-derived poly(ethylene) terephthalate (PET, global annual production > 50 MT).[3–5] Despite the potential of HMF as a platform for the chemical industry, practical routes to FDCA and its ester derivatives have not been well established so far. This is largely due to the highly reactive formyl group (-CHO) in HMF, which results in complex polymerization and condensation reactions that lead to humins. By-product formation can be lowered by using dilute solutions, which is, however, hampering scale-up. For instance, even from reported dilute solutions of HMF (0.5–4 wt%), the oxidative esterification results in low MFDC yields and high energy cost for solvent recycling (**Table 1.1**).[6–27]

Protection of the highly reactive formyl group as its acetal with 1,3-propanediol (PD) suppresses such undesirable side reactions and allows the use of concentrated HMF solutions (10-20 wt%) for various hydrogenation and oxidation reactions.[28–33] Earlier, the potential of acetalized HMF with PD (PD-HMF) as a reactant in the one-pot oxidation and oxidative esterification with Au/CeO_2 and two equivalents of Na_2CO_3 to synthesize FDCA (> 90%) and MFDC (> 90%), respectively, using concentrated PD-HMF solutions (>10 wt%) have

been established as shown in **Figure 1.3**.[30,31] A large amount of base (200 mol% to the substrate) is required to stabilize the acetals, even in the presence of water and at high reaction temperatures (130–140 ºC), against the non-catalytic degradation of HMF in concentrated solutions.[30,31] However, the conversion of the acetal moiety in PD-HMF to carboxylic acid and methyl carboxylate groups upon oxidation or oxidative esterification, respectively, is accompanied by the release of PD in the reaction mixture. The free PD is then subject to oxidative degradation during the prolonged reactions at high temperature, limiting the PD recovery to ca. 80%.

To cope with this, later, a stepwise approach was developed using concentrated PD-HMF solutions (10–20 wt%) to ensure high FDCA productivity and PD recovery (**Figure 1.3C**).[32] The hydroxymethyl moiety in PD-HMF was oxidized to the carboxylic acid with a hydroxyapatite-supported Au catalyst (Au/HAP), producing a six-membered ring acetal form of 5-formylfuran-2-carboxylic acid (FFCA-acetal) as a key intermediate. The deprotection of the FFCA-acetal in the presence of a mineral acid, such as HCl, recovers PD and FFCA from the reaction mixture of the first oxidation step. The crude FFCA (10–20 wt%) can be selectively oxidized with Au/HAP to obtain FDCA in high yields (> 95%). The stepwise approach satisfied a high FDCA productivity and an excellent PD recovery (95%). Still, two equivalents of Na_2CO_3 base were essential in each oxidation step for stabilizing the acetal group of PD-HMF against side reactions and dissolving two products (FFCA and FDCA) in water through neutralization of carboxylic acid.[32] The latter aspect is important for designing efficient oxidation reactions, because the deposition of poorly soluble products, i.e. FFCA and FDCA in their acid form, on the catalyst surface can substantially lower the catalyst activity.

In the present study, such a stepwise approach is employed to the oxidative esterification of HMF-acetal in methanol. The benefit is that the reaction product, dimethyl furan-2,5-dicarboxylate (MFDC), can be dissolved in methanol without a base such as NaOH and Na_2CO_3 (**Scheme 2.1**). The one-pot oxidative esterification of PD-HMF reported in our previous work (**Figure 1.3B**)[31] required a high temperature, a long reaction time, and an excess amount of Na_2CO_3 (two equivalents to the substrate) to convert the highly stable six-

membered acetal ring to the methyl carboxylate. Such severe reaction conditions caused oxidative degradation of the released PD protecting agent. Among different acetals that can be used to protect the formyl group, only the six-membered ring acetal in PD-HMF could suppress extensive humin formation. On the other hand, the stepwise approach in **Figure 1.3C** do not require such harsh reaction conditions, as the oxidative transformation of the acetal moiety to the methyl carboxylate, together with the release of the protecting agent was elimimated, thus both extending the scope of acetal and preventing oxidative degradation of the protecting reagent. I used methanol as protecting agent and solvent, allowing to reduce the amount of Na_2CO_3 in each elementary step during oxidative esterification of the HMF-dimethylacetal (hereafter simply referred to as "HMF-acetal"). The proposed route consists of three independent steps (**Scheme 2.1**), (i) oxidative esterification of hydroxymethyl in HMF-acetal to methyl carboxylate with retaining dimethylacetal moiety, producing dimethylacetal form of methyl 5-formylfuran-2-carboxylate (MFFC-acetal), (ii) deprotection of acetal functional group in MFFC-acetal, and (iii) the oxidative esterification of formyl group in non-protected MFFC to obtain MFDC. This approach eliminates the need to isolate the methanol protecting reagent and its recycling after the second deprotection step, which reduces the energy consumption. Control experiments with non-protected HMF clarified the impact of the dimethylacetal functionality on side reactions during the first oxidative esterification step.

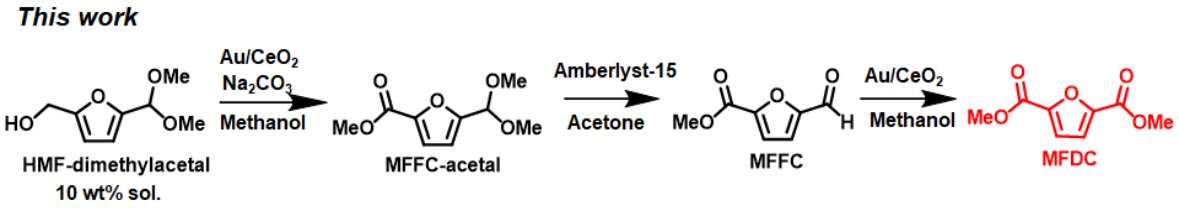

Scheme 2.1. Reaction pathway for stepwise oxidative esterification of HMF-acetal to MFDC.

2.2 Experimental section

2.2.1 Materials

HMF, 5-acetoxymethyl-2-furfuraldehyde, gold(III) chloride tetrahydrate ($HAuCl_4.4H_2O$), and indium trifluoromethanesulfonate ($In(OTf)_3$ were purchased from Sigma-Aldrich. Methyl-5-formyl-2-furancarboxylate (MFFC) was purchased from Angene chemicals. CeO_2 (JRC-CEO-1) was supplied from the Catalyst Society of Japan. Methanol super dehydrated, ethanol super dehydrated, acetone, *N,N*-dimethylformamide super dehydrated (DMF) and activated alumina were obtained from FUJIFILM Wako Pure Chemical Corporation. Trimethyl orthoformate (TMOF) and chlorobenzene were purchased from Tokyo Chemical Industry (TCI). Anhydrous NaOH, Na_2CO_3, dichloromethane, and ethyl acetate were obtained from Kanto chemical corporation. Amberlyst-15 was purchased from Acros Organics.

2.2.2 Catalyst preparation

Au/CeO_2 was synthesized by the deposition-precipitation method.[9,31] To an aqueous solution (160 mL) of $HAuCl_4.4H_2O$ (350 mg, 0.8 mmol), NaOH solution (0.2 M) was added dropwise while maintaining the pH of the resulting solution at 9.7. The solution was mixed with CeO_2 (4 g) suspended in 50 mL deionized water, followed by the addition of an aqueous NaOH to readjust the pH to 9.7. After stirring the mixture at room temperature for 18 h, a yellow solid obtained was repeatedly washed with deionized water until Cl- ions were completely removed, which was confirmed by a precipitation test using an aqueous $AgNO_3$ solution. Finally, the solid was dried at 70 °C overnight and used as an oxidation catalyst.

2.2.3 Characterization

Energy dispersive X-ray (EDX) measurements were performed to determine the chemical composition of the catalyst using an EDX spectrometer (EDX-720, Shimadzu). UV-Vis diffuse reflectance spectroscopy (UV-vis DRS) was carried out using Jasco V-650 spectrophotometer. Powder X-ray diffraction (P-XRD) measurements were performed by an

Ultima IV, Rigaku diffractometer at 40 kV and 40 mA using Cu Kα radiation (λ = 1.5418 Å) in $2\theta = 20-80°$.

2.2.4 Synthesis of (5-(dimethoxymethyl)furan-2-yl)methanol (HMF-acetal)

Typically, 5-acetoxymethyl-2-furfuraldehyde (4.2 g, 25 mmol) was dissolved in dichloromethane (180 mL). Trimethyl orthoformate (6 mL, 55 mmol), methanol (5.5 mL, 137 mmol), and Indium trifluoromethanesulfonate ($In(OTf)_3$, 0.075 g, 0.5 mol% to the substrate) were added stepwise into the solution. The reaction mixture was stirred at room temperature overnight and purged over alumina to remove excess $In(OTf)_3$. All organic volatiles were removed under reduced pressure and the crude product was dried overnight in a high vacuum. A yellowish liquid intermediate, which was obtained after vacuum evaporation, was dissolved in the mixture of ethanol (50 mL) and an aqueous Na_2CO_3 solution (1 M, 150 mL) and then stirred for 4 h at room temperature. The product was extracted with ethyl acetate (20 mL) three times and dried by a high vacuum treatment. The yield and purity of the resulting HMF-acetal were determined as 85% and > 95%, respectively, by a ^1H nuclear magnetic resonance (NMR) spectrometer (JNM-ECZ600, JEOL).

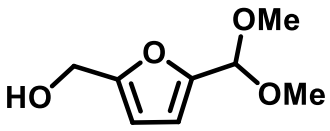

5-(dimethoxymethyl)furan-2-yl)methanol (HMF-acetal): ^1H NMR (400 MHz, $CDCl_3$) 6.39 (s, 1H), 6.27 (s, 1H), 5.4 (s, 1H), 4.6 (s, 2H), 3.35 (s, 6H) ppm; ^{13}C NMR (100 MHz, $CDCl_3$) 154.2, 150.8, 109.3, 108.3, 98.0, 57.6, 53.0 ppm.

2.2.5 Catalytic reaction

The oxidative esterification of HMF, HMF-acetal, and MFFC was conducted in Teflon-lined stainless steel autoclave reactors. The mixture of a methanolic substrate solution (100 mg, 10-20 wt%), Au/CeO_2 (100 mg), and Na_2CO_3 (1 mol% to the substrate) was stirred

at 373 K for 2 h under pressurized oxygen (0.9 MPa). The reaction mixtures were diluted with 50 mL ethyl acetate to dissolve all products, and analyzed by gas-chromatograph (GC, Shimadzu, GC-2025AF) with a flame ionization detector (FID) using chlorobenzene as an internal standard.

2.2.6 Deprotection of MFFC-acetal to MFFC

The deprotection of MFFC-acetal was performed by trans-acetalization with acetone and a solid Brønsted acid catalyst (Amberlyst-15).[39] After the first step, crude MFFC-acetal was isolated from the reaction mixture through an extraction procedure using EtOAc and subsequent evaporation. Crude MFFC-acetal (50 mg, approximately 0.25 mmol) was stirred with Amberlyst-15 (0.02 mmol, 8 mol% to the substrate) in acetone (5 mL) at 60 ºC for 1.5 h. After the reaction, the catalyst was separated by centrifugation from the reaction mixture. The reaction mixture was diluted with 50 mL ethyl acetate to dissolve all products and analyzed by GC-FID using chlorobenzene as an internal standard.

2.2.7 Reuse experiment of Au/CeO_2

The catalyst (Au/CeO_2) was recovered by centrifugation after the reaction and then washed with ethyl acetate, 0.1 M aqueous NaOH solution, and distilled water step-wisely three times to remove adsorbed species from the catalyst surface. The catalyst was dried at 70 °C overnight and used for the next run.

2.3 Results and Discussion

2.3.1 Characterization of catalysts

EDX measurements revealed that the Au loading in Au/CeO_2 was 5 wt%. The absorption band at 554 nm in the UV-Vis DRS spectrum for Au/CeO_2 evidences the formation of metallic Au nanoparticles (**Figure 2.1**).[37–38] No diffraction lines of metallic Au can be observed in its XRD pattern, implying that Au is present as small nanoparticles (**Figure 2.2**).[34–36] This is in line with the TEM analysis of Au/CeO_2 in a previous work, where the

average Au particle size was found to be 4 nm.[31] The UV-Vis DRS and XRD results are similar to previous works, emphasizing the presence of very small metallic Au nanoparticles (< 5 nm) on the CeO_2 support.

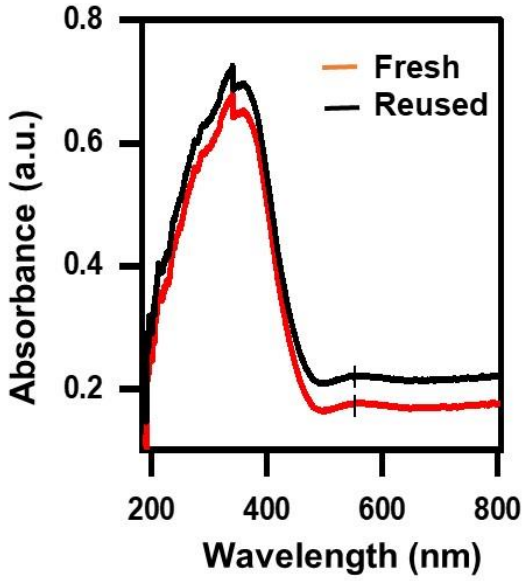

Figure 2.1. UV-Vis DRS spectra of fresh and used Au/CeO_2 catalysts.

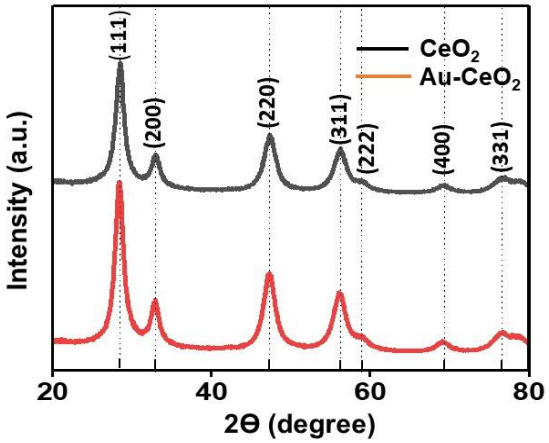

Figure 2.2. XRD patterns of (A) CeO_2 support and Au/CeO_2 catalyst.

2.3.2 Oxidative esterification of HMF-acetal and HMF (10 wt%) with Au/CeO_2

The catalytic activity of Au/CeO_2 in the oxidative esterification of HMF-acetal in methanol (10 wt%) was investigated at various temperatures, reaction times, and Na_2CO_3 contents (**Table 2.1**). The oxidative esterification of HMF-acetal in methanol produces the MFFC-acetal as the main reaction product, which is formed through the oxidation of the -CH_2OH group to -CHO, followed by hemiacetal formation with methanol and its oxidative dehydrogenation to the methyl carboxylate, as shown in **Scheme 2.2**.[9,19–21]

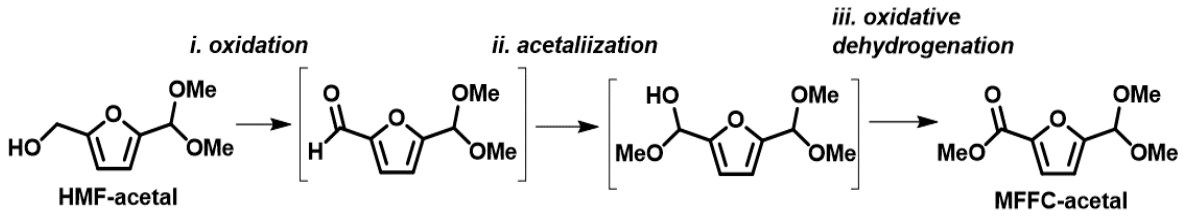

Scheme 2.2. Reaction pathway for oxidative esterification of HMF-acetal to MFFC-acetal in methanol

First, the Na_2CO_3 content was fixed at 1 mol% and optimized the reaction temperature (**entries 1–4**), as lower temperatures are typically preferred to prevent side reactions associated with the thermally less stable dimethylacetal moiety. The conversion, MFFC-acetal yield, and carbon balance increased with the reaction temperature. High MFFC-acetal yields (>90%) were obtained at 100 ºC and 110 ºC, indicating that oxidative esterification of HMF-acetal to MFFC-acetal is the dominant reaction (**entries 3 and 4**). Prolonging the reaction at 100 ºC had no positive influence on the carbon balance and the MFFC-acetal yield (**entry 5**), meaning that the reaction was completed at 100 ºC for 2 h. Increasing the Na_2CO_3 content to 2 mol% (**entry 6**) did not affect the conversion and MFFC-acetal yield. When the same reaction was carried out without Na_2CO_3 (**entry 7**), the formation of humin-type byproducts was pronounced (others yield, 33%), which demonstrated that the addition of a small amount Na_2CO_3 of 1 mol% is enough to suppress side reactions. The formation of humin-type byproducts and methyl-5-hydroxymethylfuran-2-carboxylate (MHMFC) in **entry 7** suggests that the thermal deprotection of HMF-acetal forms HMF. Thus formed HMF is involved in both side reactions and oxidative esterification to form humin-type

byproduct and MHMFC, respectively. Note that the water content of the reaction solution increases with the progress of oxidative esterification of HMF-acetal to MFFC-acetal. High MFFC-acetal yields in **entries 3**–**6** means that a small amount of Na_2CO_3(1–2 mol% to HMF-acetal) stabilizes the dimethylacetal moiety against oxidative degradation and deprotection with the formed water, leading to selective MFFC-acetal formation from the HMF-acetal.

In contrast, the substrate-to-catalyst ratio (S/C wt/wt) had less impact on the MFFC-acetal yield. **Figure 2.3** shows the effect of substrate/catalyst (S/C) ratio on product distribution in the oxidative esterification of HMF-acetal (10 wt%) in methanol under optimized reaction conditions. High MFFC-acetal yields (>90%) were obtained at S/C = 0.8, 1.0, and 1.5. In contrast, low catalyst loading (S/C = 2.0) simply decreased overall reaction rates without significant change in MFFC-acetal selectivity. The optimal S/C was found to be 1 wt/wt at 100 ºC during a 2 h reaction with 1 mol% of Na_2CO_3. These results demonstrate that the oxidative esterification conducted at 100 ºC for 2 h using a methanolic solution of HMF-acetal (10 wt%), 1 mol% of Na_2CO_3, and Au/CeO_2 (S/C = 1 wt/wt) under oxygen pressure of 0.9 MPa (**entry 3**) is optimal as the first step in the stepwise approach to synthesize MFDC.

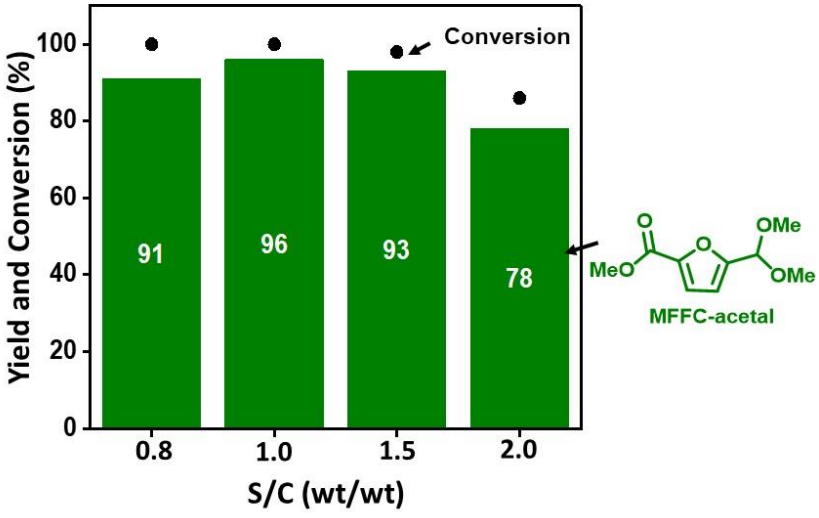

Figure 2.3. Effect of S/C ratio on the oxidative esterification of HMF-acetal to MFFC-acetal with Au/CeO_2. Green bars and black circles represent MFFC-acetal yields and HMF-acetal conversions, respectively. Reaction conditions: HMF-acetal, 100 mg; Au/CeO_2, 100 mg;

Na_2CO_3, 1 mol%; MeOH, 1 g; O_2 pressure, 0.9 MPa; temp., 100 ºC; time, 2 h; stirring rate, 600 rpm.

Table 2.1. Oxidative esterification of HMF-acetal and HMF in methanol (10 wt%) with Au/CeO_2 under pressurized oxygen.[a]

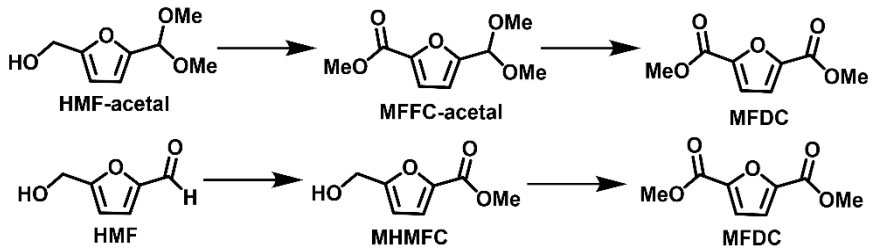

Entry	Substrate	T (°C)	t (h)	Na_2CO_3 (mol%)	Conv. (%)	Product Yield (%)			C.B. (%)
						MFFC-acetal	MHMFC	MFDC	
1	HMF-acetal	80	2	1	69	18	n.d.	3	52
2		90			85	34	n.d.	4	53
3		100			>99	96	n.d.	2	98
4		110			>99	92	n.d.	4	96
5		100	4	1	>99	92	n.d.	2	94
6				2	98	88	n.d.	2	92
7				0	98	46	13	6	67
8	HMF	100	4	1	>99	n.d.	55	37	92
9			24		>99	n.d.	34	62	96
10			48		>99	n.d.	33	56	89
11		140	4		>99	n.d.	26	48	74

[a] Reaction conditions: HMF-acetal/HMF, 100 mg; Au/CeO_2, 100 mg (S/C = 1 wt/wt); MeOH, 1 g; 0.9 MPa O_2, stirring rate 600 rpm.

Control experiments using methanolic HMF solutions (10 wt%) were studied under the optimal reaction conditions for HMF-acetal (**entries 8**–**10**). HMF was fully converted at 100 ºC for 4 h with 1 mol% of Na_2CO_3 to MHMFC (55% yield) and MFDC (37% yield) at 92%

of carbon balance (**entry 8**). MFDC formation proceeds from 4 h to 24 h (**entry 9**). Prolonging the reaction to 48 h did not increase the MFDC yield, meaning that Au/CeO_2 is less effective for the oxidative esterification of MHMFC to MDFC under the reaction conditions (**entry 10**).[9] Increasing the temperature to 140 ºC promotes the oxidative esterification of MHMFC to MFDC, but also causes humin-type byproduct formation (**entry 11**). The formation of such humin-type byproduct in concentrated HMF solutions (**entry 11**) is consistent with our previous work.[29–31] Thus, concentrated HMF solutions cannot be used to synthesize MFDC because of inefficient oxidative esterification of MHMFC at low temperatures and humin-type byproduct formation at high temperatures.[9,31]

2.3.2.1 Kinetic studies on oxidative esterification of HMF-acetal and HMF

The reaction kinetics in oxidative esterification were studied to compare the difference between HMF-acetal and HMF under optimal reaction conditions. **Figure 2.4A** displays the time courses for HMF-acetal conversion and the product yields during 4 h of the reaction. The kinetic traces were fitted with pseudo-first-order reaction kinetics, which provides reaction rate constants for each reaction step (**Figure 2.4C**). HMF-acetal was converted almost quantitatively to MFFC-acetal, while MFDC formation was negligibly small. Although only two products were detected (MFFC-acetal and MFDC), the reaction should involve several intermediates, such as the mono-acetal form of 2,5-diformylfuran with methanol (2-formyl-2-(1,1'-dimethoxymethyl)furan, DFF-mono-acetal) and the di-acetal form of 2,5-diformylfuran (2,5-bis(1,1'-dimethoxymethyl)furan, DFF-di-acetal), as shown in **Figure 2.4C**. The reaction of HMF-acetal starts from the oxidation of the free hydroxymethyl group in HMF-acetal to form DFF-mono-acetal, which is then converted to MFFC-acetal via the hemiacetal form of DFF-mono-acetal by oxidative dehydrogenation.[9,19-21] Neither DFF-mono-acetal, DFF-di-acetal nor their hemiacetals were detected in the reaction mixture (**Figure 2.4A**), suggestive of a direct route from HMF-acetal to MFFC-acetal and high stability of the dimethylacetal functionality under the reaction conditions.[31] The reaction rate constants involved in the oxidative esterification of HMF-acetal to MFFC-acetal were determined to be 3.9 h^{-1} (k_1), > 0.1 h^{-1} (k_3 and k_4), and > 0.01 h^{-}

[1] (k_2). The large value of k_1 compared to the other constants can be attributed to the high stability of the dimethylacetal functionality against side reactions and deprotection with water under the reaction conditions. The MFFC-acetal yield reached 94.3% after 1 h and remained nearly constant for 24 h , which means that the high stability of the dimethylacetal functionality prevents the subsequent oxidative esterification toward MFDC.

Figure 2.4B shows the time courses for the conversion of HMF. HMF was converted to MHMFC by oxidative esterification of the formyl group to the methyl carboxylate via the hemiacetal form of HMF with methanol, which was then involved in the subsequent oxidative esterification via MFFC to afford MFDC as shown in **Figure 2.4D**, while MFFC was detected in very small amounts (< 2%). Oxidative esterification of HMF to MFDC is therefore regarded as a combination of two reaction steps, i.e., MHMFC formation from HMF and MFDC formation from MHMFC, as shown in **Figure 2.4D**. Side reactions to produce humin-type byproduct proceeded from HMF with k_5 = 0.12 h^{-1} due to the high reactivity of the formyl group of HMF. The formation of such byproducts is expected during the oxidative esterification of HMF under these reaction conditons. Nevertheless, the relatively small reaction rate constants k_5 = 1.3 h^{-1} and k_6 = 0.2 h^{-1} in comparison to k_1 imply that high MFDC selectivity cannot be achieved from concentrated HMF solutions.

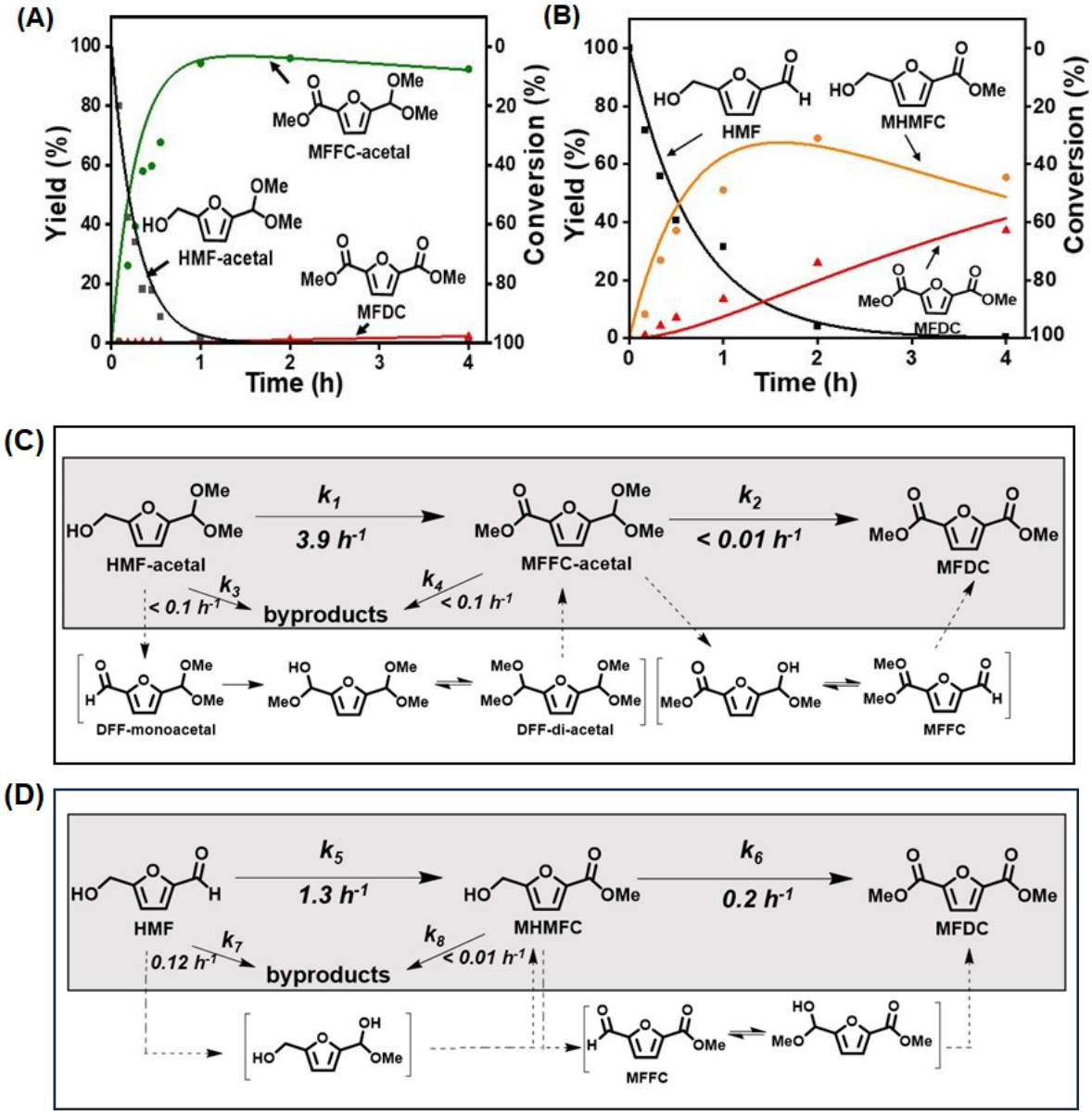

Figure 2.4. (A) Time courses for oxidative esterification of HMF-acetal (10 wt%) in methanol with Au/CeO_2. HMF-acetal conversion, black line and symbols; MFFC-acetal yield, green line and symbols; and MFDC yield, red line and symbols. (B) Time courses for oxidative esterification of HMF (10 wt%) in methanol with Au/CeO_2. HMF conversion, black line and symbols; MHMFC yield, orang line and symbols; and MFDC yield, red line and symbols. Reaction networks for the oxidative esterification of (C) HMF-acetal and (D) HMF in methanol with Au/CeO_2. Reaction Conditions: HMF/HMF-acetal, 100 mg; Au/CeO_2, 100

mg (S/C = 1 wt/wt); Na_2CO_3, 1 mol%; MeOH, 1 g; 0.9 MPa O_2, 100 ºC, 2 h, stirring rate 600 rpm.

In the oxidative esterification of HMF-acetal and HMF, a pseudo first-order model was used for curve fitting lines for the experimental data. **Figure 2.4C and 2.4D** illustrates the possible reaction pathways for the synthesis of MFDC. Based on detectable compounds (HMF-acetal, MFFC-acetal, and MFDC), reaction rate constants (k_1, k_2, k_3, and k_4) in the oxidative esterification of HMF-acetal were estimated by the following equations, assuming that two consecutive reactions (HMF-acetal to MFFC-acetal, MFFC-acetal to MFDC) as a single elementary reaction. We applied the same concept to the oxidative esterification of HMF to estimate reaction rate constants (k_5, k_6, k_7, and k_8).

$$\frac{d[\text{HMF-acetal}]}{dt} = -(k_1+k_3)[\text{HMF-acetal}] \quad \text{(S1)}$$

$$\frac{d[\text{MFFC-acetal}]}{dt} = k_1[\text{HMF-acetal}] - (k_2+k_4)[\text{MFFC-acetal}] \quad \text{(S2)}$$

$$\frac{d[\text{MFDC}]}{dt} = k_2[\text{MFFC-acetal}] \quad \text{(S3)}$$

$$\frac{d[\text{byproducts}]}{dt} = k_3[\text{HMF-acetal}] + k_4[\text{MFFC-acetal}] \quad \text{(S4)}$$

$$\frac{d[\text{HMF}]}{dt} = -(k_5+k_7)[\text{HMF}] \quad \text{(S5)}$$

$$\frac{d[\text{MHMFC}]}{dt} = k_5[\text{HMF}] - (k_6+k_8)[\text{MHMFC}] \quad \text{(S6)}$$

$$\frac{d[\text{MFDC}]}{dt} = k_6[\text{MHMFC}] \quad \text{(S7)}$$

$$\frac{d[\text{byproducts}]}{dt} = k_7[\text{HMF}] + k_8[\text{MHMFC}] \quad \text{(S8)}$$

2.3.2.2 Oxidative esterification of HMF-acetal and HMF with various concentrations

To further clarify the difference between HMF and HMF-acetal, we studied how the substrate concentration impacted the conversion and product yields using 10, 15, and 20 wt% solutions (**Figure 2.5**). All reactions were performed at 100 ºC for 2 h with 0.5–1.0 g of methanolic substrate solutions (10, 15, and 20 wt%), Au/CeO_2 (S/C = 1 wt/wt), Na_2CO_3 (1 mol%), and O_2 (0.9 MPa). High MFFC-acetal yields were obtained in all the experiments with HMF-acetal as substrate, even at a concentration of 20 wt% (yield 90%), while the MHMFC and MFDC yields decreased with increasing HMF concentration. Byproduct formation could be correlated to the initial HMF concentration. The yield of humin byproduct increased from 1% in a 10 wt% solution to 12% in a 20 wt% solution. Humin formation can be attributed to side reactions with the reactive formyl group of HMF, as reported in our previous paper.[31] These results suggest that the first oxidative esterification step of the stepwise approach can be carried out at high concentration of HMF-acetal (10–20 wt%).

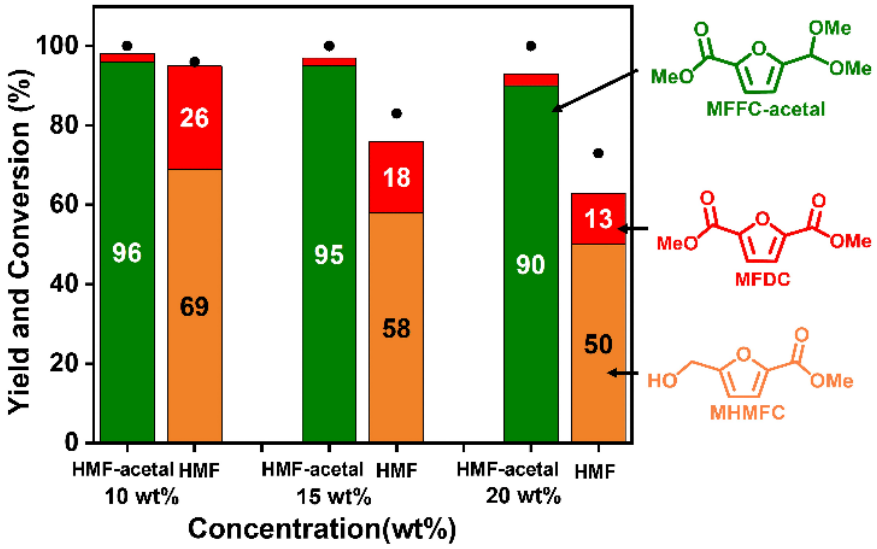

Figure 2.5. Oxidative esterification of HMF-acetal and HMF at various concentrations. Reaction conditions: HMF-acetal or HMF, 100 mg; Au/CeO_2, 100 mg (S/C = 1 wt/wt); Na_2CO_3, 1 mol%; MeOH, 0.5–1.0 g; 0.9 MPa O_2, 100 ºC, 2 h, stirring rate, 600 rpm.

2.3.3 Deprotection of MFFC-acetal to MFFC

Gregg *et al.* reported that acetals and ketals can be readily deprotected under neutral conditions with acetone and indium trifluoromethanesulfonate ($In(OTf)_3$), via *trans*-acetalization, to give the corresponding aldehydes and ketones in high yields, respectively.[39] This strategy was applied to the deprotection of MFFC-acetal. Crude MFFC-acetal was quantitatively isolated from the reaction mixture by a conventional extraction technique with EtOAc and H_2O and dissolved in acetone to prepare a 10 wt% solution for the consecutive trans-acetalization. **Table 2.2** shows the results for the *trans*-acetalization of MFFC-acetal in acetone with acid catalysts under various reaction conditions. Although the deprotection of MFFC-acetal proceeded at 100 ºC for 15 min with $In(OTf)_3$, MFFC was obtained only in a moderate yield (65%) and carbon balance (76%), mainly due to humin byproduct formation (**entry 1**). MFFC formation is based on the *trans*-acetalization of the dimethylacetal moiety in MFFC-acetal with acetone, evidenced by the formation of 2,2-dimethoxypropane as the *trans*-acetalized product as reported in the previous paper. A a commercially available sulfonated polystyrene resin (Amerlyst-15, H^+ = 4.6-4.8 mmol g^{-1}) was used as a Brønsted acid catalyst. The reaction with Amberlyst-15 (8 mol%-H^+ to MFFC-acetal) formed MFFC in a good yield (83%) and with a nearly closed carbon balance (92%) (**entry 2**). The reaction temperature and time were changed to maximize MFFC yield and carbon balance (**entries 3**–**6**). While better values of the carbon balance (> 97%) were obtained at 60 ºC (**entries 4 and 5**), there were no significant changes in MFFC-acetal conversion and MFFC yield. This can be tentatively explained by the equilibrium between the MFFC-acetal and MFFC at these reaction temperatures and at a 10 wt% MFCC-acetal concentration. Consequently, the acetone content was increased from 0.5 to 2.0 g (**entry 7**) or 4.0 g (**entry 8**) to maximize the MFFC yield, as the MFFC-acetal concentration likely determines the MFFC yield. When the MFFC-acetal concentration was decreased from 10 wt% (**entries 1**–**6**) to 2.5 wt% (**entry 7**) and 1.25 wt% (**entry 8**), MFFC was obtained in high yields (> 90%) at high MFFC-acetal conversion (≥ 95%). A high MFFC yield (95%) under the optimal reaction conditions (**entry 8**) demonstrates that the *trans*-acetalization using a solid Brønsted acid catalyst, crude

MFFC-acetal, and acetone is suitable for the deprotection step of the stepwise approach to synthesize MFDC.

Table 2.2. Deprotection of MFFC-acetal to MFFC through *trans*-acetalization with acetone.[a]

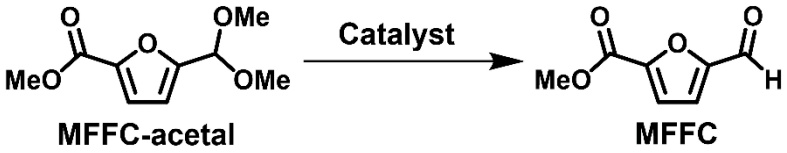

#	Catalyst	Acetone (g)	Conc. (wt%)	T (ºC)	t (min)	Conv. (%)	Product yield (%)		C. B. (%)
							MFFC	Others	
1	$In(OTf)_3$	0.50	10	100	15	89	65	24	76
2	Amberlyst-15					91	83	8	92
3	Amberlyst-15	0.50	10	80	60	90	80	10	90
4					60	75	74	1	99
5	Amberlyst-15	0.50	10	60	90	85	82	3	97
6					120	87	78	9	91
7	Amberlyst-15	2.0	2.5	60	90	95	92	3	97
8		4.0	1.25			98	95	3	97

[a] Reaction conditions: MFFC-acetal, 50 mg; $In(OTf)_3$, 1.4 mg (0.8 mol%); Amberlyst-15, 6.3 mg (8 mol%); stirring rate 600 rpm. Others include undetectable byproducts.

2.3.4 Oxidative esterification of MFFC to MFDC (10 wt%) with Au/CeO_2

The oxidative esterification of MFFC to MFDC was conducted with Au/CeO_2 in a 10 wt% methanolic solution at 100 ºC for 3 h. Commercially available MFFC was used as the model compound without any purification. **Figure 2.6A** shows the reaction results for different Na_2CO_3 loadings. While there was no difference in MFFC conversion, the MFDC yield without Na_2CO_3 was higher than those with Na_2CO_3 (4–10 mol%). The lower MFDC

yields are due to base-assisted several side reactions such as the stepwise hydrolysis of MFDC to FDCA[24,40] and the base-catalyzed Cannizaro reaction of MFFC to MHMFC, the latter of which forms the humin-type byproducts via polymerization with the unreacted substrate.[13,23] The base-free oxidative esterification of MFFC with Au/CeO_2 afforded MFDC in an excellent yield of 93%. This result is distinct from the first oxidative esterification step using HMF-acetal, which requires 1 mol% Na_2CO_3 to obtain MFFC-acetal in a high yield.

Figure 2.6B shows time courses for the oxidative esterification of MFFC without Na_2CO_3. The MFDC yield increased linearly with time, reaching a maximum of 93% at complete substrate conversion (> 99%) after 3 h. The yield of undetectable byproducts (to close the mass balance) only increased to 8% in the first 1 h and then remained almost unchanged for 3 h. As the MFDC yield did not decrease, it can be concluded that MFDC is stable under the reaction conditions.

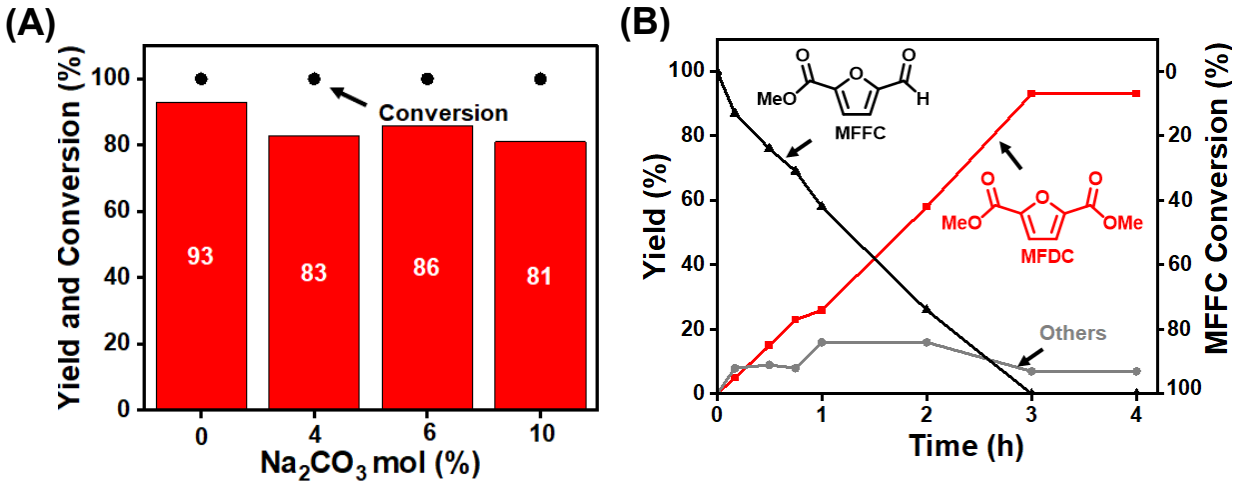

Figure 2.6 (A) Oxidative esterification of MFFC to MFDC at different Na_2CO_3 loadings. Reaction Conditions: MFFC, 50 mg; Au/CeO_2, 50 mg; MeOH, 500 mg; 100 °C, 6 h, 0.9 MPa O_2, stirring rate 600 rpm. **(**B**)** Time courses for the oxidative esterification of MFFC (10 wt%) in methanol with Au/CeO_2. MFFC conversion, black line, and symbols; MFDC yield, red line, and symbols; Others yield, grey line, and symbols (include undetectable intermediate

and byproducts). Reaction conditions: MFFC, 50 mg; Au/CeO_2, 50 mg; MeOH, 500 mg; 100 °C, 0.9 MPa O_2, stirring rate 600 rpm.

2.3.5 Recyclability and leaching test of Au/CeO_2

Five recycles were performed to evaluate the reusability of Au/CeO_2 in two oxidative esterification reactions using HMF-acetal and MFFC, which are the first and third step of the

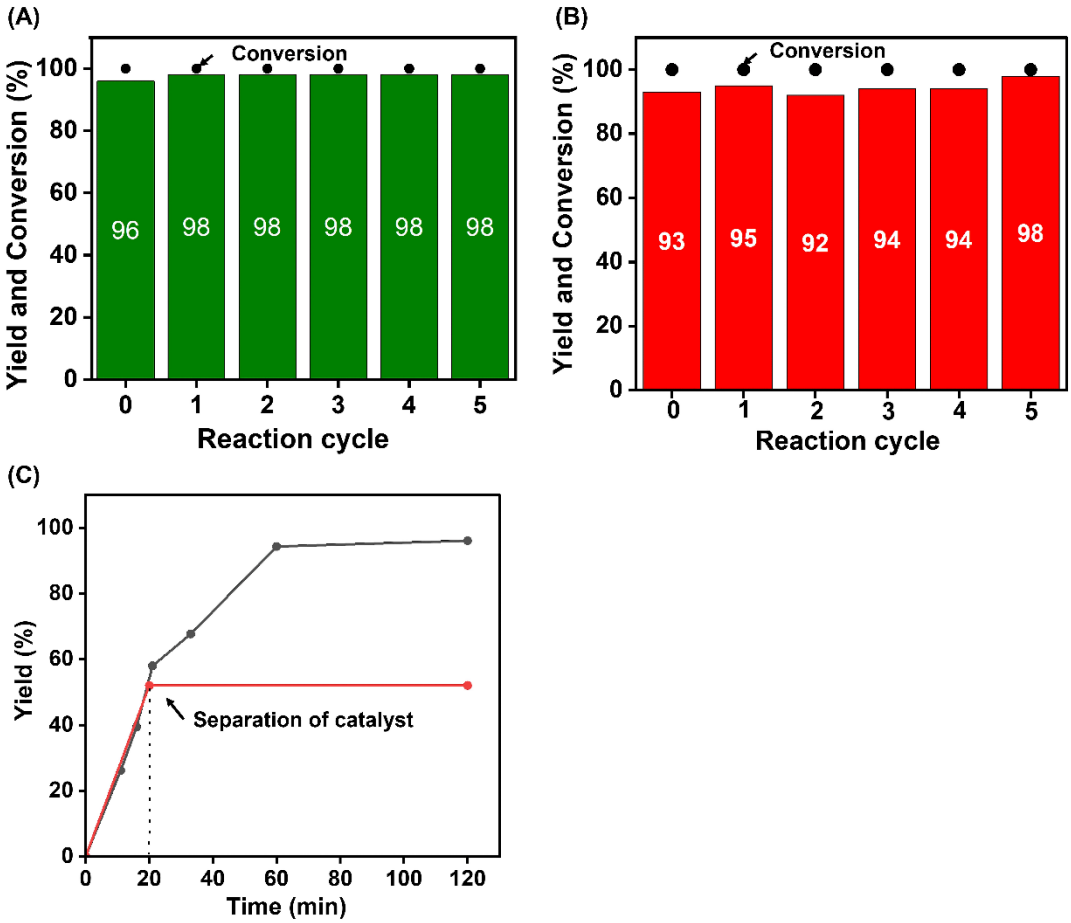

Figure 2.7. Recyclability tests of Au/CeO_2 in the oxidative esterification of (A) HMF-acetal to MFFC-acetal and (B) MFFC to MFDC. (C) Leaching test of Au/CeO_2 in the oxidative esterification of HMF-acetal to MFFC-acetal. Reaction Conditions of (A) and (C): HMF-acetal, 100 mg; Au/CeO_2, 100 mg (S/C = 1 wt/wt); Na_2CO_3, 1 mol%; MeOH, 1 g; 0.9 MPa O_2, 100 ºC, 2 h, stirring rate 600 rpm. Reaction Conditions of (B): MFFC, 50 mg; Au/CeO_2, 50 mg (S/C = 1 wt/wt); MeOH, 0.5 g; 0.9 MPa O_2, 100 ºC, 3 h, stirring rate 600 rpm.

stepwise approach, respectively. The spent catalyst (Au/CeO_2) retained its original activity, even after 5 times reuse in both reactions (**Figures 2.7A and 2.7B**),[9] which confirms the high reusability of Au/CeO_2. After five runs, the XRD pattern of the spent Au/CeO_2 does not contain diffraction lines of metallic Au, indicating that no extensive Au nanoparticle aggregation occurred during the reactions (**Figure 2.8**). A hot filtration test was performed to evaluate the heterogeneous nature of the reaction. The catalyst was filtered from the reaction solution after 20 min, and the reaction was continued for an additional 100 min without the solid catalyst (**Figure 2.7C**). As the reaction did not progress after removal of the solids, it can be concluded that Au nanoparticles do not leach into the solution. These results demonstrate the high stability of the catalysts under the reaction conditions and the heterogeneous nature of the reaction.

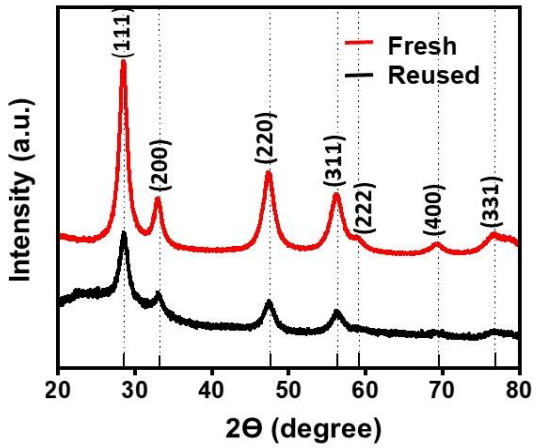

Figure 2.8. XRD patterns of fresh Au/CeO_2 and used Au/CeO_2 after fifth reuses in the oxidative esterification of HMF-acetal.

The main results for each reaction step of this approach are finally summarized in **Scheme 2.3**. The first and third step involves the use of concentrated substrate solutions (10 wt%), which significantly enhances the productivity of MFDC due to a high overall yield (85%). A small amount of Na_2CO_3 (1 mol% to HMF-acetal) was required in the first oxidative esterification step to stabilize the acetal functionality during the formation of MFFC-acetal. The Na_2CO_3 content in this stepwise approach is much lower than in the two

one-pot processes earlier describe to obtain FDCA and MFDC (200 mol% to PD-HMF).[31,32] The deprotection of MFFC-acetal to MFFC via a simple trans-acetalization reaction using a solid Brønsted acid catalyst (Amberlyst-15) is highly efficient, and MFFC could be isolated easily by evaporation of the low-boiling organic volatiles. A base-free oxidative esterification of MFFC in the third step afforded MFDC in an excellent yield.

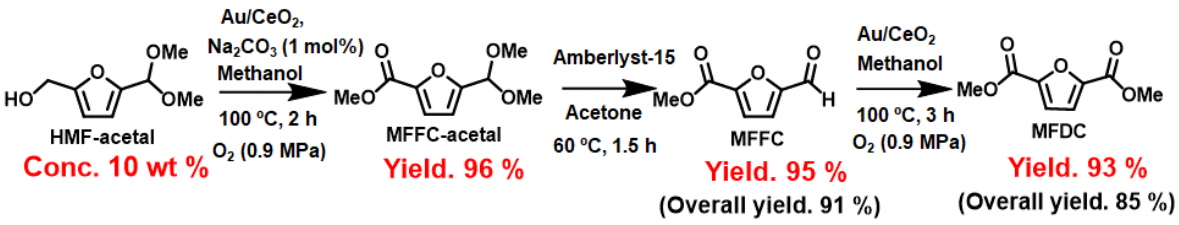

Scheme 2.3. Three-step approach to synthesize MFDC from concentrated methanolic solution of HMF-acetal (10 wt%). Overall yield was calculated based on HMF-acetal.

A significant advance in this work towards the one-pot synthesis of MFDC is to develop a reaction system using the thermally less stable HMF-dimethylacetal. Thermal stability experiments of HMF and several HMF-acetals revealed that PD-HMF exhibits a much higher stability than HMF and the HMF-dimethylacetal.[30,31] One-pot synthesis of MFDC from PD-HMF requires hash reaction conditions to promote sequential reaction steps, consisting of partial deprotection of the six-membered ring acetal to form corresponding hemiacetal, the dehydrogenation of the hemiacetal with Au/CeO_2, and trans-esterification of the resulting ester with methanol (**Scheme 2.4**). Other HMF-acetals require similar reaction conditions as for one-pot MFDC synthesis.

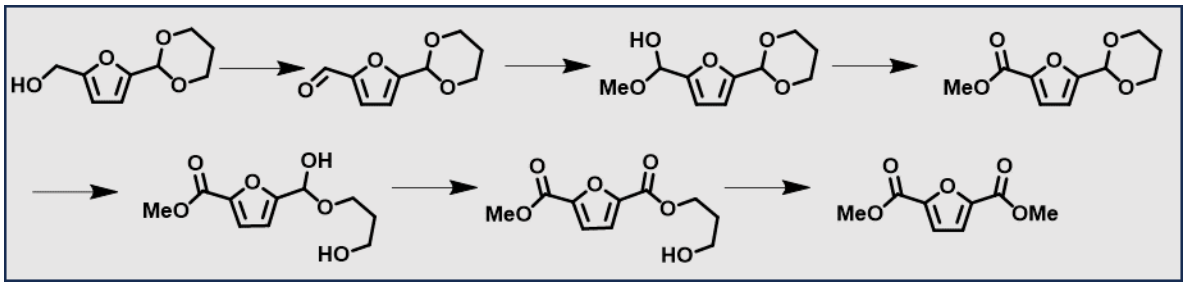

Scheme 2.4. Reaction network for the one-pot oxidative esterification of PD-HMF to MFDC in methanol with Au/CeO_2.

However, the thermally less stable HMF-dimethyl acetal is primarily involved in complex side reactions towards humins under such hash reaction conditions, likely due to the deprotection of the dimethylacetal moiety and subsequent degradation of *in-situ* formed HMF.[31] Therefore, it is not possible to use the HMF-dimethylacetal in a one-pot synthesis of MFDC (**Table 2.3**). On the other hand, the stepwise approach can eliminate the oxidative transformation of the acetal to the methyl carboxylate moiety. Using methanol as the protecting reagent in MFDC synthesis eliminates the recovery and reuse of the protecting reagent, because methanol is cheap and can in principle be obtained from renewable resources. Key advantages of the recent approach are (i) the use of HMF-dime thylacetal, (ii) very low Na_2CO_3 loading, and (iii) high reaction rates of oxidative esterification steps using concentrated solutions (~ 20 wt%), rendering the current approach ameanable to a flexible process for large-scale MFDC production.

Table 2.3. One-pot synthesis of MFDC from HMF-acetal (10 wt%) in methanol with Au/CeO_2 under pressurized oxygen.[a]

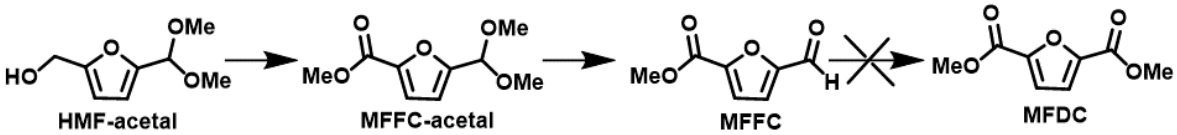

Entry	Temp. (°C)	Time (h)	Conv. (%)	Product Yield (%)				C.B. (%)
				MFFC-acetal	MFFC	MFDC	Others	
1	100	2	> 99	96	0	2	n.d.	98
2		24	> 99	90	1	3	n.d.	95
3	120	24	> 99	22	32	13	11	78

[a] Reaction conditions: HMF-acetal, 100 mg; Au/CeO_2, 100 mg; Na_2CO_3, 1 mol%; MeOH, 1 g; 0.9 MPa O_2, stirring rate 600 rpm. Others refers to MHMFC, produced via Cannizaro reaction of MFFC.

2.4 Conclusion

I have developed a highly efficient catalytic process for the stepwise synthesis of MFDC from HMF-acetal (methanolic 10–20 wt% solutions). Methanol was demonstrated for the first time to be effective protecting agent in the oxidative esterification of HMF. This strategy offered several advantages over the previous one-pot reaction strategy using 1,3-propanediol as a protecting reagent, namely (i) the amount of the basic additive can be reduced (Na_2CO_3, 1 mol%), (ii) the recovery step of the protecting agent can be omitted, and (iii) desired products (MFFC-acetal and MFDC) can be obtained in high yields using concentrated substrate solutions. Such advantages are derived from the non-oxidative transformation of the acetal group to methyl carboxylate by this stepwise approach. A one-pot reaction, including the oxidative transformation of the acetal functional group to methyl carboxylate, requires hash reaction conditions, which leads to deprotection of the thermally unstable dimethylacetal group and subsequent oxidative degradation of non-protected HMF. Due to low thermal stability compared to PD-HMF, the HMF-dimethylacetal cannot be used in a one-pot reaction approach. However, as the dimethylacetal group in HMF is stable enough against deprotection under specific reaction conditions, it can be used to obtain MFFC-acetal, which is the key to the use of dimethylacetal functionality as a protecting agent in the current reaction process. The deprotection step (MFFC-acetal to MFFC) was catalyzed by a solid Brønsted acid catalyst, which further enhances the significance of the process. Au/CeO_2 showed high catalytic performance in the oxidative esterification of HMF-acetal (10–20 wt%) and MFFC (10 wt%) for producing the target products in high yield under mild reaction conditions. Products such as MFFC-acetal, MFFC, and MFDC could be obtained from the reaction mixture in high purity after each step, extending the scope of this approach towards other valuable biobased monomers.

2.5 References

[1] M. A. Hillmyer, *Science* **2017**, 358, 868−870.

[2] Y. Zhu, C. Romain, C. K. Williams, *Nature* **2016**, 540, 354364.

[3] A. F. Sousa, C. Vilela, A. C. Fonseca, M. Matos, C. S. R. Freire, G.-J. M. Gruter, J. F. J. Coelho, A. J. D. Silvestre, *Polym. Chem.* **2015**, 6, 5961−5983.

[4] A. J. J. E. Eerhart, A. P. C. Faaij, M. K. Patel, *Energy Environ. Sci.* **2012**, *5*, 6407.

[5] S. K. Burgess, J. E. Leisen, B. E. Kraftschik, C. R. Mubarak, R. M. Kriegel, W. J. Koros, *Macromolecules* **2014**, *47*, 1383–1391.

[6] D. Zhao, T. Su, C. Len, R. Luque, Z. Yang, Green Chem. **2022**, *24*, 6782–6789.

[7] A. Abad, P. Concepción, A. Corma, H. García, Angew. Chem. Int. Ed. **2005**, *44*, 4066–4069.

[8] O. Casanova, S. Iborra, A. Corma, ChemSusChem **2009**, *2*, 1138–1144.

[9] O. Casanova, S. Iborra, A. Corma, J. Catal. **2009**, *265*, 109–116.

[10] E. Taarning, I. S. Nielsen, K. Egeblad, R. Madsen, C. H. Christensen, ChemSusChem **2008**, *1*, 75–78.

[11] F. Menegazzo, M. Signoretto, D. Marchese, F. Pinna, M. Manzoli, J. Catal. **2015**, *326*, 1–8.

[12] J. Du, H. Fang, H. Qu, J. Zhang, X. Duan, Y. Yuan, Appl. Catal. Gen. **2018**, *567*, 80–89.

[13] F. Li, X.-L. Li, C. Li, J. Shi, Y. Fu, Green Chem. **2018**, *20*, 3050–3058.

[14] A. Salazar, P. Hünemörder, J. Rabeah, A. Quade, R. V. Jagadeesh, E. Mejia, ACS Sustain. Chem. Eng. **2019**, acssuschemeng.9b00914.

[15] M. Jin, L. Yu, H. Chen, X. Ma, K. Cui, Z. Wen, Z. Ma, Y. Sang, M. Chen, Y. Li, Catal. Today **2021**, *367*, 2–8.

[16] H. Liu, W. Jia, X. Yu, X. Tang, X. Zeng, Y. Sun, T. Lei, H. Fang, T. Li, L. Lin, *ACS Catal.* **2021**, *11*, 7828–7844.

[17] H. Su, K.-X. Zhang, B. Zhang, H.-H. Wang, Q.-Y. Yu, X.-H. Li, M. Antonietti, J.-S. Chen, *J. Am. Chem. Soc.* **2017**, *139*, 811–818.

[18] S. Xu, P. Zhou, Z. Zhang, C. Yang, B. Zhang, K. Deng, S. Bottle, H. Zhu, *J. Am. Chem. Soc.* **2017**, *139*, 14775–14782.

[19] Q. Zhu, F. Wang, F. Zhang, Z. Dong, *Nanoscale* **2019**, *11*, 17736–17745.

[20] W. Zhong, H. Liu, C. Bai, S. Liao, Y. Li, *ACS Catal.* **2015**, *5*, 1850–1856.

[21] Y. Lu, Z. Zhang, H. Wang, Y. Wang, *Appl. Catal. B Environ.* **2021**, *292*, 120162.

[22] Y. Sun, H. Ma, X. Jia, J. Ma, Y. Luo, J. Gao, J. Xu, *ChemCatChem* **2016**, *8*, 2907–2911.

[23] Y. Feng, W. Jia, G. Yan, X. Zeng, J. Sperry, B. Xu, Y. Sun, X. Tang, T. Lei, L. Lin, *J. Catal.* **2020**, *381*, 570–578.

[24] J. Deng, H.-J. Song, M.-S. Cui, Y.-P. Du, Y. Fu, *ChemSusChem* **2014**, *7*, 3334–3340.

[25] H. Liu, N. Ding, J. Wei, X. Tang, X. Zeng, Y. Sun, T. Lei, H. Fang, T. Li, L. Lin, *ChemSusChem* **2020**, *13*, 4151–4158.

[26] M. Zhang, Y. Liu, B. Liu, Z. Chen, H. Xu, K. Yan, *ACS Catal.* **2020**, *10*, 5179–5189.

[27] K. Gupta, R. K. Rai, S. K. Singh, *Inorg. Chem. Front.* **2017**, *4*, 871–880.

[28] F. J. A. G. Coumans, Z. Overchenko, J. J. Wiesfeld, N. Kosinov, K. Nakajima, E. J. M. Hensen, *ACS Sustain. Chem. Eng.* **2022**, *10*, 3116–3130.

[29] T. Boonyakarn, J. J. Wiesfeld, M. Asakawa, L. Chen, A. Fukuoka, E. J. M. Hensen, K. Nakajima, *ChemSusChem* **2022**, *15*, e202200059.

[30] M. Kim, Y. Su, A. Fukuoka, E. J. M. Hensen, K. Nakajima, *Angew. Chem. Int. Ed.* **2018**, *57*, 8235–8239.

[31] M. Kim, Y. Su, T. Aoshima, A. Fukuoka, E. J. M. Hensen, K. Nakajima, *ACS Catal.* **2019**, *9*, 4277–4285.

[32] J. J. Wiesfeld, M. Asakawa, T. Aoshima, A. Fukuoka, E. J. M. Hensen, K. Nakajima, *ChemCatChem* **2022**, *14*, e202200191.

[33] J. J. Wiesfeld, M. Kim, K. Nakajima, E. J. M. Hensen, *Green Chem.* **2020**, *22*, 1229–1238.

[34] M. Haruta, *Catal. Today* **1997**, *36*, 153–166.

[35] S. Torbrügge, M. Reichling, A. Ishiyama, S. Morita, Ó. Custance, *Phys. Rev. Lett.* **2007**, *99*, 056101.

[36] M. Manzoli, F. Menegazzo, M. Signoretto, G. Cruciani, F. Pinna, *J. Catal.* **2015**, *330*, 465–473.

[37] V. Amendola, R. Pilot, M. Frasconi, O. M. Maragò, M. A. Iatì, *J. Phys. Condens. Matter* **2017**, *29*, 203002.

[38] S. Ma, D.-J. Yang, S.-J. Ding, J. Liu, W. Wang, Z.-Y. Wu, X.-D. Liu, L. Zhou, Q.-Q. Wang, *Phys. Rev. Lett.* **2021**, *126*, 173902.

[39] B. T. Gregg, K. C. Golden, J. F. Quinn, *J. Org. Chem.* **2007**, *72*, 5890–5893.

[40] X. Guo, Y. Si, Y. Huang, J. Zhang, X. Lyu, Y. Cheng, X. Li, Ind. Eng. Chem. Res. **2023**, *62*, 16309–16318.

Chapter 3

Reductive Amination of Acetal-protected 2,5-Diformylfuran to 2,5-Bis(aminomethyl)furan Using Co_2P Nanorods

Abstract

Herein, I have explored an acetal protection strategy for the stepwise synthesis of 2,5-bis(aminomethyl)furan (BAMF) by reductive amination of biomass-derived acetal-protected 2,5-diformylfuran (DFF) using Co_2P nanorods (NRs) catalyst. In the first step, the reductive amination PD-DFF with NH_3 in a methanol-water (2:1) mixture affords the acetal-protected amionomethylfuran (PD-AMF) exclusively (92%) at 120 °C for 2 h with 0.5 MPa H_2. The high stability of the six-membered ring acetal under the reaction conditions prevents the deprotection and direct synthesis of BAMF, in a single step. When, an optimum amount of acetic acid was added to the reaction mixture containing PD-AMF, BAMF was obtained selectively in high yield (94%) via partial deprotection, and the subsequent reductive amination of the *in-situ* formed hemiacetal. The Co_2P NRs catalyst exhibits high catalytic performance and reusability in both the reductive aminations of PD-DFF and PD-AMF to give the desired products in high yield. Moreover, the process was extended for producing BAMF using highly concentrated solutions of PD-DFF (10–20 wt%) to enhance productivity. A high yield of BAMF (95%) was achieved also from concentrated solutions of PD-DFF (10 wt%) derived from the protecting strategy and stepwise approach. Thus, the developed process is immensely attractive to commercialize in real-field applications.

3.1 Introduction

Recently, the conversion of biomass-derived substrates into nitrogen-containing compounds, specifically primary amines, has gained tremendous attention owing to its versatility in organic synthesis such as to produce polymers, drugs, surfactants, pharmaceuticals, agrochemicals and so on.[1–5] 2,5-bis(aminomethyl)furan (BAMF), a biomass-derived primary diamine is widespread for the synthesis of polyamides, polyurethanes and polyurea because of its superior gas barrier performance, miscibility, processibility and biocompatibility. To date, the synthesis of primary amines mainly relies on fossil resources involving harsh reaction conditions and toxic intermediates.[6,7] However, the continuous depletion of fossil fuel resources has a serious impact on the environment, which urgently requires finding an alternative renewable carbon source.[8] Notably, the catalytic reductive amination of carbonyl functionality of biomass-derived furanics to primary amines with NH_3 and H_2 is one of the promising methods for the sustainable development of human society and economy compared to conventional synthetic process using specific nitrogen source and/or stoichiometric reductants.[9] However, the direct reductive amination of carbonyl functionality to primary amines is less explored for the biomass-derived substrates and restricted to simple aryl and alkyl aldehydes (e.g., benzaldehyde)) due to the formation of secondary and tertiary amines and/or the progress of undesired over-hydrogenation of carbonyl groups and furan rings.[9] In particular, the selective reductive amination of carbonyl compounds containing reduction-sensitive functional groups such as heterocycles and halogens is highly challenging.[9] Therefore, it is urgently required to develop an efficient process for the conversion of biomass-derived substrates into primary amine derivatives.

2,5-diformylfuran (DFF) can be synthesized on a large scale from lignocellulosic biomass-derived HMF or other carbohydrates,[10–13] and it is one of the promising candidates as a BAMF precursor. However, two highly reactive formyl groups in DFF often leads to undergo condensations with primary amines and their corresponding di-imine intermediates to produce oligomeric by-products resulting in low selectivity to BAMF. Therefore, the reported BAMF yield from DFF is limited (**Table 1.2**). Kim et al obtained only a 42.6 %

yield of BAMF from DFF using acid-treated Raney Ni catalysts with a high number of oligomers.[13] To overcome these challenges, Zhang et al. introduced n-butylamine as a scavenger of dialdehydes,[14] which first reacts with DFF to form primary imines followed by undergoing transamination reaction with NH_3, and then the hydrogenation catalyzed by Co/ZrO_2 catalysts (P_{H2} = 2 MPa) affords BAMF selectively, in a high yield of 95%. However, the reaction requires a long time (10 h) and high H_2 pressure (4 MPa) for 71% of BAMF yield from 10 wt% DFF solution. Moreover, the use of an expensive and toxic protecting agent, n-butylamine, enhances the cost and environmental burden bringing down the atom-efficiency of the process. Another concern is the catalyst lifetime and stability.[21-30] Wei et al. reported an efficient one-pot reductive amination of HMF into BAMF over the Raney Ni catalyst.[22] However, the catalyst lost its original activity due to the poisoning of the catalytic active sites by strongly adsorbed NH_3 and alkyl amines. Thus, developing an effective method as well as a rational design of an efficient catalyst for the selective reductive amination of biomass-derived furanic aldehydes to BAMF is a highly desired yet challenging goal.

As already mentioned in Chapters 1 and 2, the acetal protection strategy could be a straightforward alternative in this aspect.[15–20] Protecting the reactive formyl groups of DFF with 1,3-propanediol (PD) can suppress side reactions and synthesize BAMF selectively. Our group explored several catalytic reactions from acetal-protected HMF in concentrated solutions and achieved high productivity.[15–20] Boonyakarn et al. performed the oxidation of highly concentrated acetal-protected HMF (PD-HMF) solutions (10–70 wt%) using γ-Al_2O_3-supported Ru catalyst (Ru/γ-Al_2O_3) and obtained acetal-protected DFF (PD-DFF) in excellent yields.[16]

Most of the earlier reports focused on supported metal catalysts in the reductive amination of biomass-derived furanic aldehydes.[21–30] As discussed, though the developed catalysts were highly active, the recyclability of the catalysts was significantly poor due to several factors such as strong adsorption of NH_3 on the catalytically active sites, coking, agglomeration of particles and leaching of the active species. In general, introducing the

support enhances the metal dispersion, prevents agglomeration, and increases the specific surface area of the catalyst. Moreover, strong metal-support interactions often improve the catalyst stability and enhance the activity. However, there are several drawbacks associated with the use of supported metal-based catalysts. For example, the acidic properties of the support (such as in the case of Al_2O_3) can cause strong adsorption of basic NH_3 and alkylamines over the catalyst surface.[23] In addition, carbon coking leads to the irregular blockage of ill-defined catalytically active sites.[14] In contrast, alloying nonmetal (such as Phosphorus) with metal can significantly improve the catalyst stability as well as reusability. In this direction, metal phosphide nano-alloys emerge as an efficient catalyst in the selective hydrogenation of biomass-derived furanics.[31–42] Mitsudome et al. have reported that alloying phosphorus with Co nanoparticles brought significant merits such as stabilizing the metallic state of the Co species, enhancing the d electron density of Co near fermi level facilitating its hydrogenation activity and creating precise well-defined active sites.[36] Thus, the activity of Co_2P can be controlled towards selective reductive amination reaction avoiding catalyst poisoning. Such distinctive features of metal-phosphide nano-catalysts inspired me to explore the application of cobalt phosphide nanorods (Co_2P NRs) in the selective reductive amination of biomass-derived furanics. Herein, I utilized the acetal protection strategy in designing a stepwise reductive amination of acetal-protected DFF (PD-DFF)[16] with 1,3-propanediol (PD) to synthesize 2,5-bis(aminomethyl)furan (BAMF) using Co_2P nanorods (NRs) catalyst.

3.2 Experimental Section

3.2.1 Materials.

Cobalt (II) acetylacetonate dihydrate ($Co(acac)_2 \cdot 2H_2O$) was purchased from Mitsuwa pure chemicals. DFF, 1,3-propanediol (PD), ethylene glycol (EG), trimethyl orthoformate, hexadecylamine, triphenyl phosphite, 1-octadecene, and chlorobenzene were purchased from Tokyo Chemical Industry (TCI). BAMF was obtained from Angene chemicals. Ruthenium(III) nitrosyl nitrate solution (1.5 wt% of Ru) was procured from Strem Chemicals. Nickle (III) chloride hexahydrate ($NiCl_2 \cdot 6H_2O$), nickle(III) nitrate hexahydrate

($Ni(NO_3)_2.6H_2O$), cobalt(II) nitrate trihydrate ($Co(NO_3)_2.3H_2O$), Ru/C, methanol, acetone, acetic acid (CH_3COOH), activated alumina, aqueous NH_3 solution (28 wt%), ammonium acetate (NH_4OAC) and *N,N*-dimethylformamide super dehydrated (DMF) were purchased from FUJIFILM Wako Pure Chemical Corporation. Methanolic ammonia (NH_3) solution (7N), indium trifluoromethanesulfonate ($In(OTf)_3$ and D_2O were obtained from Sigma-Aldrich. Dichloromethane, ethyl acetate, hexane, and chloroform were purchased from Kanto chemical corporation. Amberlyst-15 was purchased from Acros Organics. ZrO_2 (JRC-ZrO-9) and Al_2O_3 (JRC-AlO-2) were supplied from the Catalyst Society of Japan.

3.2.2 Catalyst preparation.

Co_2P NRs was prepared by a solvothermal process, following an earlier reported method.[36] Briefly, $Co(acac)_2.2H_2O$ (1 mmol), hexadecylamine (10 mmol) and triphenyl phosphite (10 mmol) were added to 1-octadecene (10 mL) placed in a Schlenk-flak. Then, the mixture was stirred at 150 °C for 1 h in N_2 atmosphere, followed by the temperature slowly increasing to 300 °C at a rate of 10 °C/min and continued stirring for 2 h under N_2. After cooling to room temperature, a black colloid was obtained, which was collected by centrifugation after washing with a mixed solvent; chloroform-acetone (1:1, v/v). Finally, the solid was dried overnight under a high vacuum at room temperature which afforded highly crystalline Co_2P NRs.

Ni_2P was prepared following a similar method. Typically, $NiCl_2{\cdot}6H_2O$ (1.0 mmol), hexadecylamine (10 mmol) and triphenyl phosphite (10 mmol) were added in a Schlenk flask.[43] The temperature was then slowly increased to 320 °C and the mixture was stirred for 2 h under an inert (N_2) atmosphere to afford a black colloidal solution of Ni_2P. Then, it was allowed to cool to 25 °C, subsequently the black product was collected by centrifugation after washing with chloroform and acetone (1:1, v/v). Finally, the product was dried overnight *in vacuo* at room temperature.

Al_2O_3 supported Ni catalyst was prepared through an incipient-wetness impregnation method.[23] Typically, 1.1 g $Ni(NO_3)_2.6H_2O$ (10 wt% theoretical Ni loading) was dissolved into 1.74 g deionized water. Then, 2.0 g Al_2O_3 was added into the mixture and kept for 24 h

at room temperature. After that, the mixture was dried at 110 °C for 10 h and finally reduced at 500 °C for 4 h under hydrogen flow (10 mL.min^{-1}) to obtain the desired catalyst. The Al_2O_3 and ZrO_2 supported Co catalysts were prepared following the same procedure with 1.1 g $Co(NO_3)_2.6H_2O$ (10 wt% theoretical Co loading).

Ru/Nb_2O_5 (1 wt% theoretical Ru loading) was prepared by an impregnation method.[9] 2 g of Nb_2O_5 was added into an aqueous ruthenium nitrosyl nitrate, $Ru(NO)(NO_3)_3$ solution and stirred overnight at room temperature. The mixture was then evaporated to dryness at 373 K for 1 h under vacuum and the obtained solid was reduced under hydrogen flow (10 mL.min^{-1}) at 400 °C for 2 h.

The commercially available 5 wt% Ru/C was used as received without further pretreatment.

3.2.3 Characterization.

Powder X-ray diffraction (P-XRD) measurements were performed by an Ultima IV, Rigaku diffractometer at 40 kV and 40 mA using Cu Kα radiation (λ = 1.5418 Å) in 2θ = 10−90°. X-ray photoelectron spectroscopy (XPS) analysis was performed with a JEOL JPS-9010MC X-ray photoelectron spectrometer equipped with a dual Mg/Al X-ray source. The spectra were obtained at a pass energy of 10.0 eV with an Mg Kα X-ray source. The C 1s peak at a binding energy of 284.6 eV was used as the internal reference. Transmission electron microscope (TEM) images were obtained from a Field Emission Electron Microscope (JEOL JEM-2100F).

3.2.4 Synthesis of acetal protected DFF (DFF-acetal).

Three DFF-acetals (PD-DFF, EG-DFF and Me-DFF) were prepared by the acetalization of 2,5-diformylfuran (DFF) with a suitable alcohol (such as 1,3-propanediol, PD; Ethylene Glycol, EG; and Methanol, Me) using a sulfonated polystyrene resin (Amberlyst-15, H^+ = 4.6-4.8 mmol g^{-1}) or, Indium trifluoromethanesulfonate ($In(OTf)_3$) as an acid catalyst.[15–19] Typically, to synthesize PD-DFF and EG-DFF, Amberlyst-15 (100 mg)

was added to a solution of 2,5-diformylfuran (0.5 g, 4.0 mmol) and tetrahydrofuran (THF, 15 mL). Then, the respective alcohol (PD/EG, 4.3 mmol) was added dropwise into the reaction mixture and stirred at room temperature for 24 h. After completion of the reaction, the reaction mixture was filtered to separate the resin (Amberlyst-15), followed by the solvent evaporated to obtain a crude product. The crude product containing a mixture of DFF, DFF-monoacetal and DFF-diacetal was purified by column chromatography using ethyl acetate and hexane (1:2) to separate the mono-acetalized DFF. After purification, the product was analyzed by ^{1}H nuclear magnetic resonance (NMR) spectrometer (JNM-ECZ600, JEOL), which showed the purity of PD-DFF ca. 90% and EG-DFF ca. 60%.

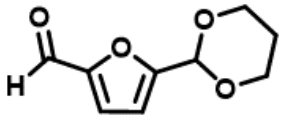

PD-DFF

5-(1,3-Dioxan-2-yl)-2-furancarboxaldehyde (PD-DFF): ^{1}H NMR (400 MHz, $CDCl_3$) 9.67 (s, 1H) 7.28 (d, 1H), 6.65 (d, 1H), 5.64 (s, 1H), 4.26 (m, 2H), 3.98 (m, 2H), 2.24 (m, 1H), 1.47 (d, 1H) ppm.

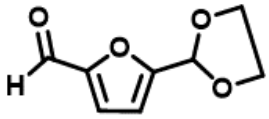

EG-DFF

5-(1,3-Dioxolan-2-yl)-2-furancarboxaldehyde (EG-DFF): ^{1}H NMR (400 MHz, $CDCl_3$) 9.67 (s, 1H) 7.21 (d, 1H), 6.63 (d, 1H), 6.00 (s, 1H), 4.13 (d, 2H), 4.05 (d, 2H) ppm.

To synthesize Me-DFF, first, 2,5-diformylfuran (0.25 g, 2.0 mmol) was dissolved in dichloromethane (DCM, 20 mL), followed by trimethyl orthoformate (TMOF, 0.5 mL, 4 mmol) and $In(OTf)_3$ (0.1 mol% to substrate, 1.4 mg) was added into the solution. Then, methanol (0.03 mL, 0.7 mmol) was added dropwise into the reaction mixture and stirred for 30 minutes at room temperature. After completion of the reaction, the reaction mixture was purged over activated alumina to remove excess $In(OTf)_3$ and followed by the filtrate was concentrated evaporating all of the organic volatiles. Next, column chromatography was

performed using ethyl acetate and hexane (1:2), with the obtained crude product to separate mono-acetalized DFF. After purification, the product was analyzed by ^{1}H nuclear magnetic resonance (NMR) spectrometer (JNM-ECZ600, JEOL), which afforded the DFF-acetal (Me-DFF) in ca. 60% purity.

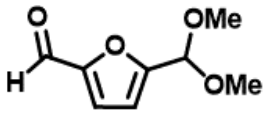

Me-DFF

5-(dimethoxymethyl)furan-2-carbaldehyde (Me-DFF): ^{1}H NMR (400 MHz, $CDCl_3$) 9.66 (s, 1H) 7.24 (d, 1H), 6.65 (d, 1H), 5.48 (s, 1H), 3.41 (s, 6H) ppm.

3.2.5 Catalytic reaction.

The reductive amination of DFF, DFF-acetal (PD-DFF, EG-DFF, and Me-DFF) and AMF-acetal (acetal-protected aminomethyl furan, PD-AMF) were conducted in pressure resistant Teflon-lined stainless steel autoclave reactors. The reductive amination of DFF and DFF-acetal (0.2 mmol) were performed in a methanolic NH_3 solution (7N) under hydrogen pressure of 0.5 MPa at 120 °C for 2 h. While the reductive amination of crude AMF-acetal (0.05 mmol, PD-AMF) was performed with optimum amount of water and acetic acid in a methanolic NH_3 solution (7N) under hydrogen pressure of 0.5 MPa at 120 °C for 3 h. After each reaction, the product distribution was monitored by ^{1}H NMR and GC-FID. The reaction mixture was diluted with 10 mL methanol to dissolve all products, and the solution was analyzed by gas-chromatograph (GC, Shimadzu, GC-4) with a flame ionization detector (FID) using chlorobenzene as an internal standard.

3.2.6 Reuse experiment of Co_2P NRs.

The catalyst was recovered by centrifugation after the reaction and then treated with 0.5 M aqueous CH_3COOH solution (10 mL) for 2 h under sonication, followed by washed with distilled water (10 mL) two times to remove adsorbed species from the catalyst surface. The catalyst was dried under a high vacuum for overnight and used for the next cycle.

3.3 Results and Discussion

3.3.1 Characterization of catalysts.

The formation of crystalline Co_2P was identified by XRD pattern. The diffraction peaks at 2θ = 40.9, 43.4, 52.6 and 56.4 º assigned to (121), (211), (230) and (320) planes, respectively, matches with the β-Co_2P (JCPDS No.054-0413) (**Figure 3.1a**).[36–38] . While Ni_2P exhibited diffraction peaks at 2θ = 40.8, 44.6, 47.6 and 54.3, corresponding to (111), (201), (210) and (300) planes, respectively, pristine-Ni_2P (JCPDS No.03-0953) (**Figure 3.1b**).[43] The Al_2O_3-supported Ni and Co catalysts showed distinct diffraction peaks of metallic Ni, Co and γ phase of Al_2O_3, respectively (**Figure 3.1, c, and d**). On the other hand, ZrO_2-supported Co and Nb_2O_5-supported Ru catalysts displayed only broad diffraction peaks of ZrO_2 and Nb_2O_5, respectively (**Figure 3.1, e, and f**). No diffraction peaks assignable to metal nanoparticles were observed, indicating high dispersion of metal. The XRD pattern of the commercial 5 wt% Ru/C indicates that along with metallic Ru nanoparticles, partially oxidized RuO_2 species are present in the catalyst (**Figure 3.1g**). Furthermore, X-ray photoelectron spectroscopy (XPS) analysis was performed to identify the chemical state of the Co species in Co_2P. The obtained Co 2p spectrum indicates sharp peaks at 777.2 and 792.4 eV, which can be assigned to those of metallic Co $2p_{3/2}$ (777.9 eV) and Co $2p_{1/2}$ (793.5 eV) (**Figure 3.2**).[36–38] Moreover, the slight shift of binding energy in the lower region suggesting transfer of electron cloud from P to Co, which enhances the electron density over metallic Co. The transmission electron microscopy (TEM) images revealed a uniform rod-shaped morphology with diameter and length of 10 and 100–150 nm of Co_2P NRs (**Figure 3.3**).

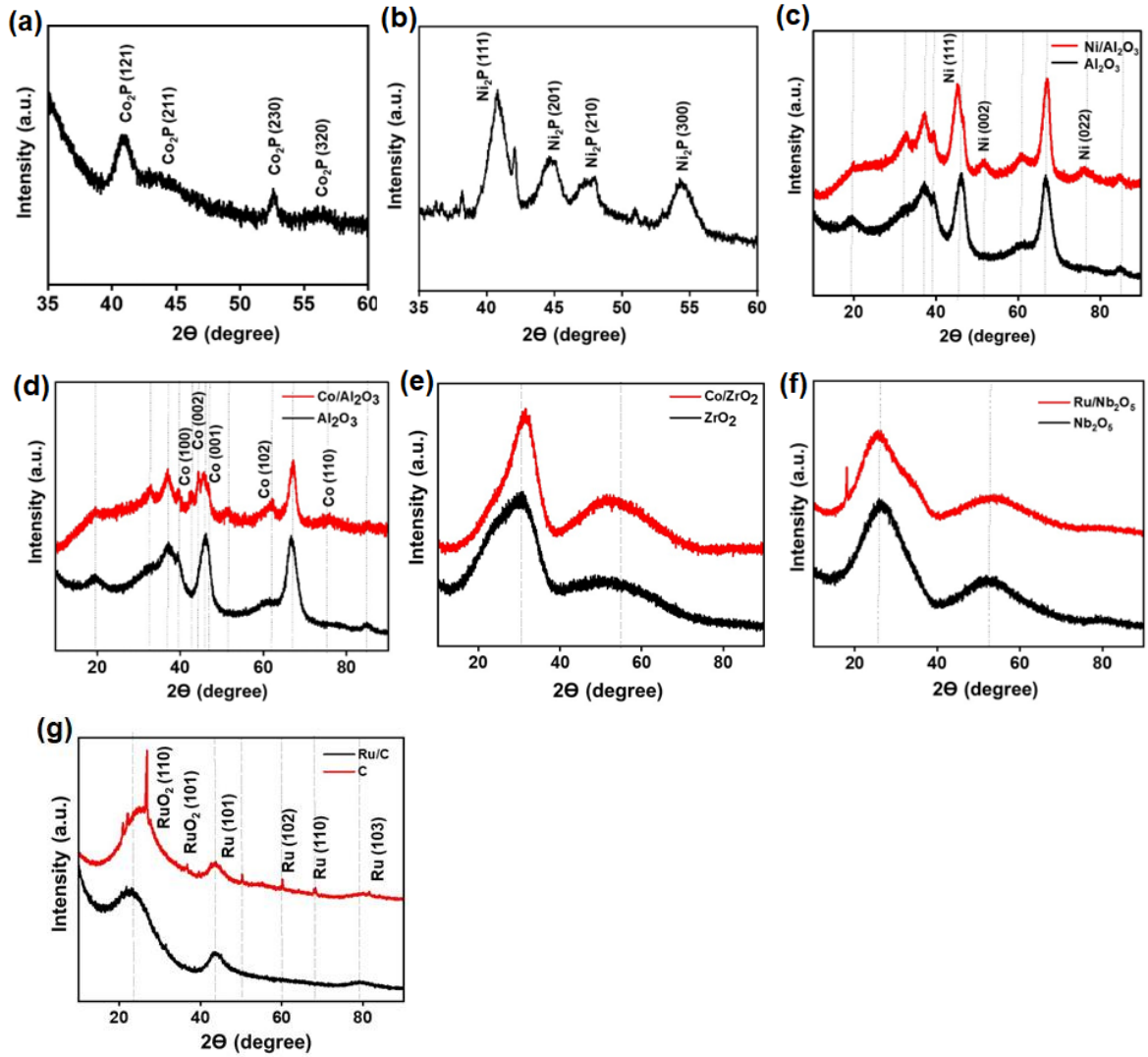

Figure 3.1. XRD patterns of (a) Co_2P, (b) Ni_2P, (c) Al_2O_3 and Ni/Al_2O_3, (d) Al_2O_3 and Co/Al_2O_3, (e) ZrO_2 and Co/ZrO_2, (f) Nb_2O_5 and Ru/Nb_2O_5, and (g) C and Ru/C, respectively.

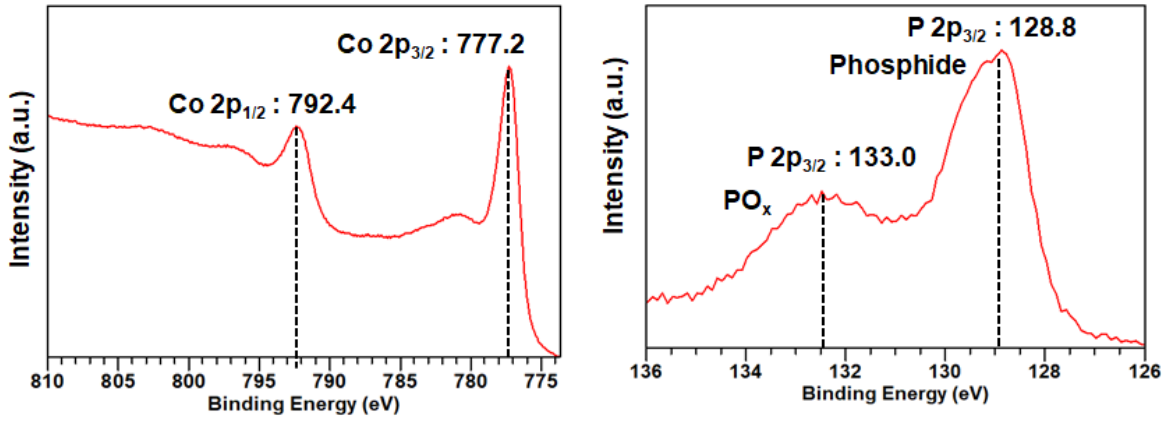

Figure 3.2. Co 2p (a) and P 2p (b) XPS spectra of Co_2P NRs.

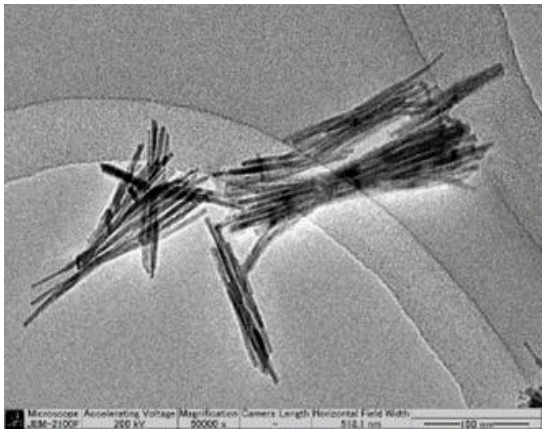

Figure 3.3. TEM images of the Co_2P NRs illustrating a rod-shaped morphology.

3.3.2 Screening of catalysts in the reductive amination of DFF-acetal (PD-DFF).

Initially, the reductive amination of DFF-acetal was investigated with several state-of-the-art catalysts in methanolic ammonia solutions at 120 °C for 2 h under 0.5 MPa hydrogen pressure (**Figure 3.4**).[9,14, 21–30] Co_2P NRs exhibit the highest activity compared to the conventional catalysts as shown in **Figure 3.4**. Reference catalysts generally require a high H_2 pressure to exhibit efficient activity. The higher hydrogenation efficiency of Co_2P NRs is associated with its unique rod-shaped morphology (**Figure 3.3**), which generates a

large content of unsaturated Co-Co active sites on the surface.[36] Mitsudome et al. demonstrated that the coordination number (CN) ratio, CN_{Co-Co}/CN_{Co-P} calculated from the crystal structure of orthorhombic Co_2P NRs, is smaller (1.6) than that of bulk Co_2P (2.0), indicating a high number of coordinatively unsaturated Co-Co sites present on the nanorod surface.[36] Moreover, XPS analysis revealed that alloying phosphorus (P) with metallic Co significantly stabilizes the metallic state of Co (0) and further increases the electron density over it, which is the main active component of the catalyst. Thus, the high abundance of well-defined active sites over the Co_2P NRs surface greatly improves its catalytic activity as compared to other benchmark catalysts (**Table 1.2**).[36].

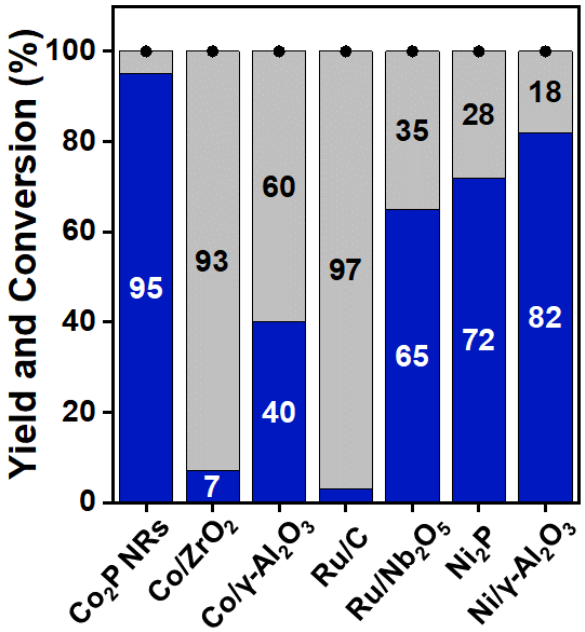

Figure 3.4. Screening of catalysts in the reductive amination of PD-DFF to PD-AMF. Blue bars and grey bars represent the PD-AMF and others yields, respectively. Black circles show the PD-DFF conversion. Reaction conditions: PD-DFF, 0.2 mmol (36 mg); NH_3-MeOH (7 N), 3 mL; 0.5 MPa H_2, 120 ºC, 2 h, stirring rate 600 rpm.

3.3.3 Reductive amination of DFF-acetal with Co_2P NRs.

The reductive amination of PD-DFF was examined with two different nitrogen (N) sources varying the solvent as shown in **Table 3.1**.[36] The reactions were conducted with Co_2P NRs catalyst at 120 °C for 2 h under pressurized hydrogen of 0.5 MPa. **Table 3.1** lists the conversion and product yield for the target reactions at various conditions. **Scheme 3.1** summarizes the reaction pathway in the reductive amination of PD-DFF to PD-AMF. The free formyl group (-CHO) of PD-DFF first reacts with the nitrogen (N) source and undergoes condensation to form a primary imine as the reaction intermediate, which is hydrogenated to PD-AMF by Co_2P NRs.

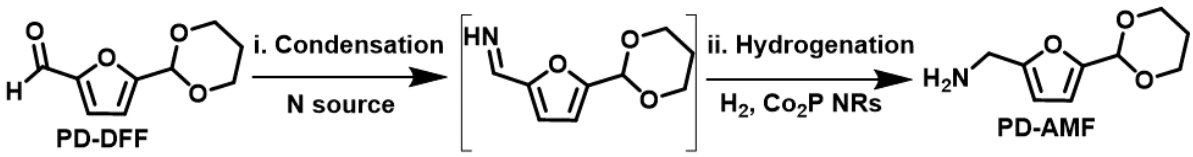

Scheme 3.1. Reaction pathway in reductive amination of PD-DFF to PD-AMF with Co_2P NRs.

A high PD-AMF yield was obtained (95%) exclusively, when the reaction was performed in a methanolic ammonia (NH_3-MeOH) solution (**Table 3.1, entry 1**). In comparison, in aqueous ammonia solution, PD-AMF was produced in moderate yield (40%), with an excess of humin-type byproducts (**Table 3.1, entry 2**). On the other hand, using NH_4OAC as the N source, in methanolic solution provided only polymerized species as major product (**Table 3.1, entry 3)**.[36] To investigate the reason for the difference in product selectivity, the pH of the reaction medium was monitored. A highly basic pH conditions (>12) were observed in the case of methanolic, and aqueous NH_3 solutions of PD-DFF (**Table 3.1, entries 1 and 2**). In the presence of NH_4OAC, the methanolic solution of PD-DFF exhibits slightly lower pH (8.2, **Table 3.1, entry 3**), which indicates that pH is presumably one of the determining factors to the selectivity depending on the stability of the acetal functionality under the reaction conditions. A lower pH leads to the deprotection of the acetal moiety of PD-DFF and produces DFF in the reaction mixture, which causes polymerization of DFF with the reaction intermediates (imine). To assure this phenomenon, the reductive amination of DFF

was performed as a control experiment. Although DFF conversion was 100%, no product was detected under the same reaction condition as PD-DFF (**Table 3.1, entry 4**).

Table 3.1. Reductive amination of PD-DFF and DFF with Co_2P NRs under pressurized hydrogen.[a]

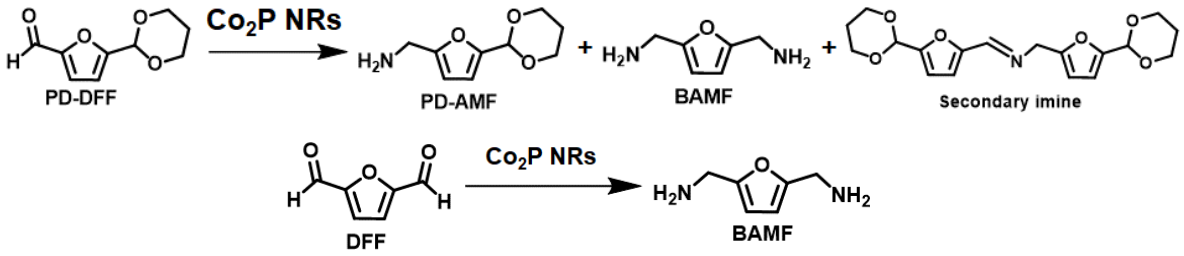

#	Substrate	N source/ Solvent	pH	Conv. (%)	Prroduct Yield (%)			C.B. (%)
					PD-AMF	BAMF	*Sec.* imine	
1	PD-DFF	NH_3/ MeOH	12.6	>99	95	n.d.	1	96
2		NH_3/ H_2O	14.2	>99	40	n.d.	3	43
3		NH_4OAC/ MeOH	8.2	>99	n.d.	n.d.	n.d.	0
4	DFF	NH_3/ MeOH	12.6	>99	n.d.	n.d.	n.d.	0

[a] Reaction condition: PD-DFF/DFF, 0.2 mmol (1.5 wt%); N source, 21 mmol; Solvent, 3 mL; Co_2P NRs (S/C = 9 wt/wt); 120 ºC; 2 h; 0.5 MPa H_2; stirring rate 600 rpm. *Sec.* imine refers to the secondary imine.

The influence of protecting functionality was further revealed by studying the reductive amination of two different DFF-acetals with ethylene glycol (EG) and methanol (Me) (**Table 3.2**). In comparison to PD-DFF, EG-DFF and Me-DFF gave the corresponding EG-AMF and Me-AMF in moderate yields along with humin-type byproducts formation under the same reaction conditions (**Table 3.2**). Control experiments revealed that the difference in AMF-acetal yield is due to the difference in the thermal degradation of acetals under the reaction conditions (**Figure 3.5**).[17,18] The order of the thermal stability of acetals

were found as follows, PD-DFF > EG-DFF > Me-DFF (**Figure 3.5**). The six-membered ring acetal in PD-DFF being thermally more stable than the five-membered ring acetal in EG-DFF and an acyclic acetal in the case of Me-DFF, displays high selectivity toward the desired product under the applied reaction conditions.

Table 3.2. Effect of protecting functionality in the reductive amination of DFF-acetal.[a]

#	Substrate	Conv. (%)	Product Yield (%)		C.B. (%)
			AMF-acetal	Others	
1	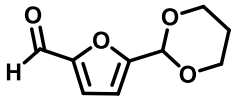 PD-DFF	100	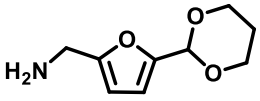 PD-AMF (95)	5	95
2	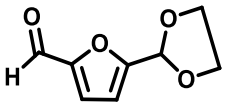 EG-DFF	100	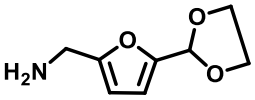 EG-AMF (55)	45	55
3	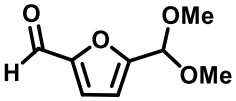 Me-DFF	100	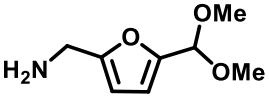 Me-AMF (47)	53	47

[a] Reaction conditions: Substrate, 0.2 mmol; Co_2P NRs, 4 mg; NH_3-MeOH (7 N), 3 mL; 120 ºC, 2 h, 0.5 MPa H_2, stirring rate 600 rpm.

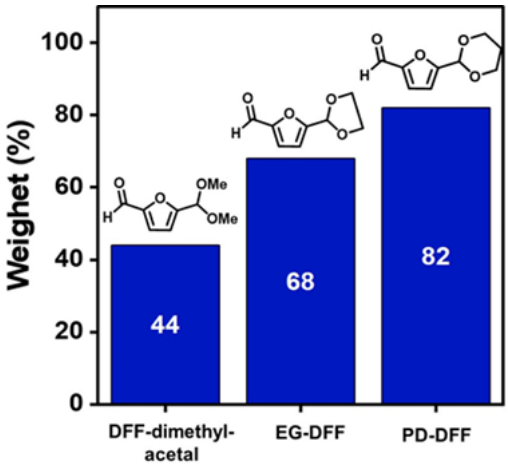

Figure 3.5. Thermal stability test of DFF-acetals. Reaction conditions: Substrate, 0.2 mmol; Super-dehydrated MeOH, 3 mL; 120 ºC; 2 h, 3 MPa Ar, stirring rate 600 rpm.

3.3.3.1 Effect of reaction parameters in the reductive amination of PD-DFF to PD-AMF.

The reductive amination of PD-DFF to PD-AMF was examined by varying the reaction temperature, hydrogen pressure, ammonia to substrate mole ratio (NH_3/PD-DFF) and catalyst loading, respectively as shown in **Figure 3.6**. **Figure 3.6a** demonstrates that varying the reaction temperature, the product distribution was significantly different, while conversion was 100% in the range of 100–140 °C. PD-AMF was obtained with a high yield of 95% at 120 °C for 2 h. By increasing or decreasing the temperatures, the PD-AMF yield decreased remarkably. **Scheme 3.1** summarizes the reaction pathway, which involves an undetectable primary imine as the reaction intermediates. A control experiment was performed prolonging the reaction time at low temperatures. The PD-AMF yield reached 96% from 45% at 100 °C in 4 h suggesting the reaction is kinetically sluggish at low temperature. Thus, the comparatively low yield of PD-AMF at low temperatures (100–110 °C) is due to the presence of undetectable intermediate. On the other hand, the high temperatures (> 120 °C) caused thermal degradation of PD-DFF resulting in low carbon balance as well as low PD-AMF yield. Therefore, to obtain PD-AMF selectively an optimum reaction temperature (120 °C) is required, where it can be produced in high yield (95%)

within a short reaction time (2 h). **Figure 3.6b** reveals the effect of H_2 pressure on the reductive amination of PD-DFF to PD-AMF, where it was observed that at low H_2 pressure due to the incomplete conversion of intermediates the yield of PD-AMF was low (48%, at 0.1 MPa H_2). The PD-AMF yield improved with the increase in H_2 pressure and reached 95% at an ambient H_2 pressure of 0.5 MPa. Further increasing the H_2 pressure impacts negatively resulting in a decrease of PD-AMF selectivity. An optimum H_2 pressure of 0.5 MPa is, therefore, suitable for the selective conversion of PD-DFF to PD-AMF. **Figure 3.6c** indicates the effect of NH_3/Sub mole ratios on the reductive amination of PD-DFF to PD-AMF. NH_3/Sub mole ratio significantly influenced the reaction efficiency, where a high NH_3/Sub mole ratio (105) was required to suppress undesirable side reactions and increase the reaction rate selectively towards primary amine (PD-AMF) formation. At the low NH_3/Sub mole ratio, the chances of side reactions such as condensation of secondary imine with the substrate (PD-DFF) and intermediates (primary imine) enhanced to produce polymeric byproducts due to the small concentration of NH_3, making the reaction less efficient. Therefore, PD-AMF yield decreased to 60% with decreasing NH_3/Sub mole ratio to 35. The effect of catalyst loading on the reaction is shown in **Figure 3.6d**. A high S/C values decrease the PD-AMF yield (34%) due to the most probable reduced hydrogenation rate of the overall reaction. However, still the high conversion (100%) at such low catalyst loading suggests that the condensation of free formyl functionality (-C=O) of PD-DFF with N source (NH_3) to form primary imine is a non-catalytic reaction (**Scheme 3.1**), which was further confirmed by a control reaction. A reaction of PD-DFF at room temperature without catalyst under the same reaction conditions within 10 min resulted in 90% conversion of PD-DFF, while no product was detected suggesting undetectable primary imine formation. In contrast, a high catalyst loading (low S/C (weight ratio), $\leq$ 9 wt/wt) simply leads to the high PD-AMF yield without changing the PD-AMF selectivity significantly. Thus, the Co_2P NRs with an optimal catalyst loading of S/C (weight ratio) = 9 showed a high catalytic activity at a comparatively lower H_2 pressure (0.5 MPa) and reaction temperature (120 °C).

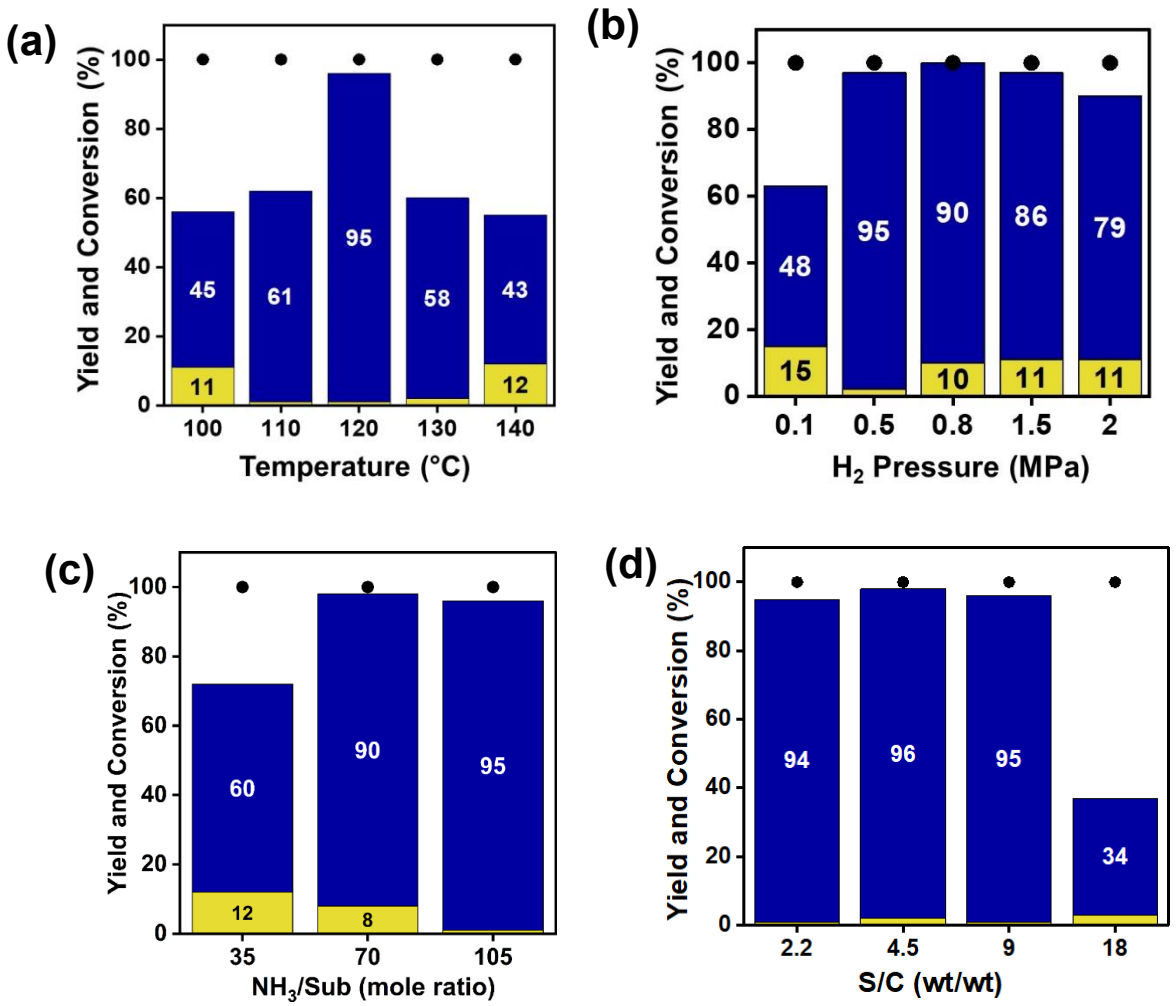

Figure 3.6. Effect of (a) temperature, (b) H_2 pressure, (c) NH_3/Sub (mole ratio), and (d) catalyst loading (S/C, wt/wt), respectively on the reductive amination of PD-DFF to PD-AMF. Blue bars and yellow bars represent the PD-AMF and secondary imine yields, respectively. Black circles show the PD-DFF conversion. Reaction conditions: [a] PD-DFF, 0.2 mmol (36 mg); Co_2P nanorods, 4 mg (S/C = 9 wt/wt); NH_3-MeOH (7 N), 3 mL; 0.5 MPa H_2, 2 h, stirring rate 600 rpm. [b] PD-DFF, 0.2 mmol (36 mg); Co_2P nanorods, 4 mg (S/C = 9 wt/wt); NH_3-MeOH (7 N), 3 mL; 120 ºC, 2 h, stirring rate 600 rpm. [c] PD-DFF, 0.2 mmol (36 mg); Co_2P nanorods, 4 mg (S/C = 9 wt/wt); NH_3-MeOH (7 N), 3 mL; 0.5 MPa H_2, 120 ºC, 2 h, stirring rate 600 rpm. [d] PD-DFF, 0.2 mmol (36 mg); Co_2P nanorods; NH_3-MeOH (7 N), 3 mL; 0.5 MPa H_2, 120 ºC, 2 h, stirring rate 600 rpm.

3.3.3.3 Reductive amination of PD-DFF to PD-AMF with various substrate concentrations.

Next, to improve the productivity of the developed process, the reductive amination of PD-DFF was studied with a methanolic ammonia solution (NH_3-MeOH) increasing its concentration to 5 wt% under the optimized reaction conditions. In concentrated solutions of PD-DFF (5 wt%), PD-AMF yield rapidly decreased from 95% to 54% (**Table 3.3, entries 1 and 2**). Due to the higher nucleophilicity of the primary amine (PD-AMF) than the NH_3, it has a higher tendency to further react with the substrate (PD-DFF) and reaction intermediates (primary imine and secondary imine) to produce subsequently secondary, tertiary amines followed by heavy byproducts (**Scheme 3.2**).[13,44] However, such challenges can be encountered by keeping a high NH_3/Sub ratio (**Table 3.3, entry 1)**.[44] Thus, the dependence of PD-AMF yield to NH_3/PD-DFF mole ratio was examined as shown in **Figure 3.6c**, where the PD-AMF yield was decreased with the decrease of NH_3/PD-DFF mole ratio in accordance with the previous reports.[44] Therefore, the low yield of PD-AMF in a concentrated solution of PD-DFF (5 wt%) can be attributed to the low NH_3/PD-DFF mole ratio (32) under the reaction condition (**Table 3.3, entry 2)**. Additionally, it is reported that by using water as a co-solvent the chemoselectivity of primary amine can be improved.[44] In the presence of water primary amine undergoes hydrolysis to form the corresponding ammonium ions which reduces its nucleophilicity and restrains further reactions to suppress byproduct formations as shown in **Scheme 3.3**.[13,44] However, excessive water can also lead to the formation of ammonium ion simultaneously by NH_3 and water, which lowers the nucleophilicity of NH_3 resulting in the reduction in the formation of corresponding imine and causing low yield of desired primary amine (**Table 3.1, entry 2**).[13,44] Therefore, an optimum amount of water (methanol to water ratio 2:1 (v/v), **Table 3.4**) was added to the methanolic ammonia solution, to improve the PD-AMF yield. After the addition of water PD-AMF yield increased to 73% even at a sufficiently low NH_3/PD-DFF mole ratio (21) under the optimized conditions (**Table 3.3, entry 3**). Further, prolonging the reaction time, the PD-AMF yield remained constant (**Table 3.3, entry 4**), indicating that further optimization of ammonia to substrate ratio using a pressurized NH_3/H_2 gas mixture is essential to obtain PD-AMF in high yields

from concentrated PD-DFF solutions due to limitation in NH_3 concentration of commercially available methanolic NH_3 solutions (≤ 7N).

Table 3.3. Reductive amination of PD-DFF with various substrate concentrations.[a]

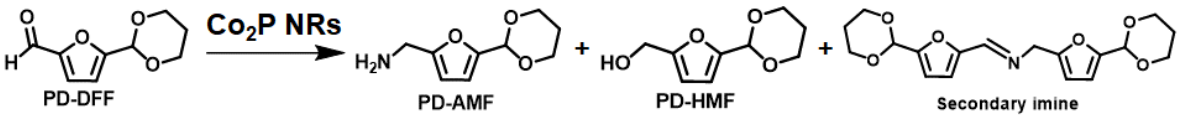

#	Conc. (wt%)	t (h)	NH_3-MeOH (mL)	D_2O (mL)	NH_3/Sub (mole ratio)	Conv. (%)	Prroduct Yield (%)			C.B. (%)
							PD-AMF	PD-HMF	Sec. imine	
1[a]	1.5	2	3	-	105	>99	95	n.d.	1	96
2[b]	5				32	>99	54	n.d.	n.d.	54
3[b]	5	2	2	1	21	>99	73	5	0.4	78
4[b]	5	4	2	1	21	>99	74	5	n.d.	79

[a] Reaction condition: [a]PD-DFF, 0.2 mmol; [b]PD-DFF, 0.65 mmol; Co_2P NRs (S/C = 9 wt/wt); 120 ºC; stirring rate 600 rpm.

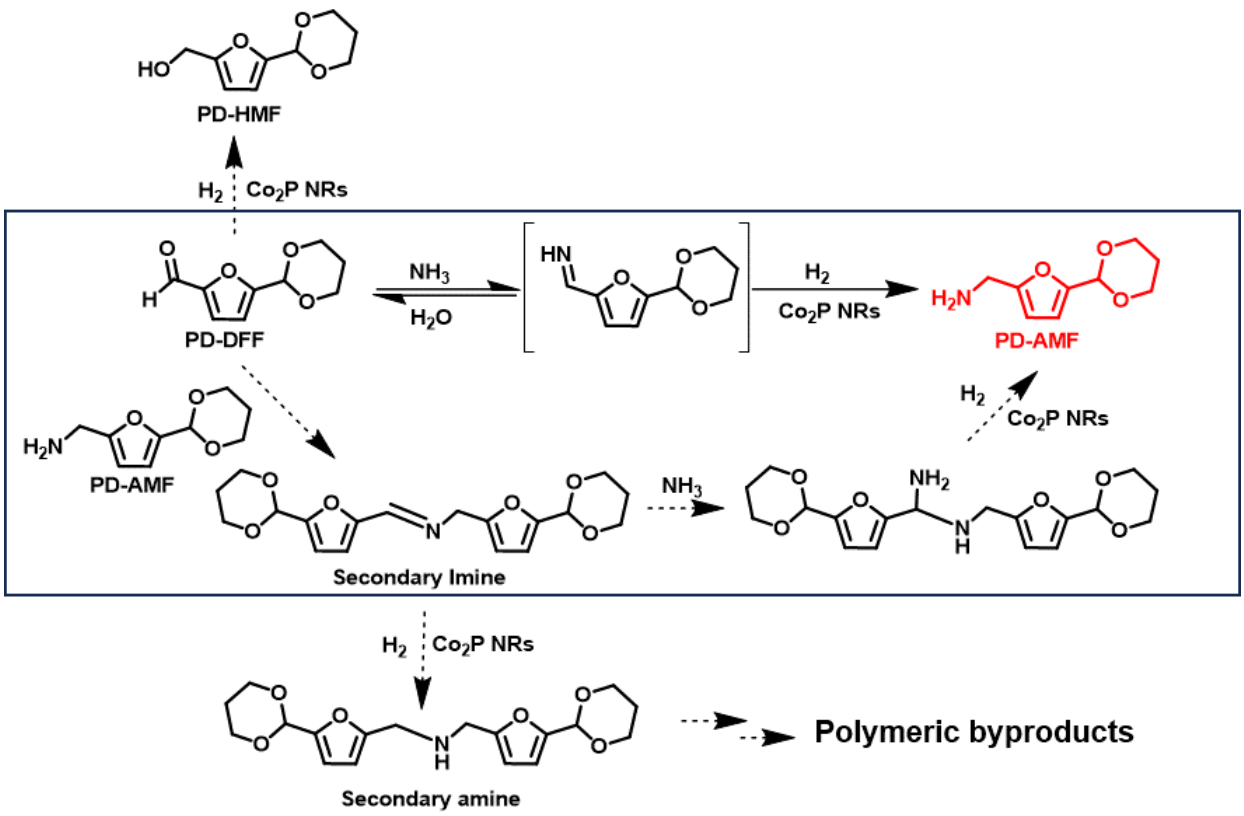

Scheme 3.2. Possible reaction pathways for the conversion of PD-DFF to PD-AMF.

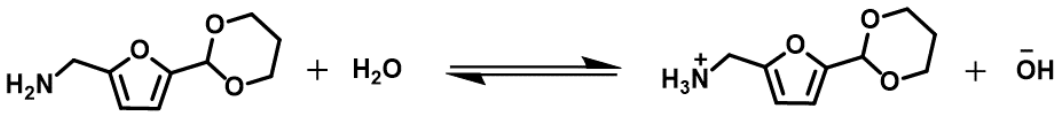

Scheme 3.3. Hydrolysis of PD-AMF to form corresponding ammonium ion.

Table 3.4. Effect of water (D_2O) content in the reductive amination of PD-DFF to PD-AMF.[a]

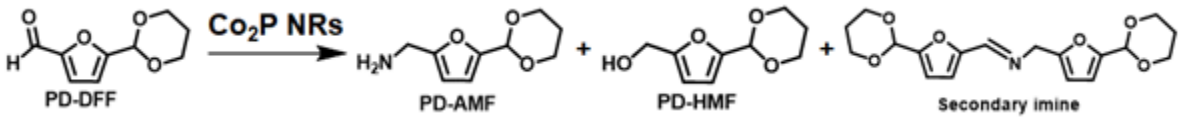

#	NH_3-MeOH (mL)	NH_3-H_2O (mL)	D_2O (mL)	NH_3/PD-DFF (mole ratio)	t (h)	Conv. (%)	Product Yield (%)			C.B. (%)
							PD-AMF	PD-HMF	*Sec.* imine	
1	3	-	0	105		100	95	n.d.	1	96
2	2	-	1	70		100	92	7	n.d.	99
3	1.5	-	1.5	52	2	100	88	11	n.d.	99
4	1	-	2	35		100	81	16	n.d.	97
5	0.5	-	2.5	17		100	68	29	n.d.	97
6	0.5	-	2.5	17	4	100	49	27	n.d.	76
7	-	1	2	70	2	100	54	6	n.d.	60

[a] Reaction conditions: PD-DFF, 0.2 mmol; Co_2P NRs, 4 mg; NH_3-MeOH (7 N), NH_3-H_2O (14.8 M), 120 ºC; 2 h, 0.5 MPa H_2, stirring rate 600 rpm.

3.3.3.4 Kinetic study in the reductive amination of PD-DFF to PD-AMF.

To clarify the reaction dynamics for the reductive amination of PD-DFF to PD-AMF in methanol and methanol-water (2:1, v/v) mixture with NH_3, the reaction kinetics was studied by monitoring the product distribution under optimized reaction conditions.[45] **Figures 3.7A and 3.7B** display the time courses for PD-DFF (1.5 wt%) conversion and

product yields in methanol and methanol-water mixture (2:1, v/v), respectively during 3 h of the reaction. The kinetic traces were fitted with pseudo-first-order reaction kinetics, which provides reaction rate constants for elementary steps (**Scheme 3.4 and 3.5**).

When the reaction was performed in methanolic NH_3 solution, PD-DFF was consumed (100%) instantly under the reaction conditions (120 ºC, 0.5 MPa H_2), whereas no desired product was observed until 20 min **(Figure 3.7A)**. At 30 min, PD-AMF was detected with 36% yield and 66% others, of which 20% was secondary imine. With the progress of the reaction, the others yield decreased, and PD-AMF yield improved, suggesting the primary imine formation is very fast, and it is a major undetectable intermediate in the initial stages of the reaction. A maximum yield of 95% PD-AMF was obtained after 2 h and kept almost constant. The rate constant for PD-AMF formation in methanolic ammonia solution was 1.5 h^{-1}, while the rate constant for byproduct formation was 1.5 h^{-1} (k_1) > 0.03 (k_2) > 0.024 h^{-1} (k_3), which reveals that the acetal functionality is high stable against deprotection and prevents side reactions (**Scheme 3.4**). In addition, due to the high NH_3/PD-DFF mole ratio (105), secondary imine formation was largely suppressed, which further reduced the chance of polymeric byproducts formation via secondary and tertiary amine formations with PD-DFF as shown in **scheme 3.2**. Based on these results, a possible reaction pathway is suggested in **Scheme 3.1**.

In comparison, a slight difference in product distribution was detected when the reaction was performed in methanol-water mixture (2:1, v/v) with NH_3. The initial trend of was same as in methanolic ammonia solution of PD-DFF (1.5 wt%) (**Figure 3.7A and 3.7B)** but comparatively faster reaction rate was confirmed ($k_4 > k_1$) in methanol-water mixture (2:1, v/v) (**Scheme 3.4 and 3.5**). During the first 10 min, no product was detected even at full conversion. Surprisingly, at 20 min, PD-AMF was present with 19% yield along with others in 81% yield of which PD-HMF and secondary imine were in 4%, and 12%, respectively. Then, the PD-AMF yield rapidly increased to 64% with a slight increase in PD-HMF yield (7%) whereas the secondary imine and undetectable products yield decreased to 5% and 24%, respectively, at 30 min. After 2 h, the PD-AMF yield reached maximum to 92% while the PD-HMF yield remained constant (7%), suggesting that PD-HMF is the major byproduct

formed among others and remaining products (undetectable primary imine and secondary imine) correspond to the reaction intermediate. Notably, although NH_3/PD-DFF mole ratio (70) was comparatively low in methanol-water (2:1, v/v) mixture, secondary imine was produced in negligible amount, indicating that the addition of water stabilizes the PD-AMF via formation of corresponding ammonium ions by hydrolysis as shown in **Scheme 3.3**, which can reduce the nucleophilicity of the PD-AMF and subsequent byproducts formation. Thus, it can be assumed that the reaction proceeds mainly involving the primary imine as an intermediate, produced via condensation of PD-DFF with NH_3 followed by hydrogenation of the primary imine gives PD-AMF. However, the presence of water induces the formation of PD-HMF by the hydrogenation of formyl group (-CHO) of PD-DFF to an alcohol (-CH_2OH) moiety. The rate constants for PD-AMF and PD-HMF formation in this system was 2.4 h^{-1} (k_4) and 0.24 h^{-1} (k_5), respectively, while no humin-type byproduct formation was observed (**Scheme 3.5)**, indicating that the hydrogenation of PD-DFF to PD-HMF is limited and the six-membered ring acetal is highly stable against deprotection even in the presence of additional water. Thus, the addition of an optimum amount of water to a methanolic ammonia solution facilitates the reductive amination of PD-DFF by decreasing the nucleophilicity of PD-AMF and subsequent byproducts formation.

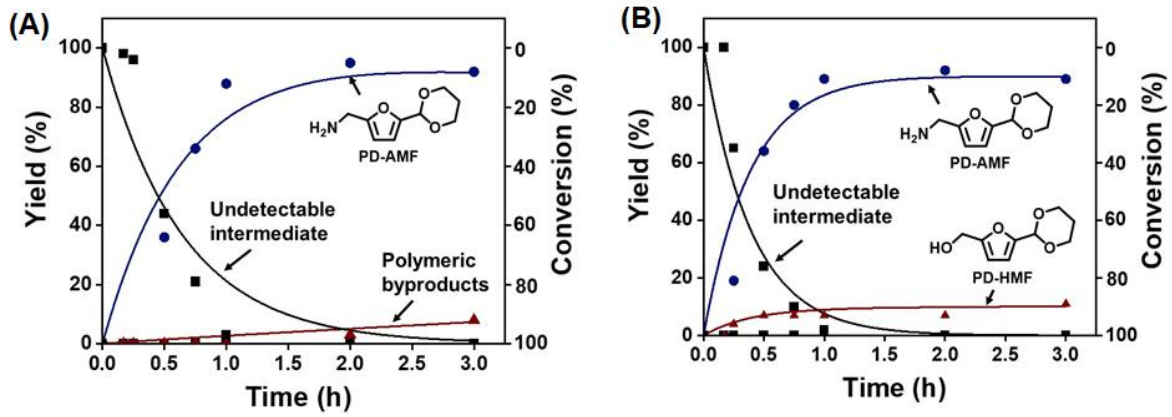

Figure 3.7. Time courses for reductive amination of PD-DFF to PD-AMF with NH_3 using Co_2P NRs in methanol (A) and methanol-water (2:1, v/v) mixture (B), respectively. Undetectable intermediate conversion, black line, and symbols; PD-AMF yield, blue line, and symbols; polymeric byproducts and PD-HMF yield, brown line, and symbols, respectively in (A) and (B). Time course lines were modelled assuming pseudo-first-order reaction model. Reaction Conditions: PD-DFF, 0.2 mmol (36 mg); Co_2P nanorods, 4 mg (S/C = 9 wt/wt); Solvent, 3 mL; 0.5 MPa H_2, 120 ºC, 3 h, stirring rate 600 rpm.

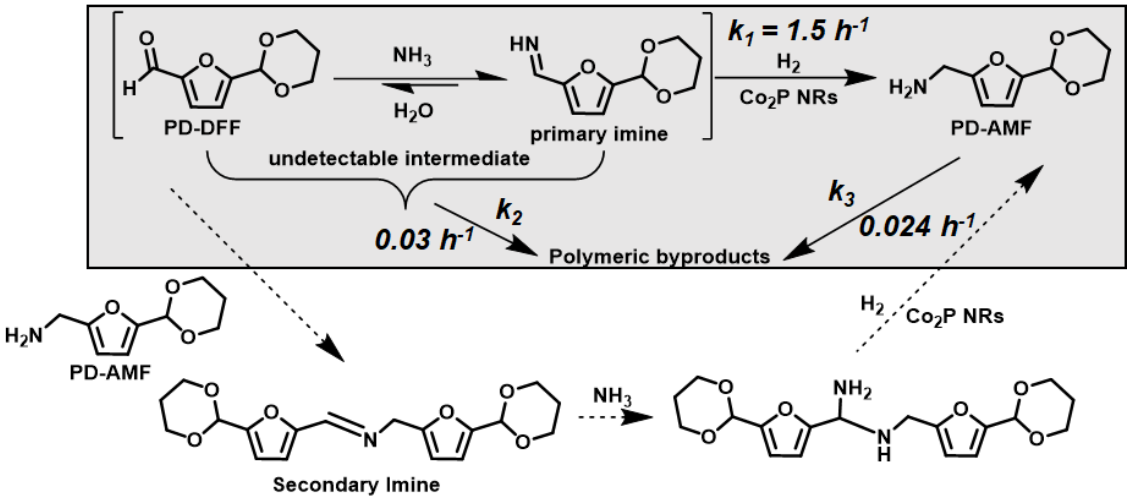

Scheme 3.4. Reaction networks for the reductive amination of PD-DFF to PD-AMF in methanol with Co_2P NRs. Grey box indicates the major reaction pathway.

Scheme 3.4 illustrates the possible reaction pathways for the synthesis of PD-AMF in methanol. Reaction rate constants (k_1, k_2, and k_3) were estimated by the following equations-

$$\frac{d[\text{undetectable intermediates}]}{dt} = -(k_1+k_2)\,[\text{undetectable intermediates}] \quad \text{(S1)}$$

$$\frac{d[\text{PD-AMF}]}{dt} = k_1\,[\text{undetectable intermediate}] - k_3\,[\text{PD-AMF}] \quad \text{(S2)}$$

$$\frac{d[\text{Polymeric byproducts}]}{dt} = k_2\,[\text{undetectable intermediate}] + k_3\,[\text{PD-AMF}] \quad \text{(S3)}$$

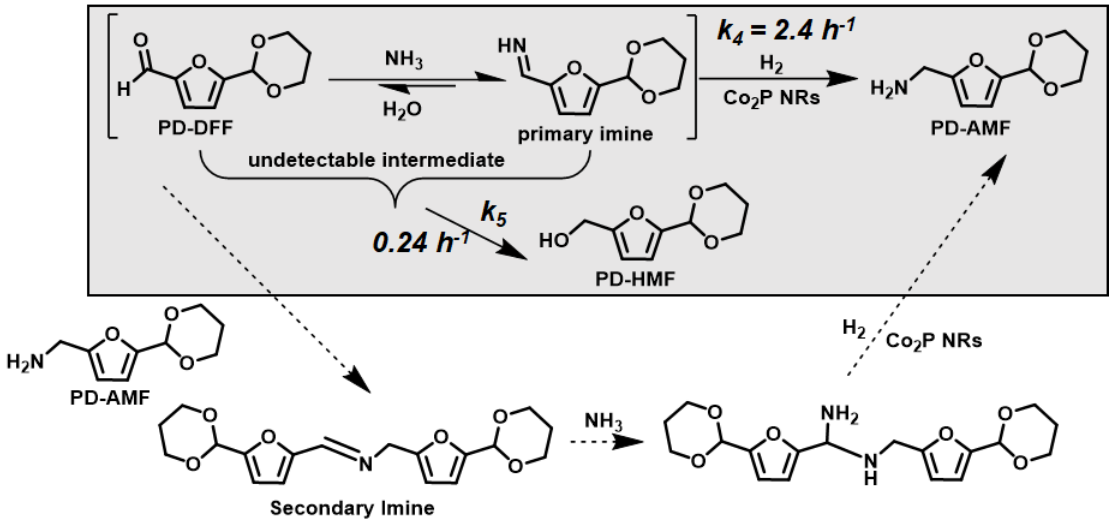

Scheme 3.5. Reaction networks for the reductive amination of PD-DFF to PD-AMF in methanol-water (2:1) mixture with Co_2P NRs. Grey box indicates the major reaction pathway.

Scheme 3.5 illustrates the possible reaction pathways for the synthesis of PD-AMF in methanol-water mixture. Reaction rate constants (k_4, and k_5) were estimated by the following equations-

$$\frac{d[\text{undetectable intermediates}]}{dt} = -(k_4+k_5)\,[\text{undetectable intermediates}] \quad \text{(S4)}$$

$$\frac{d[\text{PD-AMF}]}{dt} = k_4\,[\text{undetectable intermediate}] \quad \text{(S5)}$$

$$\frac{d[\text{PD-HMF}]}{dt} = k_5\,[\text{undetectable intermediate}] \quad \text{(S6)}$$

3.3.3.5 Recyclability of Co_2P NRs in the reductive amination of PD-DFF to PD-AMF.

The reusability of Co_2P NRs in the reductive amination of PD-DFF (1.5 wt%) was examined with NH_3 in a methanol-water (2:1, v/v) mixture under optimized reaction conditions. **Figure 3.8A** shows that the catalyst can be used for at least up to four cycles retaining its original activity.[36] XRD pattern of the spent catalyst after four runs exhibited diffraction peaks without any shift, indicating no structural change during the reactions (**Figure 3.9)**. Next, to evaluate the stability of the catalyst under the reaction conditions, a leaching test was performed. The catalyst was filtered from the reaction solution at 20 min, and the reaction was continued for an additional 100 min without a catalyst (**Figure 3.8B**). The reaction stopped completely after the removal of the catalyst, suggesting no leaching of Co nanoparticles. These results demonstrate the high stability of the catalysts under the reaction conditions and the heterogeneous nature for the reaction. The high stability and reusability of Co_2P NRs can be attributed to the alloying of a non-metal "P" atom with metallic Co, which stabilizes its intrinsic activity. In contrast, previously reported catalysts, Ni/γ-Al_2O_3, showed a significant decrease in catalytic activity during the reaction due to the structural composition changes. The γ-Al_2O_3 lost its original structure under the reaction conditions due to the formation of Ni_3N on the surface caused by strong adsorption of NH_3.[23] The reason behind such phenomenon is presumably due to the acidic nature of support (γ-Al_2O_3), which is highly susceptible to NH_3 adsorption over its surface and the high reaction temperature (160 °C) resulting in severe poisoning of active sites. Herein, such strong adsorption of NH_3 over the catalyst surface can be diminished due to the surface modification of Co alloying with P atoms instead of using conventional support material. Though NH_3 is weakly adsorbed over the Co_2P surface, such poisoning can be mitigated via simple washing treatment with a dilute acetic acid solution (0.5 M) to neutralize NH_3 as its salt.

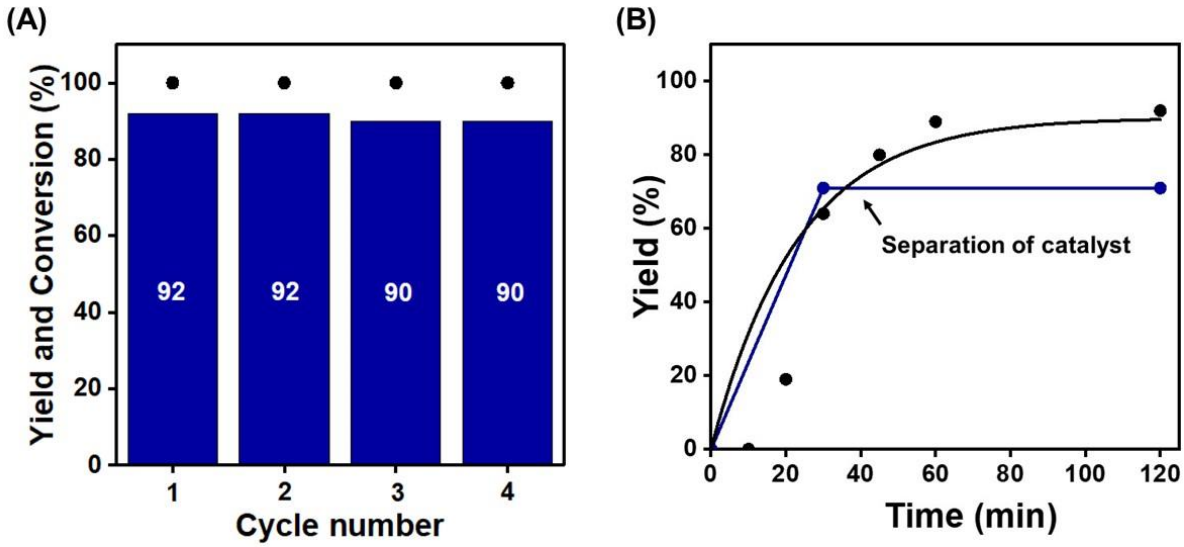

Figure 3.8. (A) Recyclability tests and (B) Leaching test of Co_2P NRs in the reductive amination of PD-DFF to PD-AMF. Reaction Conditions: PD-DFF, 0.2 mmol (36 mg); Co_2P NRs, 4 mg (S/C = 9 wt/wt); NH_3-MeOH, 2 mL; D_2O, 1 mL; 0.5 MPa H_2, 120 ºC, 2 h, stirring rate 600 rpm.

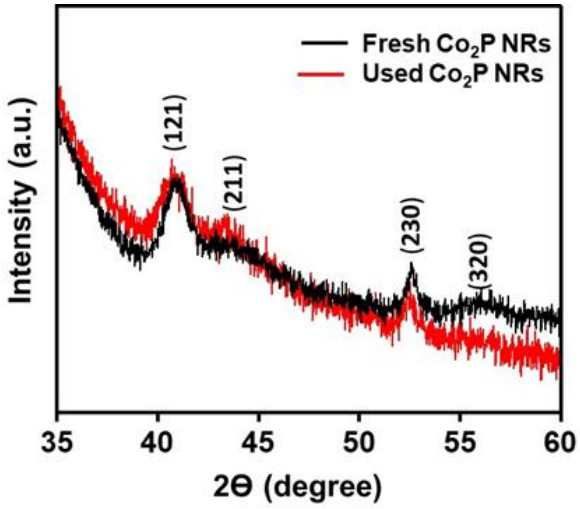

Figure 3.9. XRD patterns of fresh (black line) and used (red line) Co_2P NRs after fourth reuses in the reductive amination of PD-DFF to PD-AMF.

3.3.4 Reductive amination of PD-AMF to BAMF with Co_2P NRs varying N source.

The reductive amination of crude PD-AMF was performed with NH_3 and NH_4OAC as the nitrogen (N) sources using an optimum amount of Co_2P NRs catalyst in methanol-water mixture (2:1, v/v) at 120 °C for 3 h under H_2 pressure of 0.5 MPa. **Scheme 3.6** summarizes a possible reaction pathway for the conversion of PD-AMF to BAMF, which involves the partial hydrolysis of acetal moiety of PD-AMF to a hemiacetal, followed by a hemiaminal formation with the N source and subsequent hydrogenation to primary amine via a primary imine intermediate.

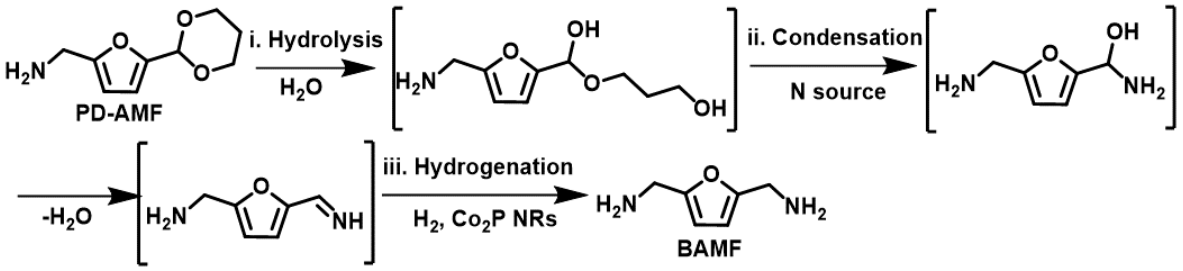

Scheme 3.6. Proposed reaction pathway for reductive amination of PD-AMF to BAMF with Co_2P NRs.

Table 3.6 lists the conversion and product yield for the target reaction at various conditions. When the reaction was conducted with NH_3 in methanol-water (2:1) mixture without any additives, PD-AMF remained stable under the reaction conditions and no product was detected (**Table 3.6, entry 1**). In contrast, in presence of NH_4OAC under the same reaction conditions, a complete conversion of PD-AMF was observed mainly with humin-type byproduct formations (**Table 3.6, entry 2)**.

Table 3.6. Reductive amination of PD-AMF to BAMF with Co_2P NRs in methanol-water (2:1, v/v) mixed solvent under pressurized H_2.[a]

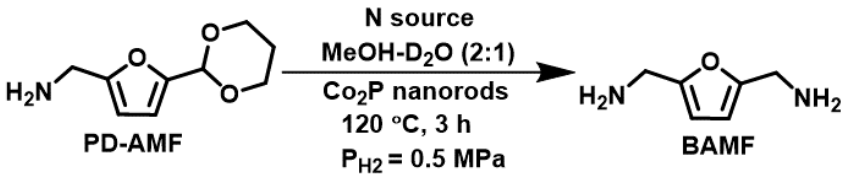

Entry	Substrate	N source	Additives	Conv. (%)	Product Yield (%)	
					BAMF	byproducts
1	PD-AMF	NH_3	-	0.5	n.d.	0.5
2		NH_4OAC	-	>99	n.d.	100

[a] Reaction condition: PD-AMF, 0.05 mmol; N source, 14 mmol; MeOH, 2 mL; D_2O, 1 mL; Co_2P NRs (4 mg, S/C = 2.3 wt/wt); 120 ºC; 3 h; 0.5 MPa H_2; stirring rate 600 rpm.

3.3.4.1 Effect of pH in the reductive amination of PD-AMF to BAMF.

To enhance the selectivity towards the desired product, the pH of the reaction mixture was tuned by the addition of CH_3COOH as an additive and the results are shown in **Table 3.7**. At high pH (12.2) conditions, the conversion of acetal moiety to a primary amine was highly challenging due to the high stability of the acetal functionality of PD-AMF (**Table 3.7**, **entry 1**). With the decrease in pH (10.6), the conversion of PD-AMF increased rapidly from 1% to 78% with a BAMF yield of 71% (**Table 3.7, entry 2**). Further decreasing the pH, the conversion of PD-AMF gradually increased the BAMF yield (**Table 3.7, entry 3**). A high yield of BAMF (94%) was obtained with the addition of an optimum amount of acetic acid (3.5 mmol) at pH = 10.1 (**Table 3.7, entry 4)**. On the other hand, the BAMF yield rapidly decreased in the presence of excess acetic acid (pH <10), even at the full conversion, suggesting that the polymerization of the BAMF with the *in-situ* formed reaction intermediates gave a low BAMF yield (**Table 3.7, entries 5**–**6**). Previous reports revealed that adding a certain amount of weak acids such as acetic acid, formic acid, and, $HCOONH_4$ favors the reductive amination reactions suppressing byproducts formation.[46,47] As described earlier, the primary amine has higher nucleophilicity than NH_3, therefore, it is more

likely to undergo condensation reactions with several reaction intermediates to produce byproducts.[13,44] However, the addition of such weak acid can reduce significantly the nucleophilicity of the primary amine facilitating its ionization to form the ammonium ions (**Scheme 3.7**).[46,47] Moreover, the weak acid environment also benefits to form the corresponding primary imine via proton donation to the -CH=O functionality, where a weak nucleophile such as NH_3 can easily attack.[46,47] Similarly, herein, the addition of acetic acid in the reductive amination of PD-AMF to BAMF promotes the hydrolysis of the acetal functionality and facilitate the subsequent reductive amination reaction as shown in **Scheme 3.6**.

Table 3.7. Effect of acetic acid (CH_3COOH) content on the reductive amination of PD-AMF to BAMF in methanol-water (2:1, v/v) mixed solvent under pressurized H_2.[a]

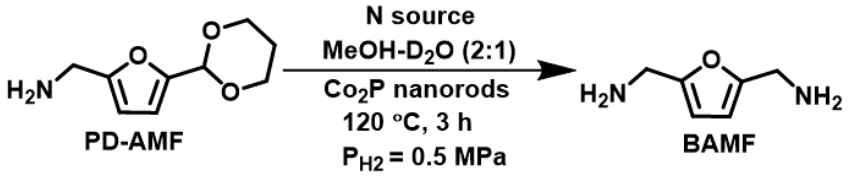

Entry	t (h)	NH_3 (mmol)	CH_3COOH (mmol)	pH	Conv. (%)	Product Yield (%)		C.B. (%)
						BAMF	Others	
1	3	14	0	12.2	1	0	1	99
2			1.7	10.6	78	71	7	93
3			2.6	10.4	81	75	6	94
4			3.5	10.1	100	94	6	94
5			7.0	9.3	100	43	57	43
6			9.6	6.8	100	34	66	34

[a] Reaction conditions: PD-AMF, 0.05 mmol; Co_2P NRs, 4 mg; NH_3-MeOH (7 N), 2 mL; D_2O, 1mL; 0.5 MPa H_2, 120 ºC, stirring rate 600 rpm. Others indicate undetectable intermediate and polymeric byproducts.

Scheme 3.7. Ionization of primary amines in presence of acetic acid to alkylammonium species.

3.3.4.2 Effect of NH_3/Sub mole ration in the reductive amination of PD-AMF to BAMF.

The influence of NH_3/Sub (NH_3/PD-AMF) mole ratio in the reductive amination of PD-AMF to BAMF was investigated as shown in **Table 3.8**. When the NH_3/PD-AMF mole ratio was sufficiently high (**Table 3.8, entries 1 and 2**), BAMF was obtained in high yield (94%) with an optimum amount of acetic acid under the optimized reaction conditions. By further decreasing the NH_3/PD-AMF mole ratio, the BAMF yield decreased from 94% to 79% **(Table 3.8, entry 3)**. These results suggest that an optimum amount of NH_3/Sub mole ratio is inevitable to suppress byproduct formation in the reductive amination reactions irrespective of the nature of substrate.[44]

Table 3.8. Effect of NH_3/PD-AMF (mole ratio) in the reductive amination of PD-AMF to BAMF with Co_2P NRs in methanol-water (2:1, v/v) mixed solvent under pressurized H_2.[a]

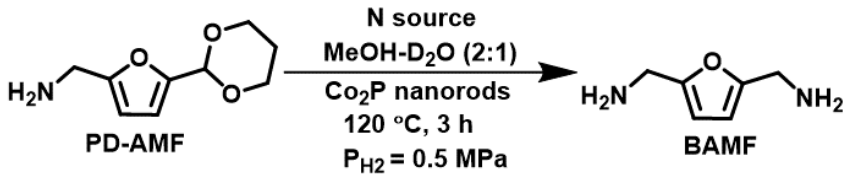

Entry	MeOH (mL)	D_2O (mL)	CH_3COOH (mL)	NH_3/PD-AMF (mole ratio)	Conv. (%)	Product Yield (%)	
						BAMF	byproducts
1	2	1	0.2	327	>99	94	6
2	1	0.5	0.1	164	>99	94	6
3	0.5	0.25	0.5	82	>99	79	21

[a] Reaction condition: PD-AMF, 0.05 mmol; NH_3-MeOH, 7 (N); MeOH-D_2O, (2:1, v/v); Co_2P NRs (S/C = 2.3 wt/wt); 120 ºC; 3 h; 0.5 MPa H_2; stirring rate 600 rpm.

3.3.4.3 Kinetic studies in the reductive amination of PD-AMF to BAMF.

Ideally, to synthesize BAMF from PD-AMF via reductive amination, first the acetal moiety of PD-AMF should be deprotected to a free formyl group (-CH=O) corresponding to AMFC (5-aminomethylfuran carbaldehyde), which can undergo condensation with a N source to form an imine, followed by hydrogenation of the imine to amine as shown in **Scheme 3.8**.

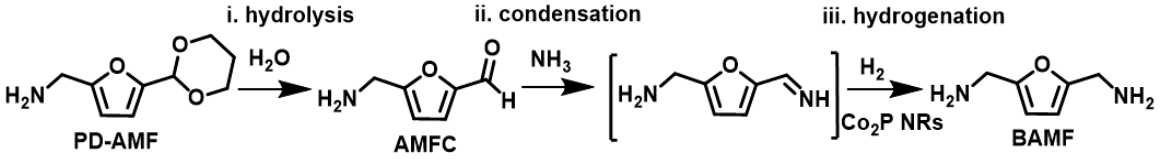

Scheme 3.8. Conventional reaction pathway for reductive amination of PD-AMF to BAMF with Co_2P NRs.

To monitor the product distributions, the reaction kinetics was studied during 4 h of the reaction. **Figure 3.10** displays the time courses for PD-AMF conversion and product yields.

The kinetic traces were fitted with pseudo-first-order reaction kinetics (**Scheme 3.9**), which provides reaction rate constants for elementary steps. In this study, during 4 h of the reaction, only PD-AMF and BAMF were detected, no reaction intermediates (AMFC and imine) were observed. At the beginning, PD-AMF was consumed, whereas any product (BAMF) was undistinguishable until 15 min, and the carbon balance was low. After 30 min, BAMF was observed with 26% yield, which rapidly increased to 75% at 1 h with almost full conversion of PD-AMF (95%). Then, BAMF yield reached slowly to 94% at 3 h with improving the carbon balance, suggesting that fully deprotection of acetal moiety under the reaction conditions (pH = 10.1) did not proceed. A partial hydrolysis of the acetal moiety most probably occurred, which further reacts instantly with NH_3 to form an undetectable primary imine as the intermediate, followed by hydrogenation of the primary imine to the desired amine (BAMF) as shown in **Scheme 3.9**. The reaction rate constants calculated for the partial hydrolysis of PD-AMF and subsequent reductive amination of the intermediate to BAMF were 2.1 h^{-1} and 3.1 h^{-1}, respectively. On the other hand, the rate constants for byproduct formation were negligibly small, following the order of $k_9 > k_8 > k_{10}$ (**Scheme 3.9**). These results indicate that for selective production of amine from the acetal, the rate of hydrolysis should be slow, but the rate of reductive amination should be comparatively faster as the generated reaction intermediates (such as AMFC after complete deprotection of PD-AMF) could lead to rapid polymerization reaction resulting in low product yield (**Table 3.7, entries 5 and 6**). Thus, a combination of NH_3 and CH_3COOH can control the reaction selectivity in this manner, where the pH was controlled by the addition of the optimum amount of CH_3COOH. It can slowly hydrolyze the acetal moiety to form a hemiacetal, and facilitate the subsequent reductive amination to BAMF by decreasing the nucleophilicity of the substrate (PD-AMF) and product (BAMF) via the formation of corresponding alkylammonium ions (**scheme 3.7**). [46, 47]

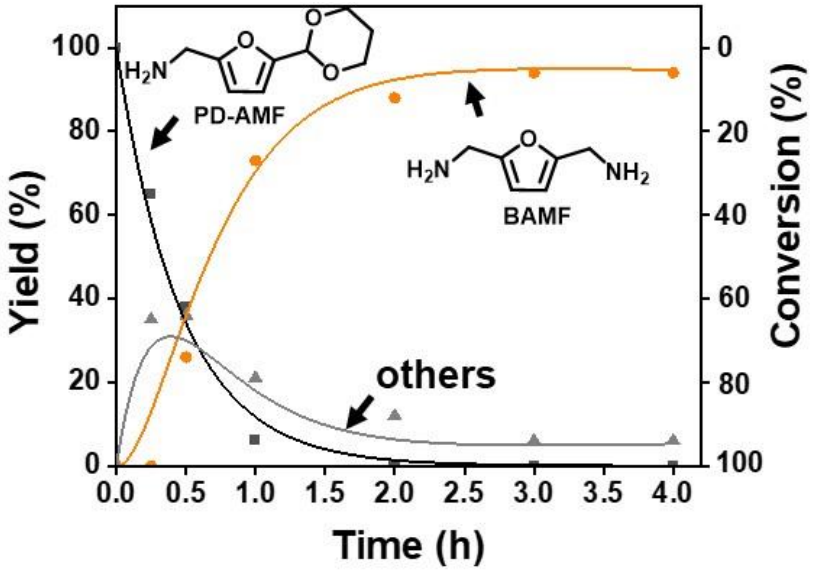

Figure 3.10. Time courses for reductive amination of PD-AMF to BAMF with NH_3 using Co_2P NRs in methanol-water (2:1) mixture. PD-AMF conversion, black line, and symbols; BAMF yield, orange line, and symbols; and others yield, grey line, and symbols. Time course lines were modelled assuming pseudo-first-order reaction model. Reaction Conditions: PD-AMF, 0.05 mmol (9 mg); Co_2P NRs, 4 mg (S/C = 2.3 wt/wt); CH_3COOH, 0.1 mL; NH_3-MeOH, 1 mL; D_2O, 0.5 mL; 0.5 MPa H_2, 120 ºC, stirring rate 600 rpm. Others indicate undetectable intermediate and polymeric byproducts.

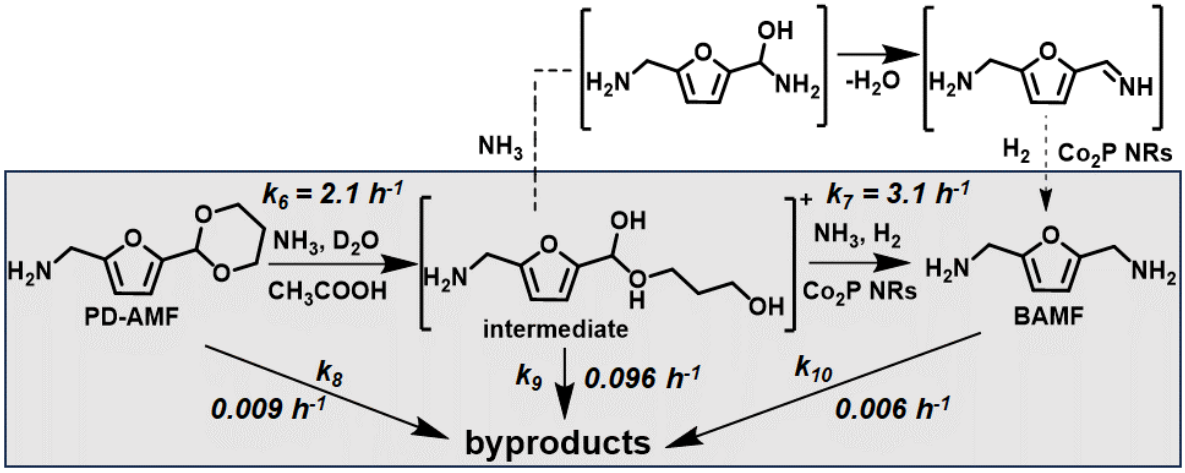

Scheme 3.9. Reaction networks for the reductive amination of PD-AMF to BAMF in methanol-water (2:1, v/v) mixture with Co_2P NRs.

Scheme 3.9 illustrates the possible reaction pathways for the synthesis of BAMF, where the conversion of intermediate to BAMF was integrated as a single step reaction. Reaction rate constants (k_6, k_7, k_8 and k_9) were estimated by the following equations-

$$\frac{d[\text{PD-AMF}]}{dt} = -(k_6+k_8)\,[\text{PD-AMF}] \quad \text{(S1)}$$

$$\frac{d[\text{intermediate}]}{dt} = k_6\,[\text{PD-AMF}] - (k_7+k_9)\,[\text{intermediate}] \quad \text{(S2)}$$

$$\frac{d[\text{BAMF}]}{dt} = k_7\,[\text{intermediate}] - k_{10}[\text{BAMF}] \quad \text{(S3)}$$

$$\frac{d[\text{byproducts}]}{dt} = k_8\,[\text{PD-AMF}] + k_9[\text{intermediate}] + k_{10}\,[\text{BAMF}] \quad \text{(S4)}$$

3.3.4.4 Recyclability of Co_2P NRs in the reductive amination of PD-AMF to BAMF.

The reusability of the Co_2P NRs was evaluated for the consecutive three runs in the conversion of PD-AMF to BAMF to confirm its stability under the reaction conditions. **Figure 3.11** reveals that the catalyst retained its original activity for at least three cycles.

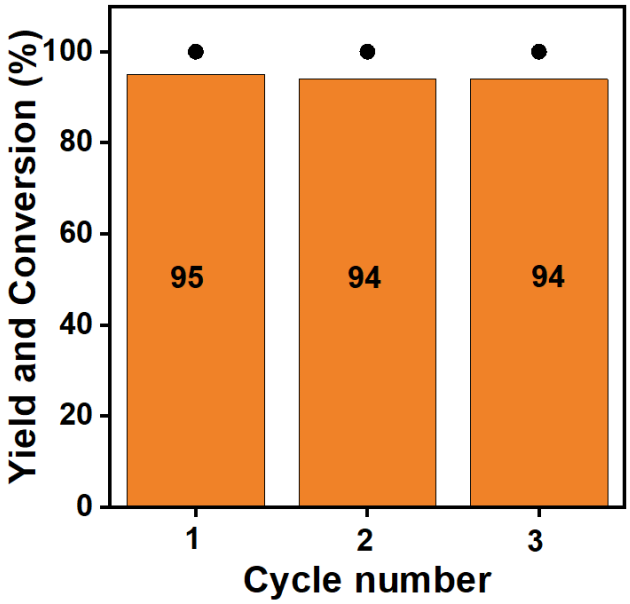

Figure 3.11. Recyclability tests of Co_2P NRs in the reductive amination of PD-AMF to BAMF. Orange bars and black circle represent the BAMF yield and PD-AMF conversion, respectively. Reaction Conditions: PD-AMF, 0.05 mmol (9 mg); Co_2P nanorods, 4 mg (S/C = 2.3 wt/wt); NH_3-MeOH (7 N), 1 mL; D_2O, 0.5 mL; CH_3COOH, 0.1 mL; 0.5 MPa H_2, 120 ºC, 3 h, stirring rate 600 rpm.

3.3.5 Stepwise reductive amination of concentrated PD-DFF solutions (5–20%) to BAMF with pressurized NH_3/H_2 gases.

With an aim to produce BAMF on a large scale, a stepwise reductive amination of concentrated PD-DFF solution (5–20 wt%) was designed with pressurized NH_3/H_2 gases and Co_2P NRs catalyst due to the limitation of NH_3 concentration in commercially available methanolic NH_3 solutions. The preliminary studies revealed that a high NH_3/Sub ratio is essential to achieve high selectivity of the desired product. Therefore, the reactions of concentrated PD-DFF solutions (5–20 wt%) in a methanol-water (2:1, v/v) mixture were conducted under pressurized NH_3 and H_2 gases at 120 °C for 4 h. In the first step, PD-AMF was afforded in high yield (ca. 90%) from 5 and 10 wt% solutions of PD-DFF under the applied reaction conditions (**Table 3.5, entries 1-3**), whereas further increasing concentrations (such as 15 and 20 wt% solutions of PD-DFF) resulted in PD-AMF with moderate yields (**Table 3.5, entries 4 and 5**), indicating that additional optimization of ammonia pressure is required to obtain PD-AMF in high yields from > 10 wt% PD-DFF solutions. Nevertheless, the second step reductive amination was performed with 10 wt% PD-AMF solution in methanol-water (2:1, v/v) mixture to produce BAMF. A 10 wt% solution of crude PD-AMF (10 wt%, 0.7 mmol, 130 mg) with CH_3COOH (3.5 mmol) in the presence of Co_2P NRs catalyst (60 mg, S/C = 2.2 wt/wt) gave BAMF in high yield (95%) under the optimum reaction condition (P_{NH3}, 0.6 MPa and P_{H2},1.2 MPa, 120 °C, 4 h). In this two-step approach, the overall yield of BAMF reached 89% from a 10 wt% solution of PD-DFF, which significantly raised the feasibility of the process (**Scheme 3.10**).

Table 3.5. Reductive amination of PD-DFF with various substrate concentrations using pressurized NH_3/H_2 gases in methanol-water (2:1, v/v) mixed solvent.[a]

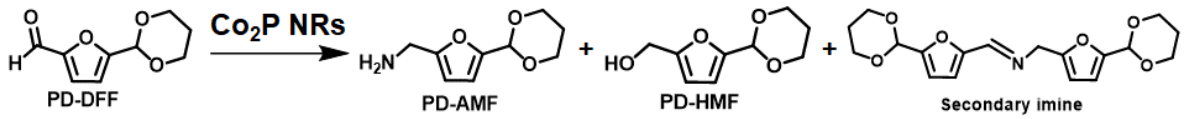

Entry	PD-DFF Conc. (wt%)	P_{NH3}/P_{H2} (MPa)	t (h)	Conv. (%)	Product Yield (%)			C.B. (%)
					PD-AMF	PD-HMF	Sec. imine	
1	5	0.35/0.65	4	>99	89	4	2	95
2	10	0.6/1.2	2	>99	94	5	n.d.	99
3	10	0.6/1.2	4	>99	92	5	1	98
4	15	0.9/1.8	4	>99	77	4	1	82
5	20	0.9/1.8	4	>99	66	3	1	70

[a] Reaction condition: PD-DFF, 0.65 mmol (5 wt%); 1.3 mmol (10 wt%); 2.1 mmol (15 wt%); and 2.8 mmol (20 wt%); Co_2P NRs (S/C = 9 wt/wt); MeOH, 2 mL; D_2O, 1 mL; 120 ºC; stirring rate 600 rpm.

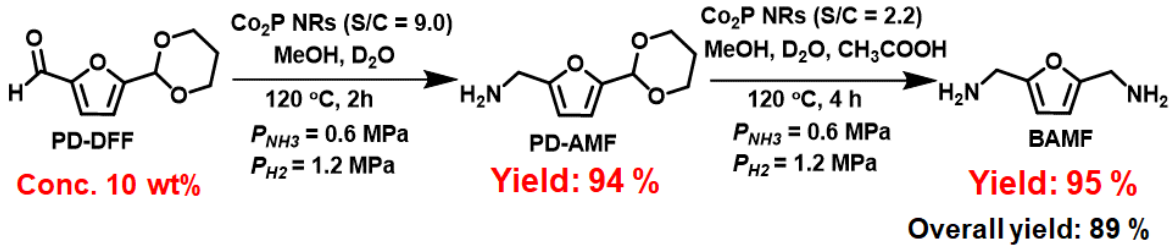

Scheme 3.10. Stepwise approach to synthesize BAMF from concentrated solution of PD-DFF (10 wt%) with pressurized NH_3/H_2 gas mixture.

3.4 Conclusions

A highly efficient catalytic process for the stepwise synthesis of BAMF via reductive amination of PD-DFF with NH_3 in methanol-water (2:1, v/v) mixed solvent using Co_2P NRs catalyst has been developed. Protecting one of the highly reactive formyl groups of DFF with

a stable six-membered ring acetal significantly suppresses the byproduct formation and affords high productivity in highly concentrated solutions of PD-DFF (10 wt%). The first step corresponding to the reductive amination of PD-DFF to PD-AMF was studied by varying the temperature, hydrogen pressure, NH_3/Sub mole ratio and water content, where each parameter plays a crucial role in determining the high yield and selectivity. The Co_2P NRs catalyst shows outstanding performance compared to state-of-art catalysts under mild reaction conditions and can be reused several times retaining its activity. In the second step, the pH of the reaction mixture was controlled by the addition of the optimum amount of acetic acid to promote the partial hydrolysis of PD-AMF. It also facilitates the subsequent reductive amination to give BAMF selectively. The present process involved highly concentrated solutions of PD-DFF (10 wt%) for the synthesis of BAMF, thus making the process industrially feasible for the large-scale production of BAMF.

3.5 References

[1] J. M. García, F. C. García, F. Serna, J. L. De La Peña, *Prog. Polym. Sci.* **2010**, *35*, 623–686.

[2] J. Reglero Ruiz, M. Trigo-López, F. García, J. García, *Polymers* **2017**, *9*, 414.

[3] H. Zeng, Z. Guan, *J. Am. Chem. Soc.* **2011**, *133*, 1159–1161.

[4] A. Kumar, D. Armstrong, G. Peters, M. Nagala, S. Shirran, *Chem. Commun.* **2021**, *57*, 6153–6156.

[5] D. Pingen, J. B. Schwaderer, J. Walter, J. Wen, G. Murray, D. Vogt, S. Mecking, *ChemCatChem* **2018**, *10*, 3027–3033.

[6] L. Bini, C. Müller, J. Wilting, L. Von Chrzanowski, A. L. Spek, D. Vogt, *J. Am. Chem. Soc.* **2007**, *129*, 12622–12623.

[7] M. Niwa, *J. Catal.* **1981**, *70*, 1–13.

[8] I. Delidovich, P. J. C. Hausoul, L. Deng, R. Pfützenreuter, M. Rose, R. Palkovits, *Chem. Rev.* **2016**, *116*, 1540–1599.

[9] T. Komanoya, T. Kinemura, Y. Kita, K. Kamata, M. Hara, *J. Am. Chem. Soc.* **2017**, *139*, 11493–11499.

[10] Y. Xu, X. Jia, J. Ma, J. Gao, F. Xia, X. Li, J. Xu, *Green Chem.* **2018**, *20*, 2697–2701.

[11] Z.-Z. Yang, J. Deng, T. Pan, Q.-X. Guo, Y. Fu, *Green Chem.* **2012**, *14*, 2986.

[12] R. Fang, R. Luque, Y. Li, *Green Chem.* **2017**, *19*, 647–655.

[13] N.-T. Le, A. Byun, Y. Han, K.-I. Lee, H. Kim, *Green Sustain. Chem.* **2015**, *05*, 115–127.

[14] H. Qi, F. Liu, L. Zhang, L. Li, Y. Su, J. Yang, R. Hao, A. Wang, T. Zhang, *Green Chem.* **2020**, *22*, 6897–6901.

[15] F. J. A. G. Coumans, Z. Overchenko, J. J. Wiesfeld, N. Kosinov, K. Nakajima, E. J. M. Hensen, *ACS Sustain. Chem. Eng.* **2022**, *10*, 3116–3130.

[16] T. Boonyakarn, J. J. Wiesfeld, M. Asakawa, L. Chen, A. Fukuoka, E. J. M. Hensen, K. Nakajima, *ChemSusChem* **2022**, *15*, e202200059.

[17] M. Kim, Y. Su, A. Fukuoka, E. J. M. Hensen, K. Nakajima, *Angew. Chem. Int. Ed.* **2018**, *57*, 8235–8239.

[18] M. Kim, Y. Su, T. Aoshima, A. Fukuoka, E. J. M. Hensen, K. Nakajima, *ACS Catal.* **2019**, *9*, 4277–4285.

[19] J. J. Wiesfeld, M. Asakawa, T. Aoshima, A. Fukuoka, E. J. M. Hensen, K. Nakajima, *ChemCatChem* **2022**, *14*, e202200191.

[20] J. J. Wiesfeld, M. Kim, K. Nakajima, E. J. M. Hensen, *Green Chem.* **2020**, *22*, 1229–1238.

[21] K. Zhou, R. Xie, M. Xiao, D. Guo, Z. Cai, S. Kang, Y. Xu, J. Wei, *ChemCatChem* **2021**, *13*, 2074–2085.

[22] Z. Wei, Y. Cheng, K. Zhou, Y. Zeng, E. Yao, Q. Li, Y. Liu, Y. Sun, *ChemSusChem* **2021**, *14*, 2308–2312.

[23] Z. Wei, Y. Cheng, H. Huang, Z. Ma, K. Zhou, Y. Liu, *ChemSusChem* **2022**, *15*, e202200233.

[24] Y. Kita, M. Kuwabara, S. Yamadera, K. Kamata, M. Hara, *Chem. Sci.* **2020**, *11*, 9884–9890.

[25] H. Yuan, B. T. Kusema, Z. Yan, S. Streiff, F. Shi, *RSC Adv.* **2019**, *9*, 38877–38881.

[26] Yogita, K. T. V. Rao, P. M. Kumar, N. Lingaiah, *Sustain. Energy Fuels* **2022**, *6*, 4692–4705.

[27] M. Chatterjee, T. Ishizaka, H. Kawanami, *Green Chem.* **2016**, *18*, 487–496.

[28] Z. Pan, Q. Zhang, W. Wang, L. Wang, G.-H. Wang, *ACS Sustain. Chem. Eng.* **2022**, *10*, 3777–3786.

[29] G. Hahn, P. Kunnas, N. De Jonge, R. Kempe, *Nat. Catal.* **2018**, *2*, 71–77.

[30] Y. Zhang, H. Yang, Q. Chi, Z. Zhang, *ChemSusChem* **2019**, *12*, 1246–1255.

[31] Y. Shi, B. Zhang, *Chem. Soc. Rev.* **2016**, *45*, 1529–1541.

[32] Y. Wang, B. Kong, D. Zhao, H. Wang, C. Selomulya, *Nano Today* **2017**, *15*, 26–55.

[33] T. Liu, D. Liu, F. Qu, D. Wang, L. Zhang, R. Ge, S. Hao, Y. Ma, G. Du, A. M. Asiri, L. Chen, X. Sun, *Adv. Energy Mater.* **2017**, *7*, 1700020.

[34] A. Sumboja, T. An, H. Y. Goh, M. Lübke, D. P. Howard, Y. Xu, A. D. Handoko, Y. Zong, Z. Liu, *ACS Appl. Mater. Interfaces* **2018**, *10*, 15673–15680.

[35] H. Zhang, D.-H. Ha, R. Hovden, L. F. Kourkoutis, R. D. Robinson, *Nano Lett.* **2011**, *11*, 188–197.

[36] M. Sheng, S. Fujita, S. Yamaguchi, J. Yamasaki, K. Nakajima, S. Yamazoe, T. Mizugaki, T. Mitsudome, *JACS Au* **2021**, *1*, 501–507.

[37] H. Ishikawa, M. Sheng, A. Nakata, K. Nakajima, S. Yamazoe, J. Yamasaki, S. Yamaguchi, T. Mizugaki, T. Mitsudome, *ACS Catal.* **2021**, *11*, 750–757

[38] M. Sheng, S. Yamaguchi, A. Nakata, S. Yamazoe, K. Nakajima, J. Yamasaki, T. Mizugaki, T. Mitsudome, *ACS Sustain. Chem. Eng.* **2021**, *9*, 11238–11246.

[39] P. Liu, J. A. Rodriguez, *J. Am. Chem. Soc.* **2005**, *127*, 14871–14878.

[40] R. Gao, L. Pan, H. Wang, X. Zhang, L. Wang, J.-J. Zou, *ACS Catal.* **2018**, *8*, 8420–8429.

[41] S. Yamaguchi, S. Fujita, K. Nakajima, S. Yamazoe, J. Yamasaki, T. Mizugaki, T. Mitsudome, *ACS Sustain. Chem. Eng.* **2021**, *9*, 6347–6354.

[42] S. Yamaguchi, S. Fujita, K. Nakajima, S. Yamazoe, J. Yamasaki, T. Mizugaki, T. Mitsudome, *Green Chem.* **2021**, *23*, 2010–2016.

[43] S. Fujita, K. Imagawa, S. Yamaguchi, J. Yamasaki, S. Yamazoe, T. Mizugaki, T. Mitsudome, *Sci. Rep.* **2021**, *11*, 10673.

[44] W. Chen, Y. Sun, J. Du, Z. Si, X. Tang, X. Zeng, L. Lin, S. Liu, T. Lei, *J. Chem. Technol. Biotechnol.* **2018**, *93*, 3028–3034.

[45] S. Song, Y. Wang, N. Yan, *Mol. Catal.* **2018**, *454*, 87–93.

[46] T. Gross, A. M. Seayad, M. Ahmad, M. Beller, *Org. Lett.* **2002**, *4*, 2055–2058.

[47] S. Ogo, K. Uehara, T. Abura, S. Fukuzumi, *J. Am. Chem. Soc.* **2004**, *126*, 3020–3021.

Chapter 4

Reductive Amination of Methyl-5-formyl-2-furancarboxylate to Methyl-5-(aminomethyl)-2-furancarboxylate with Co_2P NRs.

Abstract

Herein, I designed a new efficient route for the synthesis of a valuable primary amine, Methyl-5-(aminomethyl)-2-furancarboxylate (MAMFC) via the reductive amination of biomass-derived methyl-5-formyl-2-furancarboxylate (MFFC), which can be obtained through the oxidative esterification of HMF. In this study, the catalytic performance of Co_2P NRs was investigated to produce MAMFC under mild reaction conditions. The reductive amination of MFFC in a methanolic solution using pressurized NH_3 and H_2 with Co_2P NRs at 130 °C in 2 h affords MAMFC in a moderate yield of 54%. Kinetic study suggests that the produced MAMFC further reacts with the *in-situ* formed reaction intermediates, which restrict to elevate MAMFC yield. Nevertheless, the present study alights a direction for the synthesis of a new bio-based primary amine.

4.1 Introduction.

Primary amines are one of the attractive key intermediates in polymer industries due to their wide applications to produce polyamides, polyurea, polyurethanes and so forth.[1–5] MAMFC is a valuable primary amine that can be transformed into an attractive polyamide, poly(iminomethylene(cis-tetrahydro-2,5-furandiyl)carbonyl) (PITC) via the formation of 8-oxa-3-azabicyclo[3.2.1]octan-2-one and several precursors of anticancer drugs such as G-quadruplex.[6–9] However, the synthesis of MAMFC from biomass-derived substrate is commonly rare. In this direction, MFFC is a versatile biomass-derived platform molecule obtained by selective aerobic oxidative esterification of HMF.[10–15] Valorization of MFFC can achieve upgrading chemicals such as MFDC and MAMFC.[10–17] MAMFC can be synthesized via catalytic reductive amination of MFFC. (**Scheme 4.1**)

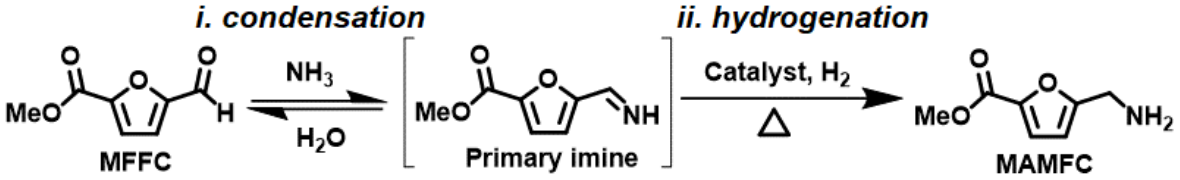

Scheme 4.1. Reaction pathway for the conversion of MFFC to MAMFC.

Nevertheless, there has been no efficient synthetic procedure to produce MAMFC in the previous papers. The current restriction in the reductive amination reactions is unfavorable side reactions due to the high nucleophilicity of the primary amines, which often undergo a condensation reaction with the highly reactive formyl and imine functionalities to secondary, tertiary amine and/or polymeric species as byproducts.[18–20] In addition, the undesired hydrogenation of the formyl group and furan ring further limits the product selectivity.[18–20] Therefore, it is highly challenging to synthesize selectively the desired products via reductive amination of biomass-derived substrates. To suppress such byproduct formation, previously we used the acetal protection strategy in several catalytic reactions, wherein the reactive formyl group was passivated with an acetal functionality to avoid direct contact with the reaction intermediates resulting in the polymerization reaction.[21–25] For example, BAMF was successfully obtained in high yield using the acetal-protected DFF (PD-

DFF) with 1,3-propanediol (PD) even from highly concentrated solutions (10 wt%) (**Chapter 3**). Protecting the highly reactive formyl groups of DFF with a stable six-membered ring acetal not only suppresses the byproduct formation but also enhances productivity. Meanwhile, the high stability of the six-membered ring acetal under the reaction conditions prevents the deprotection and direct synthesis of BAMF even in the presence of water. An optimum amount of acetic acid was, therefore, added to promote the partial hydrolysis of acetal functionality and facilitate the subsequent reductive amination.[26–27] In this regard, such acetal protection strategy cannot be simply applicable in the reductive amination of MFFC to MAMFC due to such high stability of the acetal functionality under the basic reaction conditions, and the addition of water and acetic acid to accelerate the deprotection can negatively impact the desired reaction as the ester (-COOMe) functionality of MFFC has high tendency to follow base-catalyzed hydrolysis to form FFCA and AMFCA as the byproducts, making the reductive amination of MFFC miserable. Nevertheless, the Co_2P NRs showed high catalytic activity, stability, and reusability in the reductive amination of several biomass-derived substrates, where catalyst deactivation is one of the common issues due to poisoning of catalytically active sites.[28–30] Moreover, Co_2P NRs exhibited an outstanding performance under relatively mild reaction conditions in the reductive amination of PD-AMF to BAMF compared to benchmark catalysts. So, herein, I extended the application of Co_2P NRs in the reductive amination of MFFC to produce MAMFC selectively.

4.2 Experimental Section

4.2.1 Materials

Cobalt(II) acetylacetonate dihydrate ($Co(acac)_2 \cdot 2H_2O$) was purchased from Mitsuwa pure chemicals. Ruthenium(III) nitrosyl nitrate solution (1.5 wt% of Ru) was procured from Strem Chemicals. Hexadecylamine, triphenyl phosphite, 1-octadecene, and chlorobenzene were purchased from Tokyo Chemical Industry (TCI). MFFC was obtained from Angene chemicals. MAMFC was purchased from Chemspace LLC. $Ni(NO_3)_2.6H_2O$, HT, methanol, acetone, and *N,N*-dimethylformamide super dehydrated (DMF) were obtained from FUJIFILM Wako Pure Chemical Corporation. Chloroform was purchased from Kanto

chemical corporation. Aerosil-380 (SiO_2) was obtained from Evonik industries. Nb_2O_5 (JRC-NBO-1) and Al_2O_3 (JRC-AlO-2) were supplied from the Catalyst Society of Japan.

4.2.1 Catalyst preparation

Co_2P NRs, Ni/Al_2O_3 and Ru/Nb_2O_5 catalysts were prepared following the procedures as mentioned in Chapter 2.

The HT, SiO_2, Al_2O_3 and Nb_2O_5 supported Co_2P NRs were prepared following the same procedure.[30] For example, to prepare Co_2P NRs/HT, first, 50 mg of Co_2P NRs was dispersed in 50 mL hexane via sonication. Then, 1.0 g of the HT was added into it and continued the sonication for 2 h. Finally, the hexane was removed by vacuum evaporation from the mixture and the obtained product was dried overnight under vacuum at room temperature.

4.2.2 Characterization of catalyst

Powder X-ray diffraction (P-XRD) measurements were performed by an Ultima IV, Rigaku diffractometer at 40 kV and 40 mA using Cu Kα radiation (λ = 1.5418 Å) in 2θ = 5−90°. N_2 adsorption-desorption isotherms were acquired using BELSORP II (BEL JAPAN. INC.). The BET equation was applied in the range of p/p_0 = 0.05-0.30 to calculate the specific surface area.

4.2.3 Catalytic reaction

The reductive amination of MFFC was conducted in a pressure resistant Teflon-lined stainless steel autoclave reactor. A mixture of MFFC (0.05 mmol, 10 mg) and Co_2P NRs (5 mg) in a methanolic solution was stirred under pressurized NH_3 and H_2 at 130 °C for 6 h. After the reaction, the reaction mixture was diluted with 10 mL methanol to dissolve all products, and the solution was analyzed by gas-chromatograph (GC, Shimadzu, GC-4) with a flame ionization detector (FID) using chlorobenzene as an internal standard.

4.3 Result and Discussion

4.3.1 Characterization of catalysts.

The formation of highly crystalline Co_2P was confirmed by XRD measurement. The diffraction peaks at 2θ = 40.9, 43.4, 52.6 and 56.4 º assigned to (121), (211), (230) and (320) planes, respectively, matches with the β-Co_2P (JCPDS No.00-054-0413) (**Figure 4.1a**).[28-30] No diffraction peaks related to Co_2P NRs and Ru were observed for HT- and SiO_2-supported Co_2P NRs catalysts and Ru/Nb_2O_5 indicating the presence of the highly dispersed metal nanoparticles (**Figure 4.1, b, c, and f**). On the other hand, very weak diffraction peaks corresponded to (230) and (121) planes of Co_2P NRs were observed in Co_2P/Al_2O_3 and Co_2P/Nb_2O_5, respectively (**Figure 4.1, d, and e**). Ni/Al_2O_3 exhibited diffraction peaks assignable to metallic Ni and Al_2O_3 (γ phase), respectively (**Figure 4.1g**). The specific surface area of the Co_2P NRs and supported Co_2P NRs were calculated using BET method from N_2 adsorption-desorption isotherms. The surface area of Co_2P NRs was 23.4 m^2g^{-1}, while the surface area HT-, SiO_2-, Al_2O_3- and Nb_2O_5-supported Co_2P NRs were 44.9, 403.2, 190.1, and 162.8 m^2g^{-1}, respectively, suggesting the high dispersion of metal nanoparticles on the support.

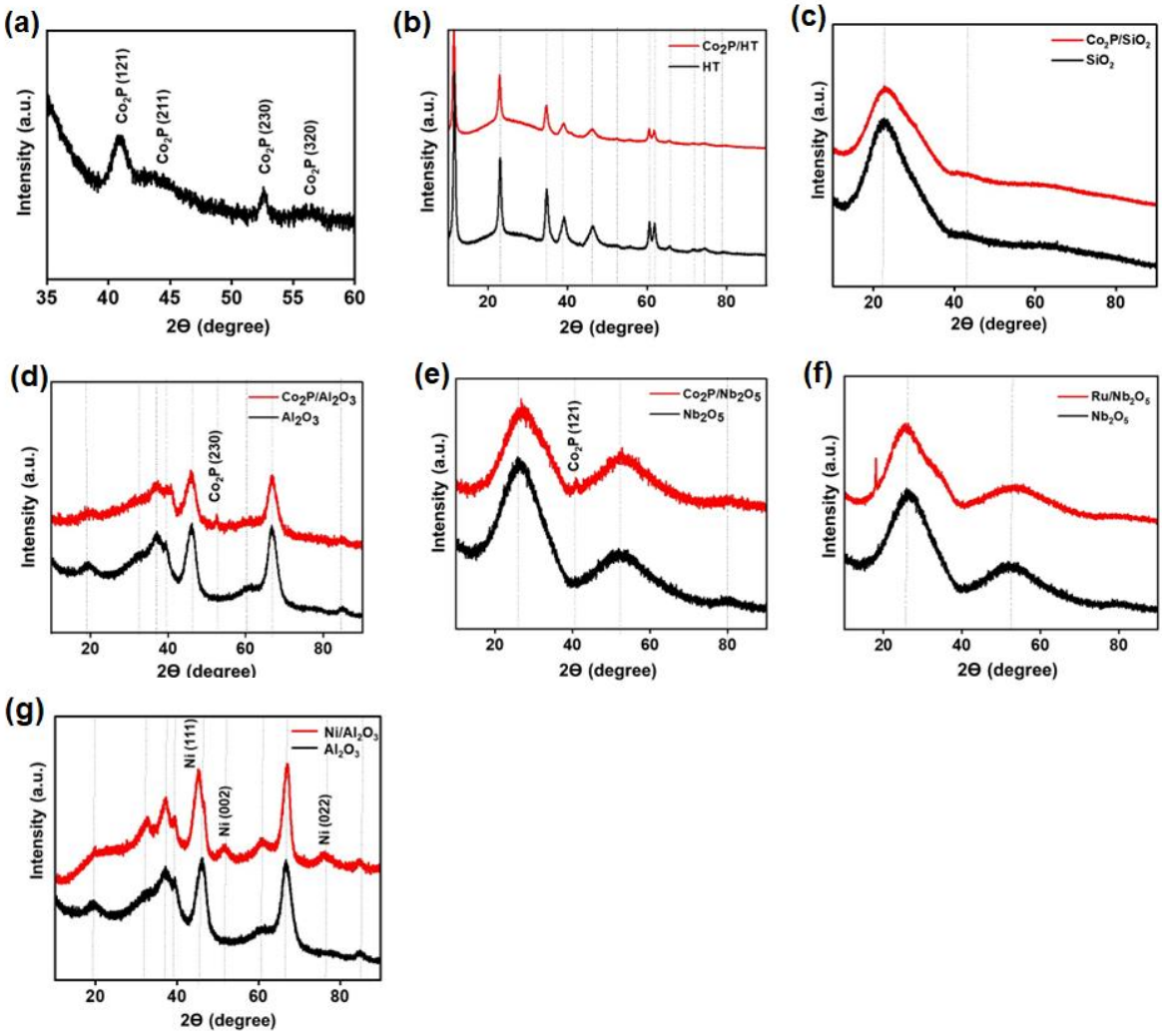

Figure 4.1. XRD patterns of (a) Co_2P NRs, (b) HT and Co_2P/HT, (c) SiO_2 and Co_2P/SiO_2, (d) Al_2O_3 and Co_2P/Al_2O_3, (e) Nb_2O_5 and Co_2P/Nb_2O_5, (f) Nb_2O_5 and Ru/Nb_2O_5, and (g) Al_2O_3 and Ni/Al_2O_3, respectively.

4.3.2 Reductive amination of MFFC to MAMFC with Co_2P NRs.

The reductive amination of MFFC proceeds via the condensation of formyl group (-CHO) and NH_3 to produce a primary imine as shown in **Scheme 4.1**. First, the reaction parameters were optimized for the conversion of MFFC to MAMFC using Co_2P NRs catalyst.

4.3.2.1 Effect of temperature.

The effect of reaction temperature was examined in the range of 120–150 °C for the reductive amination of MFFC in a methanolic solution using pressurized NH_3 and H_2. **Table 4.1** summarizes the conversion and product yield at various reaction temperatures. Almost full conversion was observed at above 120 °C, while product yields were significantly different depending on the temperatures. MAMFC was obtained with 32% yield at 120 °C for 6 h, which gradually increased with increasing the reaction temperature from 120 to 140 °C, suggesting that MAMFC is produced from undetectable intermediates included in "others" at 120 °C. Furthermore, a high reaction temperature (150 °C) gave a low yield of MAMFC, most probably due to the degradation of MAMFC and undetectable intermediates (**entry 4)**. Prolonging the reaction time at 130 °C resulted in a high MAMFC yield (**entry 5**), while the same reaction at 140 °C gave a poor MAMFC yield (**entry 6**).

Table 4.1. Effect of temperature in the reductive amination of MFFC with Co_2P NRs.[a]

Entry	T (°C)	t (h)	Conv. (%)	Product Yield (%)	
				MAMFC	Others
1	120	6	>99	32	68
2	130		>99	41	59
3	140		>99	47	53
4	150		>99	35	65
5	130	8	>99	57	43
6	140		>99	26	74

[a] Reaction conditions: MFFC, 10 mg; Co_2P NRs, 4 mg (S/C = 2.5 wt/wt); methanol, 3 mL; P_{NH3} = 0.2 MPa, P_{H2} = 0.5 MPa. Others refer to undatable intermediate and polymeric byproducts.

4.3.2.2 Effect of NH_3 pressure.

The synthesis of MAMFC via the reductive amination of MFFC strongly depends on the NH_3 concentration. The reductive amination reaction often involves undesirable side reactions due to high nucleophilicity of primary amine than NH_3, which undergoes oligomerization reaction with the reactive formyl group and reaction intermediates (imine) to form polymeric byproducts as shown in **Scheme 4.2**. Such undesirable reactions can be suppressed at high NH_3/Sub ratio.[31,32] However, excess amount of NH_3 causes catalyst poisoning due to the strong adsorption over the catalytically active sites. Therefore, an optimum amount of NH_3 concentration is required to promote the desired reaction. Herein, I look for a suitable NH_3 pressure (P_{NH3}) in the reductive amination of MFFC to facilitate the synthesis of MAMFC. The reactions were performed at 130 °C for 6 h with different NH_3 pressures under 0.5 MPa H_2 pressure. **Figure 4.4** shows the effect of NH_3 pressure on the product distribution, which revealed that 0.3 MPa NH_3 pressure is idle to obtain MAMFC efficiently via the reductive amination of MFFC. Further increasing NH_3 pressure results in decrease of MAMFC yield from 50% (P_{NH3}, 0.3 MPa) to 37% (P_{NH3}, 0.4 MPa) due to most probable catalyst poisoning.

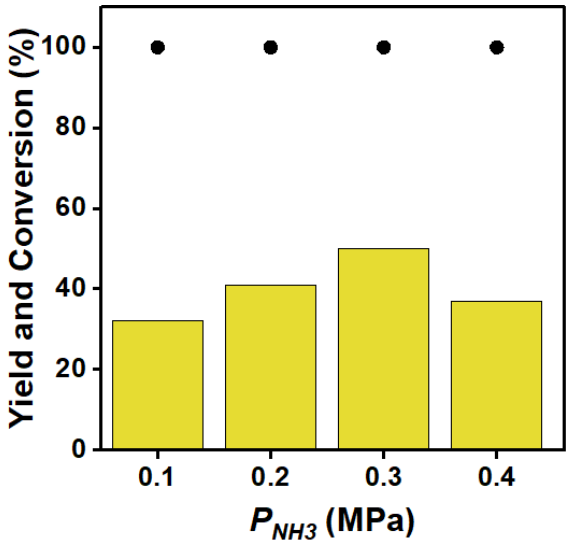

Figure 4.4. Effect of NH_3 pressure on the reductive amination of MFFC to MAMFC. Black circles and yellow bars represent MFFC conversion and MAMFC yield, respectively. Reaction conditions: MFFC, 0.05 mmol (10 mg); Co_2P NRs, 4 mg (S/C = 2.5 wt/wt); methanol, 3 mL; P_{H2} = 0.5 MPa, 130 °C, 6 h, stirring rate 600 rpm.

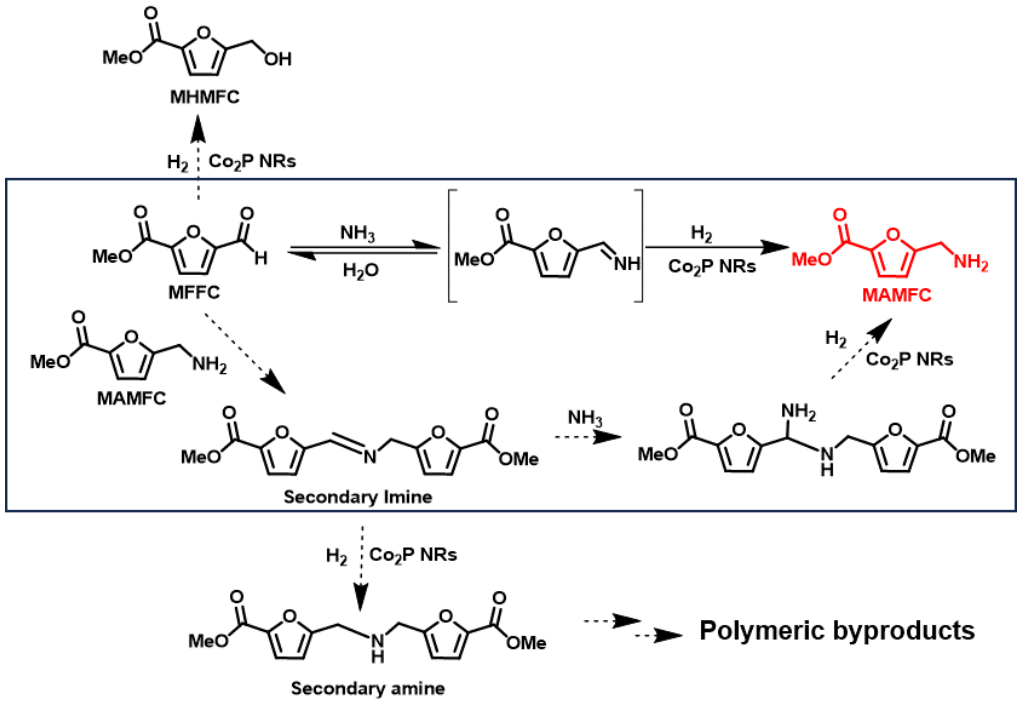

Scheme 4.2. Possible reaction pathways in the reductive amination of MFFC to MAMFC.

4.3.2.3 Effect of H_2 pressure.

The H_2 pressure significantly influences this reaction. **Figure 4.5** demonstrates the effect of H_2 pressure at a range of 0.1 to 0.7 MPa under the optimized reaction temperature and NH_3 pressure for 6 h. A relatively low H_2 pressure ($\leq P_{NH3}$) results the poor MAMFC yield (8–12%), while a high yield (50%) of MAMFC was obtained at 0.5 MPa H_2 pressure ($>P_{NH3}$). No significant change in MAMFC yield (47%) was observed by further increasing the H_2 pressure (P_{H2}) to 0.7 MPa, indicating that a competitive adsorption between NH_3 and H_2 occurs over the catalyst surface. At low H_2 pressures (< 0.5 MPa) poor yield of MAMFC was obtained due to incomplete hydrogenation of the reaction intermediates. Notably, no detection of secondary imine indicates that reaction proceeds mainly via primary imine pathway. In addition, the hydrogenation of MFFC to MHMFC was largely suppressed in the range of 0.1–0.7 MPa H_2 pressure (P_{H2}) under the optimized NH_3 pressure (P_{NH3}, 0.3 MPa).

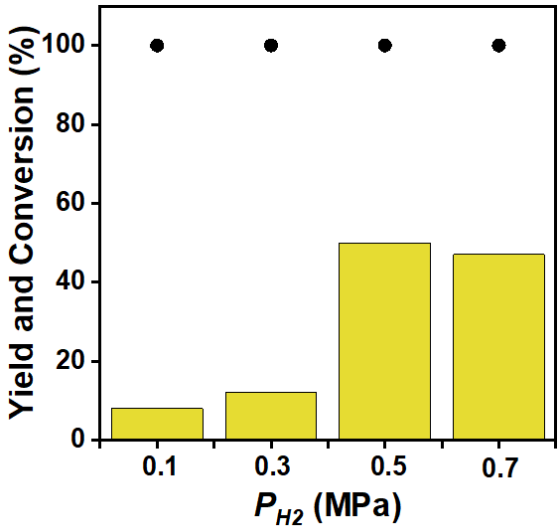

Figure 4.5. Effect of H_2 pressure on the reductive amination of MFFC to MAMFC. Black circles and yellow bars represent the MFFC conversion and MAMFC yields, respectively. Reaction conditions: MFFC, 0.05 mmol (10 mg); Co_2P NRs, 4 mg (S/C = 2.5 wt/wt); methanol, 3 mL; P_{NH3} = 0.3 MPa, 130 °C, 6 h, stirring rate 600 rpm.

4.3.2.4 Effect of solvent.

The choice of solvent played a crucial role in directing the products selectivity in the reductive amination of PD-HMF. The reductive amination of MFFC was studied varying several organic solvents such as methanol, methanol-water mixture, ethanol, tetrahydrofuran (THF) and 1,4-dioxane (**Table 4.2**). Among different solvents, the reductive amination of MFFC to MAMFC was only favored in methanol because of its polar protic nature, which facilitates the imine formation followed by the hydrogenation to primary amine selectively. Notably, it is reported that a combination of water-organic solvent mixture facilitates the reductive amination reaction toward primary amine formation by suppressing the nucleophilicity of the primary amine via hydrolysis with water. However, herein, due to highly basic reaction conditions (pH = ~12), the addition of water induces other undesirable reactions, *i.e.*, the base-catalyzed hydrolysis of -COOMe functionality of MFFC to -COOH resulting in FFCA and AMFCA formation (**Scheme 4.3**). Therefore, methanol was selected as a suitable solvent for further study.

Table 4.2. Effect of solvent in the reductive amination of MFFC with Co_2P NRs.[a]

Entry	Solvent	Conv. (%)	Product Yield (%)	
			MAMFC	Others
1	Methanol	>99	50	50
2	Methanol-water (2:1)	>99	n.d.	100
3	Ethanol	>99	n.d.	100
4	THF	>99	n.d.	100
5	1,4-dioxane	>99	n.d.	100

[a] Reaction conditions: MFFC, 10 mg; Co_2P NRs, 4 mg (S/C = 2.5 wt/wt); Solvent, 3 mL; P_{NH3} = 0.3 MPa, P_{H2} = 0.5 MPa, 130 °C, 6 h, stirring rate 600 rpm. Others refer to secondary imine, FFCA, AMFCA, undetectable intermediates and polymeric byproducts.

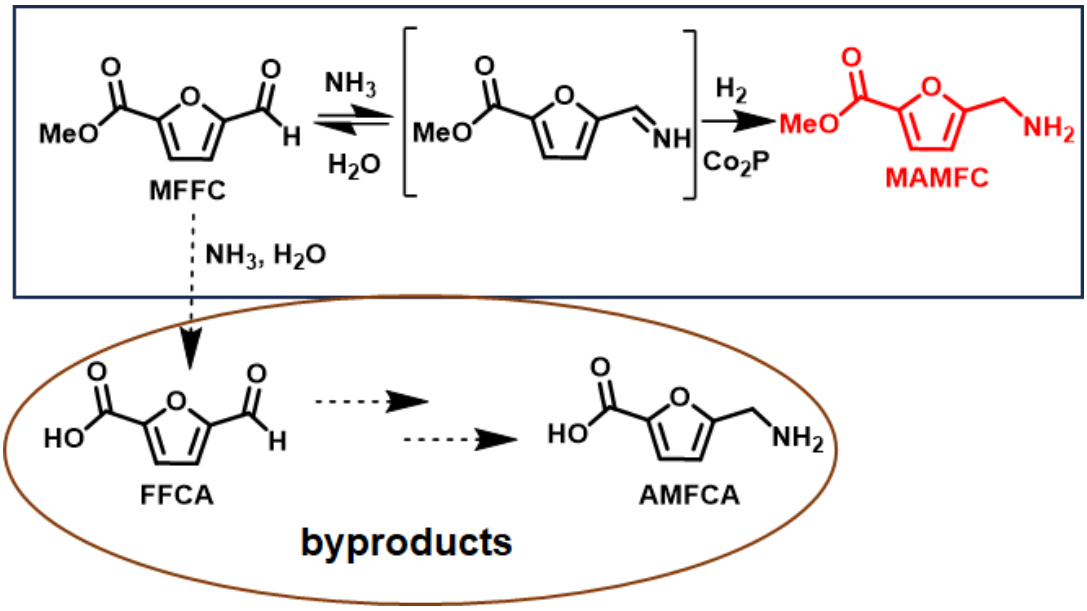

Scheme 4.3. Reductive amination of MFFC to MAMFC in methanol–water mixture.

4.3.2.5 Effect of catalyst loading.

The impact of substrate to catalyst weight ratio (S/C) on the product distribution was examined under the optimized reaction conditions as shown in **Figure 4.6**. MFFC conversion was almost full (>99) in the range of S/C (weight ratio) 1.0 to 3.5, while at high S/C (3.5) (*i.e.*, low catalyst loading) MAMFC yield was significantly low (24%). MAMFC yield substantially improved by increasing the catalyst loadings, which reached the maximum at S/C = 2. A further decrease of S/C weight ratio decreased the MAMFC yield, indicating that catalyst assisted side reactions might be proceed at high catalyst loading. Thus, an optimum amount of catalyst loading (5 mg, S/C = 2 wt/wt) is required for the efficient conversion of MFFC to MAMFC.

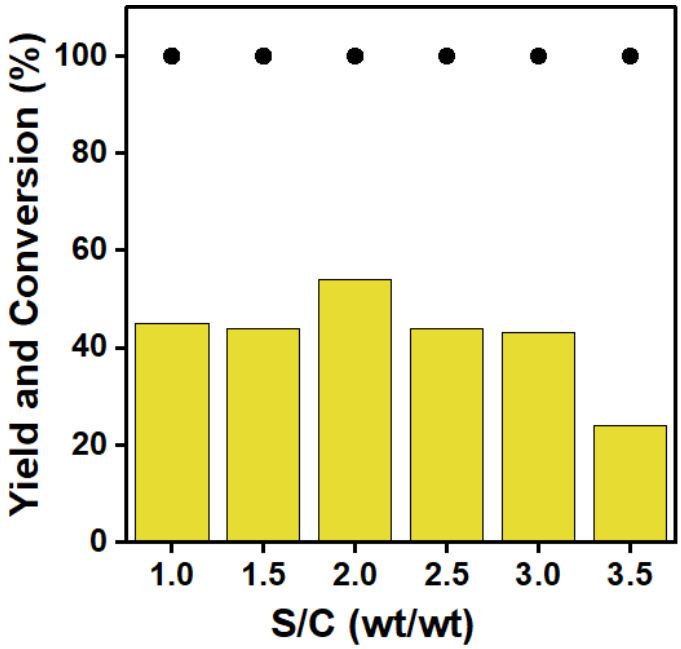

Figure 4.6. Effect of catalyst loading (S/C) on the reductive amination of MFFC to MAMFC. Black circles and yellow bars represent the MFFC conversion and MAMFC yields, respectively. Reaction conditions: MFFC, 0.05 mmol (10 mg); Co_2P NRs, methanol, 3 mL; P_{NH3} = 0.3 MPa, P_{H2} = 0.5 MPa, 130 °C, 6 h, stirring rate 600 rpm.

4.3.2.6 Comparison of catalytic activity of Co_2P NRs.

To enhance the catalytic activity of Co_2P NRs in the reductive amination of MFFC, a series of supported Co_2P NRs catalysts were prepared using several metal oxides as support (such as Nb_2O_5, Al_2O_3, SiO_2 and HT). The catalytic performance of supported Co_2P NRs was investigated in methanolic solution using pressurized NH_3 and H_2 under optimized conditions at 130 °C for 2 h and the results are described in **Table 4.3**. In comparison to the supported Co_2P NRs catalyst, the bare Co_2P NRs showed the highest catalytic activity. MAMFC was obtained in 54% yield with Co_2P NRs, while using supported Co_2P NRs, MAMFC yield declined to ca. 20% (**entries 1**–**5**). Previous study indicates that though the dispersion of Co_2P NRs enhanced after incorporation of a support material, metal-support interactions and electronic properties of the metal strongly influence the hydrogenation efficiency of Co_2P NRs. Furthermore, we screened several reported catalysts such as Ni/Al_2O_3 and Ru/Nb_2O_5 in

the reductive amination of MFFC to improve the MAMFC yield (**entries 6**–**7**). Among all of them, Co_2P NRs showed the highest catalytic activity.

Table 4.3. Screening of catalysts in the reductive amination of MFFC.[a]

Entry	Catalyst	Conv. (%)	Product Yield (%)	
			MAMFC	Others
1	Co_2P	>99	54	46
2	Co_2P/HT	>99	16	84
3	Co_2P/SiO_2	>99	14	86
4	Co_2P/Al_2O_3	>99	19	81
5	Co_2P/Nb_2O_5	>99	21	79
6	Ni/Al_2O_3	>99	31	69
8	Ru/Nb_2O_5	>99	36	64

[a] Reaction conditions: MFFC, 0.05 mmol (10 mg); methanol, 3 mL; P_{NH3} = 0.3 MPa, P_{H2} = 0.5 MPa, 130 °C, 2 h, stirring rate 600 rpm. Others refer to undetectable intermediate, secondary imine and byproducts.

4.3.2.7 Time profile for reductive amination of MFFC to MAMFC.

The product distribution for the reaction was monitored for 10 h under optimized reaction conditions. **Figure 4.4.A** displays the time course for the MFFC conversion and variation of product yields. Almost complete conversion of MFFC was observed at the beginning of the reaction, while reaction intermediates were undetectable due to the highly reactive nature of the imines. At 30 min, MAMFC was obtained with 36% yield as a sole product, which steadily increased to 50% in 1 h. After 2 h, a maximum yield of 54% of MAMFC was obtained. Prolonging the reaction time to 4 h, MAMFC yield gradually decreased from 54% to 25%. Further extending the reaction time, MAMFC yield reached 50% at 8 h and remained almost constant (48%) till 10 h. These results indicate that the reaction between MFFC and NH_3 is quite fast, which produces mainly a primary imine as the

intermediate (**Figure 4.7B**). Moreover, the abrupt variation of MAMFC yield suggests that it further reacts with the highly reactive *in-situ* formed primary imine or substrate (MFFC) to produce polymeric imine species as byproducts (**Scheme 4.2**).

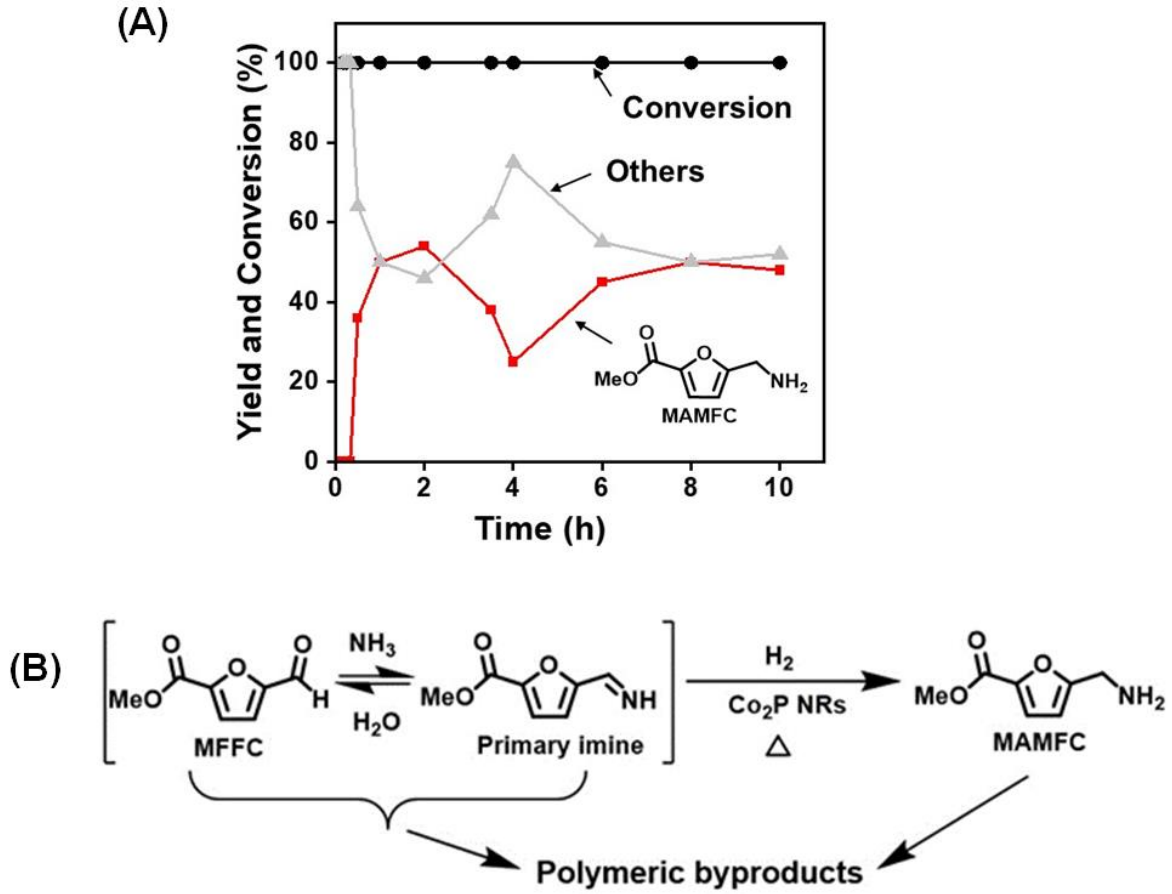

Figure 4.4. Time course for the reductive amination of MFFC to MAMFC with NH_3 using Co_2P NRs in methanol (A). MFFC conversion, Black line, and symbols; MAMFC yield, red line, and symbols. Reaction pathways for reductive amination of MFFC to MAMFC with NH_3 using Co_2P NRs in methanol (B). Reaction Conditions: MFFC, 0.05 mmol (10 mg); Co_2P NRs, 5 mg (S/C = 2 wt/wt); Solvent, 3 mL; 0.3 MPa NH_3, 0.5 MPa H_2, 130 ºC, stirring rate 600 rpm.

4.4 Conclusion

In brief, I produced a precious biobased amine, MAMFC, by the reductive amination of MFFC with Co_2P NRs. In this study, the effect of reaction parameters such as temperature, ammonia, and hydrogen pressure were thoroughly investigated, which significantly influenced the reaction selectivity. Furthermore, the impact of catalyst was examined varying catalyst loading. The catalytic activity of Co_2P NRs was compared with several benchmark catalysts, wherein the Co_2P NRs showed highest catalytic activity. The highest yield of 54% MAMFC was obtained at 130 °C for 2 h under the optimized reaction conditions. Kinetic study indicates that MAMFC further reacts with the *in–situ* formed reaction intermediates, which results in low MAMFC yield. The present study will inspire readers to further develop the reaction system to produce MAMFC in high yield following a sustainable pathway.

4.5 References

[1] J. M. García, F. C. García, F. Serna, J. L. De La Peña, *Prog. Polym. Sci.* **2010**, *35*, 623–686.

[2] J. Reglero Ruiz, M. Trigo-López, F. García, J. García, *Polymers* **2017**, *9*, 414.

[3] H. Zeng, Z. Guan, *J. Am. Chem. Soc.* **2011**, *133*, 1159–1161.

[4] A. Kumar, D. Armstrong, G. Peters, M. Nagala, S. Shirran, *Chem. Commun.* **2021**, *57*, 6153–6156.

[5] D. Pingen, J. B. Schwaderer, J. Walter, J. Wen, G. Murray, D. Vogt, S. Mecking, *ChemCatChem* **2018**, *10*, 3027–3033.

[6] C. P. Woroch, A. W. Lankenau, M. W. Kanan, *Macromolecules* **2021**, *54*, 9978–9983.

[7] A. W. Lankenau, M. W. Kanan, *Chem. Sci.* **2020**, *11*, 248–252.

[8] H. Singh, K. Arora, S. Tapadar, T. K. Chakraborty, *J. Theor. Comput. Chem.* **2004**, *03*, 555–566.

[9] T. K. Chakraborty, A. Arora, S. Roy, N. Kumar, S. Maiti, *J. Med. Chem.* **2007**, *50*, 5539–5542.

[10] D. Zhao, T. Su, C. Len, R. Luque, Z. Yang, Green Chem. **2022**, *24*, 6782–6789.

[11] A. Abad, P. Concepción, A. Corma, H. García, Angew. Chem. Int. Ed. **2005**, *44*, 4066–4069.

[12] O. Casanova, S. Iborra, A. Corma, ChemSusChem **2009**, *2*, 1138–1144.

[13] O. Casanova, S. Iborra, A. Corma, J. Catal. **2009**, *265*, 109–116.

[14] E. Taarning, I. S. Nielsen, K. Egeblad, R. Madsen, C. H. Christensen, ChemSusChem **2008**, *1*, 75–78.

[15] F. Menegazzo, M. Signoretto, D. Marchese, F. Pinna, M. Manzoli, J. Catal. **2015**, *326*, 1–8.

[16] J. Du, H. Fang, H. Qu, J. Zhang, X. Duan, Y. Yuan, Appl. Catal. Gen. **2018**, *567*, 80–89.

[17] F. Li, X.-L. Li, C. Li, J. Shi, Y. Fu, Green Chem. **2018**, *20*, 3050–3058.

[18] T. Komanoya, T. Kinemura, Y. Kita, K. Kamata, M. Hara, *J. Am. Chem. Soc.* **2017**, *139*, 11493–11499.

[19] N.-T. Le, A. Byun, Y. Han, K.-I. Lee, H. Kim, *Green Sustain. Chem.* **2015**, *05*, 115–127.

[20] H. Qi, F. Liu, L. Zhang, L. Li, Y. Su, J. Yang, R. Hao, A. Wang, T. Zhang, *Green Chem.* **2020**, *22*, 6897–6901.

[21] T. Boonyakarn, J. J. Wiesfeld, M. Asakawa, L. Chen, A. Fukuoka, E. J. M. Hensen, K. Nakajima, *ChemSusChem* **2022**, *15*, e202200059.

[22] M. Kim, Y. Su, A. Fukuoka, E. J. M. Hensen, K. Nakajima, *Angew. Chem. Int. Ed.* **2018**, *57*, 8235–8239.

[23] M. Kim, Y. Su, T. Aoshima, A. Fukuoka, E. J. M. Hensen, K. Nakajima, *ACS Catal.* **2019**, *9*, 4277–4285.

[24] J. J. Wiesfeld, M. Asakawa, T. Aoshima, A. Fukuoka, E. J. M. Hensen, K. Nakajima, *ChemCatChem* **2022**, *14*, e202200191.

[25] J. J. Wiesfeld, M. Kim, K. Nakajima, E. J. M. Hensen, *Green Chem.* **2020**, *22*, 1229–1238.

[26] T. Gross, A. M. Seayad, M. Ahmad, M. Beller, *Org. Lett.* **2002**, *4*, 2055–2058.

[27] S. Ogo, K. Uehara, T. Abura, S. Fukuzumi, *J. Am. Chem. Soc.* **2004**, *126*, 3020–3021.

[28] M. Sheng, S. Fujita, S. Yamaguchi, J. Yamasaki, K. Nakajima, S. Yamazoe, T. Mizugaki, T. Mitsudome, *JACS Au* **2021**, *1*, 501–507.

[29] H. Ishikawa, M. Sheng, A. Nakata, K. Nakajima, S. Yamazoe, J. Yamasaki, S. Yamaguchi, T. Mizugaki, T. Mitsudome, *ACS Catal.* **2021**, *11*, 750–757

[30] M. Sheng, S. Yamaguchi, A. Nakata, S. Yamazoe, K. Nakajima, J. Yamasaki, T. Mizugaki, T. Mitsudome, *ACS Sustain. Chem. Eng.* **2021**, *9*, 11238–11246.

[31] Z. Wei, Y. Cheng, H. Huang, Z. Ma, K. Zhou, Y. Liu, *ChemSusChem* **2022**, *15*, e202200233.

[32] W. Chen, Y. Sun, J. Du, Z. Si, X. Tang, X. Zeng, L. Lin, S. Liu, T. Lei, *J. Chem. Technol. Biotechnol.* **2018**, *93*, 3028–3034.

Chapter 5

Summary and Outlook

Over the past years, the rapid consumption of fossil-based resources to produce chemicals and fuels has raised the substantial energy crisis along with their adverse environmental impact. The utilization of sustainable and renewable carbon sources in the chemical industry is of utmost importance for building a sustainable society. In this regard, non-edible biomass is widely recognized as one of the promising carbon sources due to its abundance and renewable nature. A variety of valuable compounds can be synthesized by valorization of the lignocellulosic biomass (**Figure 1.2**). Among these, 5-hydroxymethylfurfural (HMF), a platform molecule, obtained by the acid dehydration of biomass-derived glucose, serves as a potential intermediate with wide applications in organic synthesis, pharmaceuticals, transportation fuels and chemical industries. For example, oxidation of 5-HMF produces FDCA, which is regarded as one of the "top 10+4" bio-based chemicals. The co-polymerization of FDCA or the ester-derivatives (such as MFDC) with ethylene glycol yields the biobased poly(ethylene furanoate) polyester (PEF), which is a suitable replacement for petroleum-derived poly(ethylene) terephthalate (PET, global annual production > 50 MT). Furthermore, recently, the synthesis of primary amines from biomass-derived substrates has gained significant attention due to their wide applications in polymer industries. In this direction, BAMF and MAMFC are a new class of biomass-derived primary amines that can be obtained via the reductive amination of HMF or HMF-derivatives (such as DFF and MFFC). Despite the potential of HMF as a platform for the chemical industry, the selective conversion of HMF to desired chemicals is highly challenging. This is largely due to the highly reactive formyl group (-CHO) in HMF, which results in complex polymerization and condensation reactions that lead to humins. By-product formation can be lowered by using dilute solutions, which is, however, hampering scale-up limiting the industrialization of the developed process.

In Chapter 2, a highly efficient catalytic process for the stepwise synthesis of MFDC from a concentrated solution of HMF (10–20 wt%) using methanol as an acetalizing agent is developed. Methanol was demonstrated for the first time to be an effective protecting agent in the oxidative esterification of HMF. The developed process consists of three steps: 1) the oxidative esterification of HMF-acetal to MFFC-acetal, 2) the deprotection of MFFC-acetal to MFFC and, 3) the production of MFDC via oxidative esterification of MFFC. The significance of the process is that the amount of the basic additive can be reduced (Na_2CO_3, 1 mol%) largely, and the desired products (MFFC-acetal and MFDC) can be obtained in high yields using concentrated substrate solutions in two oxidative esterification steps with reusable solid catalysts. The oxidative esterifications of HMF-acetal (10–20 wt%) and MFFC (10 wt%) were performed with CeO_2-supported Au catalyst (Au/CeO_2), which gave high product yields (90–95%) under mild reaction conditions. Moreover, the deprotection step (MFFC-acetal to MFFC) was designed using a solid Brønsted acid catalyst, which further increased the sustainability of the process. Products such as MFFC-acetal, MFFC, and MFDC could be obtained from the reaction mixture in high purity after each step, extending the scope of this approach toward other valuable biobased monomers.

Chapter 3 demonstrates the high-yielding synthesis of 2,5-bis(aminomethyl)furan (BAMF) via reductive amination of acetal-protected 2,5-diformylfuran (DFF) with 1,3-propanediol (PD-DFF). The highly reactive formyl groups in DFF induce polymerization with the *in-situ* formed primary imine and amines. To suppress such byproduct formation, an acetal protection strategy was applied for the stepwise synthesis of BAMF from concentrated DFF-acetal solutions (10 wt%). The reductive amination of PD-DFF (10 wt%) in a binary solvent of methanol and water (2:1, v/v) with NH_3 and Co_2P NRs catalyst afforded the corresponding primary amine with retaining acetal functionality (PD-AMF) in high yield (94%). In the second step, pH of the reaction mixture was adjusted by the addition of acetic acid to promote the partial hydrolysis of the acetal moiety during the reductive amination of PD-AMF. BAMF was obtained in a high yield (95%) from a 10 wt% PD-AMF solution under the optimal reaction conditions (P_{NH3} = 0.6 MPa, P_{H2} = 1.2 MPa, 120 °C, 4 h). Co_2P NRs showed outstanding catalytic performance compared to state-of-art catalysts and can be

reused several times while retaining its original activity. Moreover, the present process involved concentrated solutions (10 wt%) in two reductive amination steps, thus making the process industrially feasible for the large-scale production of BAMF.

In Chapter 4, Co_2P NRs were applied to the synthesis of methyl 5-aminomethylfuran-2-carboxylate (MAMFC), one of the valuable biomass-derived primary amines, which can be produced via the reductive amination of MFFC**.** There has been no efficient synthetic procedure to produce MAMFC in the previous papers. Herein, I studied the reductive amination of MFFC in a methanolic solution using pressurized NH_3 and H_2 with Co_2P NRs. The reaction parameters were optimized to maximize the MAMFC yield. MAMFC was obtained with the highest yield of 54% at 130 °C in 2 h under the optimized reaction conditions (P_{NH3} = 0.3 MPa and P_{H2} = 0.5 MPa).

My dissertation is focused on the synthesis of possible building blocks of bio-based polymers via efficient transformation of biomass-derived substrates to mitigate our dependency on fossil-based resources. In this direction, I was successful in developing efficient pathways for the high yield synthesis of several monomers of bio-based polymers such as MFDC and BAMF, from highly concentrated solutions of respective substrates involving an acetal protection strategy as described in **Chapters 2** and **3**, which greatly enhanced the productivity of the processes. The developed methods beyond literature can be directly employed to commercialize in real fields. Moreover, in **Chapter 4**, I showed a new reaction pathway for the synthesis of biomass-derived amino-acid derivatives (such as MAMFC) which have wide applications in polyamide industries.

List of Publications

Journal publications

Nirupama Sheet, Ryota Osuga, Nao Arai, Jan J. Wiesfeld, Satoshi Suganuma, Takayuki Aoshima, Atsushi Fukuoka, Emiel J.M. Hensen, Kiyotaka Nakajima*; A protection Strategy for High-yield Synthesis of Dimethyl Furan-2.5-dicarboxylate from 5-Hydroxymethylfurfural Using Methanol as an Acetalizing Agent". (Submitted to ***ChemCatChem***)

Nirupama Sheet, Ryota Osuga, Satoshi Suganuma, Atsushi Fukuoka, Takato Mitsudome, Kiyotaka Nakajima*; Reductive amination of acetal-protected 2,5-diformylfuran to 2,5-Bis(aminomethyl)furan using Co_2P Nanorods (NRs) catalyst. (In preparation)

Journal publications (not related to thesis)

Nirupama Sheet, Ankit Kumar, Mahendra K. Awasthi, Tushar A. Kharde, Sanjay K. singh* "One-pot Upcycling of Waste Plastics for Selective Hydrogen Production at Low-Temperature ", ***ChemCatChem*** **2023**, e202300574, 1–10. DOI. 10.1002/cctc.202300574

Patent

Sanjay K. Singh*, Nirupama Sheet, Mahendr K. Awasthi "Catalytic process for hydrogen production from polyethylene terpthalate (PET) waste", ***India Patent*** **2020**, 422056

Conference contributions

Nirupama Sheet, Jan J. Wiesfield, Atsushi Fukuoka, Kiyotaka Nakajima. Oxidative Esterification of Dimethylacetal-protected HMF (10 wt%) with Au/CeO_2. Post Symposium of TOCAT9, 60th Aurora seminar and the 9^{th} International Symposium of Institute for Catalysis. Sapporo, Japan, August 1st, 2022. (Poster)

Nirupama Sheet, Jan J. Wiesfield, Atsushi Fukuoka, Kiyotaka Nakajima. Protection strategy for selective oxidative esterification of HMF-dimethylacetal to dimethylfuran-2-5-dicarboxylate with Au/CeO_2. Nagano Conv. of JPI (52nd Petroleum-Petrochemical Symposium of JPI), Nagano, Japan, October 27–28, 2022. (Oral)

Nirupama Sheet, Nao Arai, Jan J. Wiesfield, Ryota Osuga, Atsushi Fukuoka, Kiyotaka Nakajima. Protection strategy for selective oxidative esterification of HMF-dimethylacetal to dimethylfuran-2-5-dicarboxylate with supported Au catalysts. Result Report Meeting/Industry-University Workshop, IRCCS, Kyoto University Uji Campus, Japan, February 27–28, 2023. (Poster)

Nirupama Sheet, Ryota Osuga, Satoshi Suganuma, Atsushi Fukuoka, Takato Mitsudeme, Kiyotaka Nakajima. Reductive amination of acetal-protected 2,5-diformylfuran (DFF) to 2,5-bis(aminomethyl)furan (BAMF) using Co_2P nanorod (NRs) catalyst. ICAT International Symposium on Catalysis 2023. Institute for Catalysis, Hokkaido University, Sapporo, Japan, July 18–19, 2023. (Poster)

Nirupama Sheet, Nao Arai, Jan J. Wiesfield, Ryota Osuga, Atsushi Fukuoka, Kiyotaka Nakajima. Protection strategy for selective oxidative esterification of HMF-dimethylacetal to dimethylfuran-2-5-dicarboxylate. EuropaCat2023, Prague, Czech Republic, Europe, August 26–September 1, 2023. (Poster)

Nirupama Sheet, Ryota Osuga, Satoshi Suganuma, Atsushi Fukuoka, Takato Mitsudome, Kiyotaka Nakajima. Reductive amination of acetal-protected 2,5-diformylfuran to 2,5-Bis(aminomethyl)furan using Co_2P Nanorods (NRs) catalyst. Osaka Conv. of JPI (53 rd Petroleum-Petrochemical Symposium of JPI), Osaka, Japan, October 27–28, 2023. (Oral)

Acknowledgement

With deep regards and respect, I want to express my deep sense of gratitude to my supervisor Prof. Atsushi Fukuoka. He always inspired us to find nobility within our research. His motto is that the research should not be limited to laboratory rather it should be implied in real field, which immensely attracted me in designing novel industry-relevant synthetic route to produce biomass-derived monomers of polymers. The synthesis of monomers of bio-based polymers can significantly contribute to developing a sustainable society. In this direction, his valuable suggestions really helped me in the progress of my PhD thesis.

I would like to express my sincere thanks to Prof. Kiyotaka Nakajima for providing such a golden platform to work under his guidance. I gratefully acknowledge his constant encouragement, help and valuable suggestions to complete my PhD thesis. He has always motivated and supports me in different ways. He provides me with several opportunities to explore domestic as well as international conferences. By active participation in these scientific symposiums, I gathered a lot of knowledge, which will be helpful to be established in my academic career. In addition, pursuing research in a highly facilitated and well-organized laboratory within a healthy environment was a pleasure for me, which was only possible by the join efforts of Prof. Atsushi Fukuoka and Prof. Kiyotaka Nakajima. So, I am thankful to both from the bottom of my heart.

I am grateful to Dr. Ryota Osuga for his unlimited help, time, and support. He always took effort to carefully examine my research papers, conference abstracts, preparing presentation slides and so on. I appreciate his polite behavior, which made it easy to approach him without any hesitation. I am also thankful to Dr. Abhijit Shrotri and Dr. Satoshi Suganuma for their support and help in various aspects.

I would like to acknowledge to my advisors Prof. Ken-ichi Shimizu, and Prof. Jun-ya Hasegawa, for their valuable suggestions, and motivation during the seminars to show reasonable directions in my projects.

I am grateful to Hokkaido University DX Doctoral Fellowship and AGS Scholarship for the financial support.

I extend my thanks to my group members Dr. Shaikh Nazmul Hasan Mohammad Dostagir, Dr. Yayati Naresh Palai, Dr. Jan J. Wiesfled, Dr. Daniele Padovan, Dr. Navya Subray Bhat, Mr. Zizan Wang, Mr. Shi Quan, Mr. Susanta Humar Sahoo, Ms. Nao Arai, Ms. Harumi Ikuta, Mr. Agora Chin, Mr. yuan Yutong, Mr. yangyang Ao, and Ms. Qing Yang for their co-operation and help during the project to make it successful.

I wish to express my special gratitude to Dr. Abhijit Shrotri and Dr. Shaikh Nazmul Hasan Mohammad Dostagir for introducing me to the opportunity to be part of the Fukuoka laboratory (Catalytic Transformation Laboratory). They helped me to know about the research environment and Japanese cultures before arriving in Japan, which was beneficial for me to be well-settled after arriving in Japan.

I am especially thankful to Dr. Yayati Naresh Palai, and Dr. Jan J. Wiesfled. Initially, they helped me to become familiar within the laboratory and taught various research activities and characterization techniques, which helped me to grow and be an independent researcher. Moreover, they were always more like friends than being senior researchers, with whom I enjoyed several get togethers, dinner parties, tours and so on, which are not forgettable.

In the last year of my PhD, Dr. Navya Subray Bhat became a member of our laboratory, who is a very nice person. Within a short period, we became very good friends. I received a partner to share my happiness, sorrow, and every small moment. I hope we can get in touch in future also. I will not say “Thanks” to her, as by Indian cultures in friendship, “No Thank you” and “No sorry”.

I would like to thank Ms. Haruna Ito, Secretary of Prof. Kiyotaka Nakajima, and Ms. Yumiko Yokoyama, Secretary of Prof. Atsushi Fukuoka for their immense support. Leaving so far from my family, they never realized the absence of my family. They were like actual family members to me. For every small purpose such as to buy personal groceries, health

checkup, home maintenance, postal services and in uncountable numbers they were by my side for always like pillars. I never felt that I am in a foreign country because of their presence.

Finally, I want to express my deepest love and gratitude to my parents for their unconditional love and support without which my journey is incomplete and extend thanks to my friends who were always beside me during this journey.

Appendix

Dehydrogenation of 5-Hydroxymethylfurfural (HMF) to 2,5-Diformylfuran Using an Acetal Protection Strategy

Abstract

Development of a sustainable process for the conversion of bio-based substrates to valuable building blocks is highly efficient in view of green chemistry. In this direction, I demonstrated an additive-free dehydrogenation of biomass-derived HMF to DFF, which is a potential intermediate in organic synthesis. The conversion of HMF to DFF via dehydrogenation will be highly efficient compared to the conventional oxidation process wherein over-oxidation and byproduct formation are frequent. To prevent the byproduct formation via self-condensation of HMF, the "acetal-protection strategy" could be a straightforward method. Nevertheless, though the process is simple yet highly challenging. Preliminary study indicates that the conversion of alcohol moiety to an aldehyde functionality without any oxidant requires high activation energy means high reaction temperature. While the thermal stability of the product is sufficiently low constraining the production with a percentage (<10%) only. Therefore, the development of a suitable catalyst for low-temperature dehydrogenation of PD-HMF to PD-DFF will be required to establish sustainable production of DFF from HMF.

Introduction

HMF is a versatile lignocellulosic biomass-derived platform molecule, which can be upgraded to a variety of commodity chemicals.[1–8] Recently, the selective conversion of HMF to DFF has gained significant attention owing to its potential applications in chemical industries.[1] For example, it can be used as a precursor for adhesives, binders, heterocyclic ligands, furan–urea resins, and so on.[1] HMF can be converted to DFF via oxidation or a dehydrogenation process. Previous studies focusing on the conversion of HMF to DFF mainly involve oxidative transformation using conventional oxidants such as Potassium dichromate (K_2Cr_2O7), Barium manganate ($BaMnO_4$), 2,2,6,6-tetramethylpiperidine-1-oxide (TEMPO) and so on.[1,9,10] Furthermore, several green oxidants such as air, oxygen, and H_2O_2 have been utilized to accomplish the oxidation of HMF to DFF. [1,9,10] Nevertheless, the formyl group (-CHO) in HMF has a higher tendency to oxidize to FDCA involving 5-(hydroxymethyl)furan-2-carboxylic acid (HMFA) and 5-formylfuran-2-carboxylic acid (FFCA) as intermediates (**Scheme A1**).[1,9] While, to synthesize DFF from HMF, selective oxidation of the hydroxymethyl (-CH_2OH) group of HMF to formyl group (-CHO) is particularly required.[9] However, due to undesirable geminal diol formation, which is mainly promoted by water, DFF further oxidized to FFCA and subsequently converted to FDCA (**Scheme A2**).[9] Therefore, controlling the oxidation of HMF to a desired intermediate is highly challenging due to the undesirable over oxidation. Thus, an efficient process for the selective oxidation of the -CH_2OH group to the -CHO group is highly appealing yet challenging.

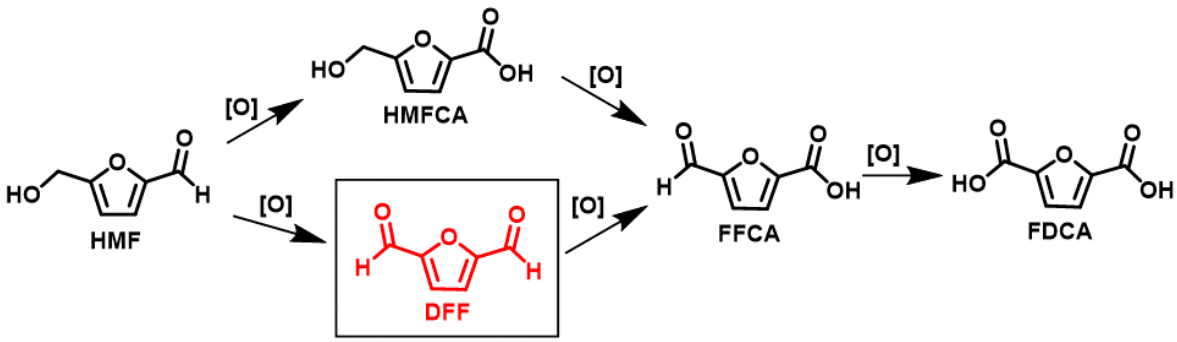

Scheme A1. Reaction Pathway for the oxidation of HMF to FDCA.

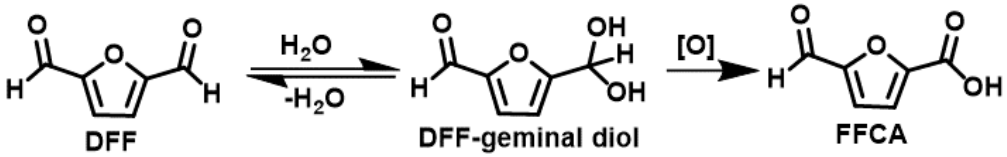

Scheme A2. Reaction Pathway for the conversion of HMF to FFCA.

In this regard, the selective oxidation of HMF to DFF has been developed using anhydrous and non-protic solvents (such as *N,N*-dimethylformamide (DMF), toluene, and so on) with several supported noble metals (Ru, Pd, Au) and metal oxide catalyst (containing Mn, V, Cu, Co and Fe). For example, Takagaki et al. reported a 92% yield of DFF via aerobic oxidation of HMF over a Ru/hydrotalcite catalyst at 120 °C in DMF.[11] Nie et al. obtained a 96% selectivity of DFF in toluene using Ru/C under an oxygen pressure of 2 MPa.[12] However, still, inevitable problems such as health, and process safety (flammability, explosion) remain in the oxidation process of HMF to DFF.[9] In contrast, the dehydrogenation process (an oxidant-free methodology) could be an alternative and attractive way to suppress the over-oxidation.[9,12,13] To date, limited studies for the dehydrogenation of HMF to DFF have been reported. For example, Chatterjee et al. reported the dehydrogenation of 5-HMF to DFF over an activated carbon-supported rhodium (Rh/C) catalyst at 150 °C using compressed carbon dioxide ($scCO_2$) as a hydrogen acceptor.[9] In the absence of CO_2, the conversion of HMF was very poor resulting in unknown byproducts. While $scCO_2$ facilitates the reaction by removing hydrogen and consequently shifting the equilibrium in the forward direction.[9] Thus, for effective conversion of HMF to DFF a high CO_2 (8 MPa) pressure and high temperature was required, which significantly reduced the sustainability of the process.[9] In the alternative, visible-light-driven acceptorless photocatalytic dehydrogenation of alcohols into the corresponding aldehyde has attracted wide attention due to its mild reaction conditions.[14–19] For instance, Liang et al. reported a Ni/ACN photocatalyst[10] and Wang et al introduced a more efficient Pt/CdS[11] for the dehydrogenation of HMF to DFF upon visible-light illumination at room temperature but still the processes require long reaction time. Moreover, previous studies indicated that in addition to the semiconductor-based photocatalyst, a suitable cocatalyst is necessary to develop an

effective photocatalytic system, which is quite challenging.[11] Therefore, to establish an efficient procedure for the selective conversion of HMF to DFF is highly desirable. Thus, herein, I designed an efficient dehydrogenation process for the conversion of HMF to DFF involving the "acetal protection strategy" to suppress polymerized byproducts formation in addition to over oxidation caused by the self-condensation of formyl group of HMF with hydroxymethyl functionalities (-CH_2OH).[20–24] I used acetal-protected HMF with 1,3-propanediol (PD) to protect the formyl group and investigated the dehydrogenation of PD-HMF to PD-DFF with heterogeneous supported-metal catalysts.

Experimental Section

Materials

5-Acetoxymethyl-2-furfuraldehyde, gold(III) chloride tetrahydrate ($HAuCl_4.4H_2O$), and indium trifluoromethanesulfonate ($In(OTf)_3$ were purchased from Sigma-Aldrich. TiO_2 and was supplied from the Ishihara Sangyo Kaisha, LTD. (Japan). 1,3-propanediol (PD) was purchased from Tokyo Chemical Industry (TCI). Nickle(III) chloride hexahydrate ($NiCl_2 \cdot 6H_2O$), nickle(III) nitrate hexahydrate ($Ni(NO_3)_2.6H_2O$), cupper(II) nitrate trihydrate ($Cu(NO_3)_2.3H_2O$), Ru/C, Rh/C, Pd/C, Pt/C, HT, anhydrous NaOH, Na_2CO_3, activated alumina, toluene and *N,N*-dimethylformamide super dehydrated (DMF) were obtained from FUJIFILM Wako Pure Chemical Corporation. Trimethyl orthoformate (TMOF) and chlorobenzene were purchased from Tokyo Chemical Industry (TCI). Dichloromethane and ethyl acetate were obtained from Kanto chemical corporation.

Catalyst preparation

The commercially available 5 wt% Ru/C, Rh/C, Pt/C and Pd/C were used as received without further pretreatment.

TiO_2 and HT supported Au catalysts were synthesized by the deposition-precipitation method.[20–24] To an aqueous solution (160 mL) of $HAuCl_4.4H_2O$ (350 mg, 0.8 mmol), NaOH solution (0.2 M) was added dropwise while maintaining the pH of the resulting solution at

9.7. The solution was mixed with the support material (TiO_2 or HT) suspended in 50 mL deionized water, followed by the addition of an aqueous NaOH to readjust the pH to 9.7. After stirring the mixture at room temperature for 18 h, a solid obtained was repeatedly washed with deionized water until Cl^- ions were completely removed, which was confirmed by a precipitation test using an aqueous $AgNO_3$ solution. Finally, the solid was dried at 70 °C overnight and used in the catalytic reaction.

Al_2O_3 supported monometallic Ni and bimetallic Cu-Ni catalysts were prepared through an incipient-wetness impregnation method.[25] In brief, to prepare Ni/Al_2O_3 (10 wt% theoretical Ni loading), 1.1 g $Ni(NO_3)_2.6H_2O$ was dissolved into 1.74 g deionized water. Then, 2.0 g Al_2O_3 was added into the mixture and kept for 24 h at room temperature. After that, the mixture was dried at 110 °C for 10 h and finally reduced at 500 °C for 4 h under hydrogen flow to obtain the desired catalyst. Bimetallic $Cu-Ni/Al_2O_3$ catalyst was prepared following the same procedure where 0.5 g $Cu(NO_3)_2.3H_2O$ and 0.22 g $Ni(NO_3)_2.6H_2O$ were added to obtain $6Cu-2Ni/Al_2O_3$ catalyst (Theoretical Cu loading, 6 wt% and Ni loading 2 wt%).

Ni_2P/CeO_2 was prepared following an earlier reported procedure.[26] Typically, $NiCl_2{\cdot}6H_2O$ (1.0 mmol), hexadecylamine (10 mmol) and triphenyl phosphite (10 mmol) were added in a Schlenk flask. The temperature was then slowly increased to 320 °C and the mixture was stirred for 2 h under an inert (N_2) atmosphere to afford a black colloidal solution of Ni_2P. Then, it was allowed to cool to 25 °C, subsequently the black product was collected by centrifugation after washing with a mixed solvent; chloroform-acetone (1:1, v/v). Finally, the product was dried overnight *in vacuo* at room temperature. The obtained powder (Ni_2P, 30 mg) was dispersed in 100 mL hexane via sonication for 1 h. Then, 1.0 g CeO_2 was added into the mixture and stirred for 6 h at room temperature. Thereafter, hexane was removed by vacuum evaporation and the obtained product was further dried *in vacuo* overnight at room temperature to afford Ni_2P/CeO_2 powder.

Characterization of catalyst

Powder X-ray diffraction (P-XRD) measurements were performed by an Ultima IV, Rigaku diffractometer at 40 kV and 40 mA using Cu Kα radiation (λ = 1.5418 Å) in 2θ = 10−90°.

Synthesis of HMF-acetal (PD-HMF)

Typically, 5-acetoxymethyl-2-furfuraldehyde (4.2 g, 25 mmol) was dissolved in dichloromethane (180 mL). Trimethyl orthoformate (6 mL, 55 mmol), 1,3-propanediol (4.5 mL, 62 mmol), and Indium trifluoromethanesulfonate ($In(OTf)_3$, 0.075 g, 0.5 mol% to the substrate) were added stepwise into the solution. The reaction mixture was stirred at room temperature overnight and purged over alumina to remove excess $In(OTf)_3$. All organic volatiles were removed under reduced pressure and the crude product was dried overnight in a high vacuum. A colorless intermediate, which was obtained after vacuum evaporation, was dissolved in the mixture of ethanol (50 mL) and an aqueous Na_2CO_3 solution (1 M, 150 mL) and then stirred for 4 h at room temperature. The product was extracted with ethyl acetate (20 mL) three times and dried by a high vacuum treatment. The yield and purity of the resulting HMF-acetal were determined as 90% and 83%, respectively, by a ^{1}H nuclear magnetic resonance (NMR) spectrometer (JNM-ECZ600, JEOL).

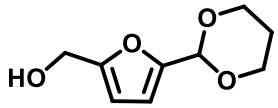

PD-HMF

^{1}H NMR (400 MHz, $CDCl_3$); 6.39 (d, 1H), 6.27 (d, 1H), 5.56 (s, 1H), 4.60 (d, 2H), 4.26 (m, 2H), 3.96 (m, 2H), 2.26 (m, 1H), 1.46 (m, 1H)

Catalytic reaction

The dehydrogenation of PD-HMF was conducted in Teflon-lined stainless steel autoclave reactors. A mixture of substrate (PD-HMF, 37 mg), and catalyst (S/C = 1 wt/wt)

in toluene was stirred at 130 °C for 16 h under an inert atmosphere (Ar, 3 MPa). The reaction mixtures were diluted with 10 mL methanol to dissolve all products, and analyzed by gas-chromatograph (GC, Shimadzu, GC-4) with a flame ionization detector (FID) using chlorobenzene as an internal standard.

Result and Discussion

Characterization of Catalysts

All the catalysts were preliminarily characterized by P-XRD to identify the crystaline phase of the catalysts. The commercial C-supported Ru, Rh, Pd and Pt catalysts (5 wt% metal loading) showed the characteistics peaks for activated C and metal (Ru, Rh, Pd and Pt) nanoparticles, respectively as shown in **Figure A1**, while partialy oxidized Ru and Pd nanoparticles were found in case of Ru/C and Pd/C, respectively. No diffraction peaks of metallic Au can be observed for TiO_2- and HT-supported Au catalysts in its XRD pattern. Simiarly, CeO_2-supported Ni_2P showed mainly diffraction peaks for the CeO_2 support, indicating high dispersion of the metal nanoparticles. On the other hand, Ni/Al_2O_3 and Cu-Ni/Al_2O_3 exhibited distinct diffraction peaks fo respective metal (Ni, Cu) nanoparticles and Al_2O_3 (γ phase).

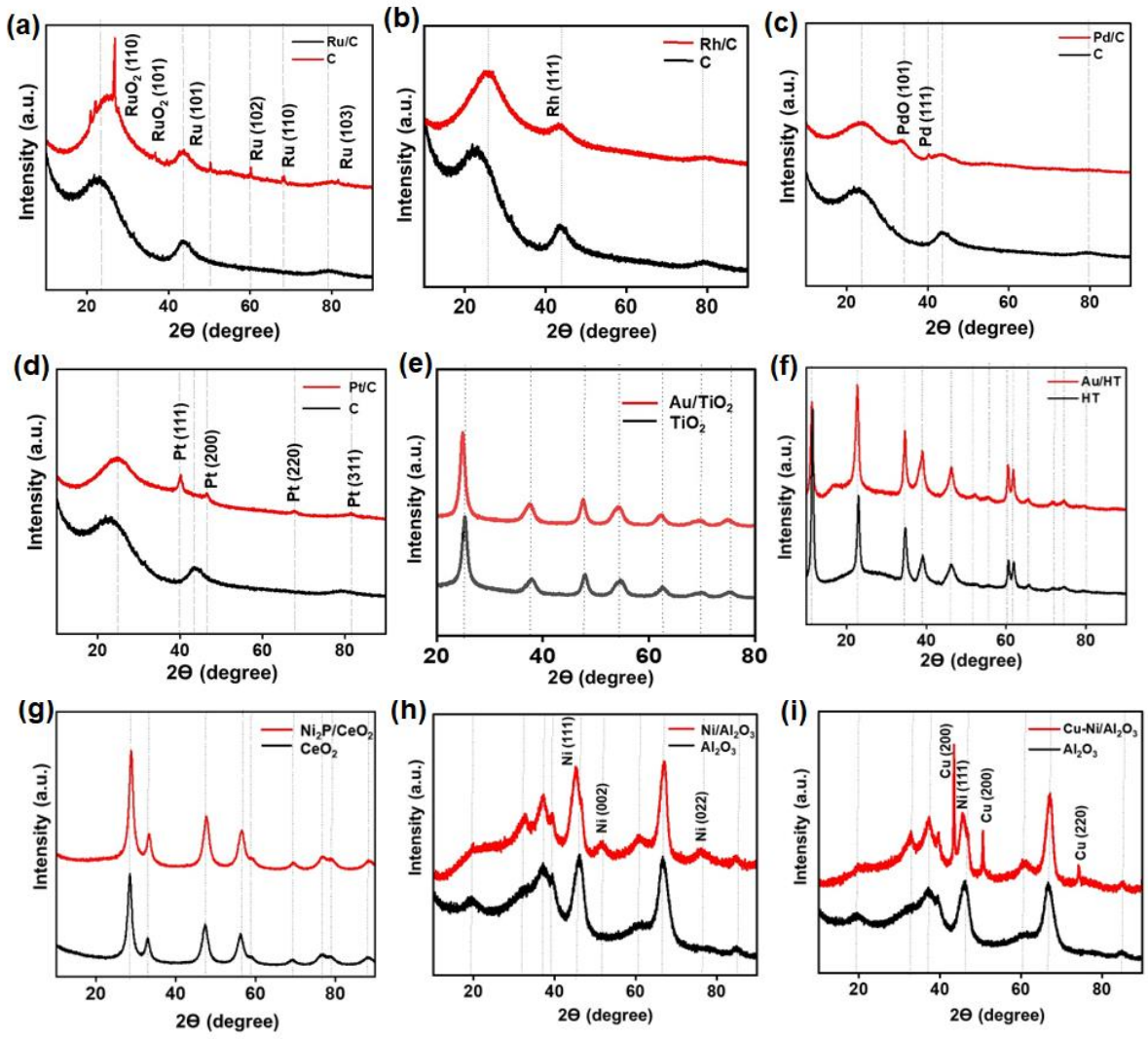

Figure A1. XRD patterns of (a) C and Ru/C, (b) C and Rh/C, (c) C and Pd/C, (d) C and Pt/C, (e) TiO_2 and Au/TiO_2, (f) HT and Au/HT, (g) CeO_2 and Ni_2P/CeO_2, (h) Al_2O_3 and Ni/Al_2O_3, and (i) Al_2O_3 and $Cu\text{-}Ni/Al_2O_3$, respectively.

Dehydrogenation of HMF-acetal (PD-HMF) to DFF-acetal (PD-DFF).

Initially, the dehydrogenation of PD-HMF to PD-DFF was studied using conventional catalysts with various combinations of metal (Ru, Rh, Pd, Pt, Au, Ni, Cu) and support (C, γ-Al_2O_3, TiO_2, CeO_2) which are well-known as active catalysts for the dehydrogenation of alcohol to aldehyde of various organic substrates. **Figure A2** shows the results for the dehydrogenation of PD-HMF to PD-DFF with the applied catalysts. The reactions were performed in toluene under an inert (Ar) atmosphere at 160 °C for 16 h. The supported noble metal catalysts (Ru, Rh, Pd, Pt and Au) showed quite high PD-HMF conversion (≥ 90%) while Al_2O_3 supported Ni and CeO_2 supported Ni_2P catalysts gave a moderate HMF conversion (ca. 35%). On the other hand, doping Cu to Ni/Al_2O_3 catalyst, conversion increased largely from 38% to 85% indicating that the catalytic activity strongly depended on the metal used. Nevertheless, the product yield was extremely low under the applied reaction conditions. Among all, Au/TiO_2 showed the highest yield of PD-DFF with a PD-HMF conversion of 90%. Therefore, further investigation to optimize the reaction conditions and maximize the product yield was continued using several supported Au catalysts.

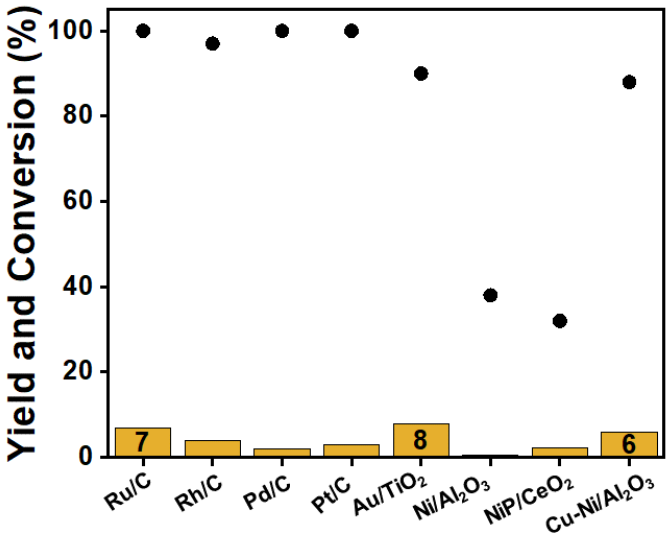

Figure A2. Screening of catalysts in the dehydrogenation of PD-HMF to PD-DFF. Reaction conditions: PD-HMF, 0.2 mmol (37 mg); catalyst (S/C =1 wt/wt); toluene, 1 mL; 160 °C, 16 h, Ar, 3 MPa.

First, the reaction temperature for the dehydrogenation of PD-HMF was optimized with Au/TiO_2 shown in **Table A1**. At 130 °C, a very low conversion of PD-HMF was obtained. With the increase in reaction temperature, PD-HMF conversion steadily increased, while PD-DFF selectivity remains same at 130–150 ºC. Prolonging the reaction time to 24 h at 150 °C resulted in lowering PD-DFF selectivity, suggesting that higher temperature and longer reaction time causes the degradation of PD-DFF. A control experiment was performed in the absence of a catalyst to monitor the thermal stability of the product under otherwise identical conditions. **Figure A3** revealed that the PD-DFF is stable ≤ 130 °C. However, high temperature (> 130 °C) caused severe degradation of the desired product (PD-DFF) which limits the study of dehydrogenation of PD-HMF to PD-DFF at low temperature (≤ 130 °C) to avoid thermal degradation of the product.

Table A1. Effect of temperature in the dehydrogenation of PD-HMF with Au/TiO_2.[a]

Entry	T (°C)	t (h)	Conv. (%)	Product Selectivity (%)		C.B. (%)
				PD-DFF	Others	
1	130	16	18	22	78	86
2	140		46	24	76	65
3	150		70	24	76	47
4	160		90	9	91	18
5	150	24	79	15	72	33

[a] Reaction conditions: PD-HMF, 0.2 mmol (37 mg); Au/TiO_2, 37 mg; toluene, 1 mL; Ar, 3 MPa. Others indicate undetectable byproducts.

Next, Hydrotalcite (HT)-supported Au catalysts with different Au (wt%) loadings were prepared and examined in the dehydrogenation of PD-HMF to PD-DFF at 130 °C under the same reaction conditions to increase the PD-HMF conversion and PD-DFF selectivity (**Table A2**). Substituting TiO_2 with HT significantly improved PD-DFF selectivity. In addition, PD-HMF conversion increased with increasing Au content, which indicates Au nanoparticles to be the active site (**Table A2, entries 1**–**4**). However, extending reaction time

did not improve both PD-HMF conversion and PD-DFF selectivity. These results suggest that monometallic Au alone is not effective even at high loadings to activate PD-HMF at low temperature (**Table A2, entry 5**).

Table A2. Dehydrogenation of PD-HMF with Au/HT.[a]

Entry	Au (wt%)	T (°C)	t (h)	Conv. (%)	Product Selectivity (%)		C.B. (%)
					PD-DFF	Others	
1	0.04	130	16	2	50	50	99
2	0.6			6	83	17	99
3	2			16	50	50	92
4	26			16	62	38	94
5	26	130	72	13	39	61	92

[a] Reaction conditions: PD-HMF, 0.2 mmol (37 mg); Au/TiO_2, 37 mg; toluene, 1 mL; Ar, 3 MPa. Others indicate undetectable byproducts.

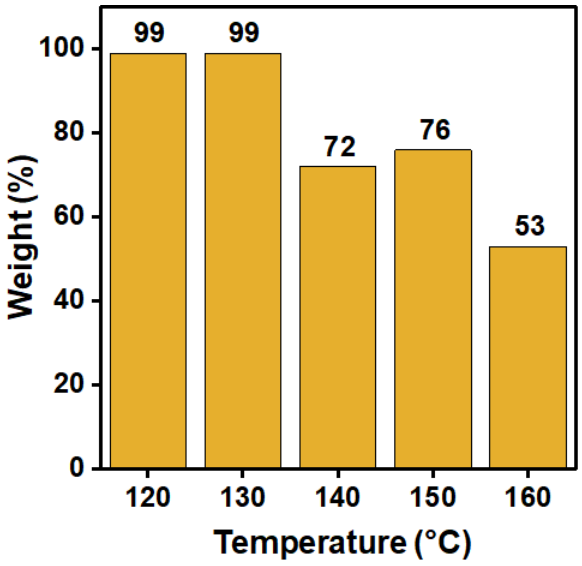

Figure A3. Stability test of PD-DFF in absence of catalyst. Reaction conditions: PD-DFF, 0.05 mmol (10 mg); toluene, 1 mL; 24 h, Ar, 3 MPa.

Conclusion

An additive-free dehydrogenation of HMF to DFF was investigated with several supported noble (Ru, Rh, Pd, Pt and Au) and non-noble metals (Ni and Cu) catalysts protecting the reactive formyl group of HMF with a stable acetal functionality (PD). Experimental results suggest that the conversion of HMF to DFF requires a high reaction temperature while the obtained product yield was very low. A control experiment to determine the thermal stability of the product was conducted, which indicates that the product is highly unstable at high temperature limiting the product yield. Therefore, a suitable catalyst for low temperature dehydrogenation of PD-HMF to PD-DFF will be developed and further study will be continued.

References

[1] C. P. Woroch, A. W. Lankenau, M. W. Kanan, *Macromolecules* **2021**, *54*, 9978–9983.

[2] L. Hu, G. Zhao, W. Hao, X. Tang, Y. Sun, L. Lin, S. Liu, *RSC Adv.* **2012**, *2*, 11184.

[3] Y. Román-Leshkov, C. J. Barrett, Z. Y. Liu, J. A. Dumesic, *Nature* **2007**, *447*, 982–985.

[4] B. Liu, Z. Zhang, *ChemSusChem* **2016**, *9*, 2015–2036.

[5] A. Corma, S. Iborra, A. Velty, *Chem. Rev.* **2007**, *107*, 2411–2502.

[6] Y. Y. Gorbanev, S. K. Klitgaard, J. M. Woodley, C. H. Christensen, A. Riisager, *ChemSusChem* **2009**, *2*, 672–675.

[7] Z. Zhang, K. Deng, *ACS Catal.* **2015**, *5*, 6529–6544.

[8] M. Chatterjee, T. Ishizaka, A. Chatterjee, H. Kawanami, *Green Chem.* **2017**, *19*, 1315–1326.

[9] W. Liang, R. Zhu, X. Li, J. Deng, Y. Fu, *Green Chem.* **2021**, *23*, 6604–6613.

[10] J. Wang, Y. Yuan, K. Ren, B. Wang, Z. Li, *J. Catal.* **2023**, *417*, 178–184.

[11] A. Takagaki, M. Takahashi, S. Nishimura, K. Ebitani, *ACS Catal.* **2011**, *1*, 1562–1565.

[12] J. Nie, J. Xie, H. Liu, *J. Catal.* **2013**, *301*, 83–91.

[13] T. Mitsudome, Y. Mikami, H. Funai, T. Mizugaki, K. Jitsukawa, K. Kaneda, *Angew. Chem. Int. Ed.* **2008**, *47*, 138–141.

[14] T. Mitsudome, Y. Mikami, K. Ebata, T. Mizugaki, K. Jitsukawa, K. Kaneda, *Chem. Commun.* **2008**, 4804.

[15] D. Huang, H. Wang, Y. Wu, *Molecules* **2022**, *27*, 8537.

[16] J. Dai, *Green Energy Environ.* **2021**, *6*, 22–32.

[17] H. Zhang, Z. Feng, Y. Zhu, Y. Wu, T. Wu, *J. Photochem. Photobiol. Chem.* **2019**, *371*, 1–9.

[18] S. Xu, P. Zhou, Z. Zhang, C. Yang, B. Zhang, K. Deng, S. Bottle, H. Zhu, *J. Am. Chem. Soc.* **2017**, *139*, 14775–14782.

[19] S. Yurdakal, B. S. Tek, O. Alagöz, V. Augugliaro, V. Loddo, G. Palmisano, L. Palmisano, *ACS Sustain. Chem. Eng.* **2013**, *1*, 456–461.

[20] T. Boonyakarn, J. J. Wiesfeld, M. Asakawa, L. Chen, A. Fukuoka, E. J. M. Hensen, K. Nakajima, *ChemSusChem* **2022**, *15*, e202200059.

[21] M. Kim, Y. Su, A. Fukuoka, E. J. M. Hensen, K. Nakajima, *Angew. Chem. Int. Ed.* **2018**, *57*, 8235–8239.

[22] M. Kim, Y. Su, T. Aoshima, A. Fukuoka, E. J. M. Hensen, K. Nakajima, *ACS Catal.* **2019**, *9*, 4277–4285.

[23] J. J. Wiesfeld, M. Asakawa, T. Aoshima, A. Fukuoka, E. J. M. Hensen, K. Nakajima, *ChemCatChem* **2022**, *14*, e202200191.

[24] J. J. Wiesfeld, M. Kim, K. Nakajima, E. J. M. Hensen, *Green Chem.* **2020**, *22*, 1229–1238.

[25] Z. Wei, Y. Cheng, H. Huang, Z. Ma, K. Zhou, Y. Liu, *ChemSusChem* **2022**, *15*, e202200233.

[26] S. Fujita, K. Imagawa, S. Yamaguchi, J. Yamasaki, S. Yamazoe, T. Mizugaki, T. Mitsudome, *Sci. Rep.* **2021**, *11*, 10673.